Utjecaj prehrane s visokim udjelom masti i ugljikohidrata i rane primjene metformina i liraglutida na lipidom hipokampusa mužjaka i ženki odraslih Sprague Dawley štakora.

Kuharić, Marin

Permanent link / Trajna poveznica: https://urn.nsk.hr/urn:nbn:hr:152:433912

JOSIP JURAJ STROSSMAYER UNIVERSITY OF OSIJEK

FACULTY OF MEDICINE OSIJEK

Marin Kuharić

THE EFFECTS OF HIGH-FAT HIGH-SUGAR DIET AND EARLY METFORMIN AND LIRAGLUTIDE TREATMENT ON THE HIPPOCAMPAL LIPIDOME OF ADULT MALE AND FEMALE SPRAGUE DAWLEY RATS

Doctoral dissertation

Osijek, 2022

JOSIP JURAJ STROSSMAYER UNIVERSITY OF OSIJEK

FACULTY OF MEDICINE OSIJEK

Marin Kuharić

THE EFFECTS OF HIGH-FAT HIGH-SUGAR DIET AND EARLY METFORMIN AND LIRAGLUTIDE TREATMENT ON THE HIPPOCAMPAL LIPIDOME OF ADULT MALE AND FEMALE SPRAGUE DAWLEY RATS

Doctoral dissertation

Osijek, 2022

Mentor: Aleksandar Včev, MD, PhD

Co-mentor: Vedrana Ivić, PhD

The dissertation contains 163 pages.

ACKNOWLEDGEMENTS

TABLE OF CONTENTS

LIST OF ABBREVIATIONS

ABC	avidin-biotin complex
AMPK	5'-AMP-activated protein kinase
APP	amyloid precursor protein
ATP	adenosine triphosphate
BBB	blood-brain barrier
BSA	bovine serum albumin
CA1	Cornu Ammonis 1 region
CA2	Cornu Ammonis 2 region
CA3	Cornu Ammonis 3 region
CDP	cytidine diphosphate
CNS	central nervous system
CoA	Coenzyme-A
CSF	cerebrospinal fluid
DAB	3,3'-diaminobenzidine
DAG	diacylglycerol
DG	dentate gyrus
DPP-4	dipeptidyl peptidase-4
ER	endoplasmic reticulum
ERK	extracellular signal-regulated kinase
FFA	free fatty acid
GLUT	glucose transporter
GLP-1	glucagon-like peptide-1
Grb2	growth factor receptor-bound protein 2
HFHSD	high-fat high-sugar diet
HFHSD-L	high-fat high-sugar diet treated with liraglutide
HFHSD-M	high-fat high-sugar diet treated with metformin
HRP	horseradish peroxidase
IDV	integrated density value
IGF-1	insulin-like growth factor-1
IGF-1R	insulin-like growth factor-1 receptor
IGF-2	insulin-like growth factor-2

InR	insulin resistance
IR	insulin receptor
IRS	insulin receptor substrate
LTD	long-term depression
LTP	long-term potentiation
MALDI-TOF	matrix-assisted laser desorption/ionization time-of-flight
MAPK	mitogen-activated protein kinase
MEK	mitogen-activated protein kinase kinase
MetS	metabolic syndrome
mTOR	mechanistic target of rapamycin
NADH	reduced nicotinamide adenine dinucleotide
OGTT	oral glucose tolerance test
PBS	phosphate buffered saline
pTau	phosphorylated Tau protein
PDK-1	phosphoinositide-dependent kinase-1
PI3K	phosphoinositide-3-kinase
PIP3	phosphatidylinositol (3,4,5)-trisphosphate
PKB	protein-kinase B
PKC	protein-kinase C
PUFA	polyunsaturated fatty acid
ROI	region of interest
SD	standard diet
SOS	Son of Sevenless
SH2	Src homology-2
T2DM	type 2 diabetes mellitus

LIST OF TABLES

LIST OF FIGURES

1. INTRODUCTION

1.1. Metabolic syndrome

Non-communicable diseases are, by definition, chronic conditions that are not a result of an acute infectious process, but develop due to a combination of genetic, environmental, physiological and behavioral factors (1). They do not resolve spontaneously and are seldom completely cured. Their large burden on healthcare systems due to their chronicity, growing morbidity and mortality in both developed and underdeveloped parts of the world has been recognized as a major concern in recent times (2).

Metabolic syndrome (MetS) is an umbrella term for a variety of risk factors that can cause a multitude of non-communicable diseases that was first coined in 1975 by a group of German researchers (3). It has since become a focus of research in many fields, both in molecular biology and clinical areas such as gastroenterology, endocrinology, epidemiology, etc. On a cellular level, there are several metabolic abnormalities that these factors have in common. Their molecular pathophysiology is a reflection of not only increased caloric intake resulting in adipose tissue and ectopic lipid accumulation but also changes in adipocyte hormone metabolism, proinflammatory immune cell activation, disturbances of the gut microbiome, organelle dysfunction, thyroid hormone dysfunction, etc. (4, 5).

From a clinical perspective, there is not a single, unified definition of MetS. Several diagnostic criteria have been proposed and used over the past few decades. Some of the more commonly used have been ones proposed by the World Health Organization (6), International Diabetes Federation (7) and National Cholesterol Education Program (8). While not identical, they focus on the same components/risk factors, which include central obesity, dyslipidemia (an increase in plasma triglyceride levels and a decrease in plasma high-density lipoprotein cholesterol levels), hypertension and hyperglycemia. Recent advances in MetS research have shown that a significant percentage of obese individuals do not have these characteristic metabolic disturbances, which led to the introduction of the term metabolically healthy obese. On the other hand, metabolic disturbances may appear in individuals with a normal body-mass index (9, 10). This is a prime example of a necessity for personalized medicine focusing on individual preventive care and treatment plans, based on the complex nature of MetS ethiopathogenesis that includes a variety of both (epi)genetic and environmental factors. While it has many challenges, especially in terms of logistics, handling large datasets and

being translated to a clinical setting on an individual level, one area showing great promise and benefit for personalized medicine is metabolomics (or simply "omics") research, which quantifies and identifies entire groups of molecules (e.g. lipids - lipidomics, proteins - proteomics, RNA – transcriptomics, etc.) (11). This can be applied to MetS research as well.

Patients who meet the diagnostic criteria of MetS are at a much greater risk of developing atherosclerosis, which can manifest itself as coronary heart disease, peripheral vessel disease or cerebrovascular disease, among others, which in turn increase the risk for major vascular-based episodes, such as stroke and heart attack. Clear connections have also been made between MetS and increased risk for many other clinical entities, including common cancers and both male and female infertility (12, 13). Another major consequence of MetS is the development of insulin resistance (InR), the key pathophysiological factor in type 2 diabetes mellitus (T2DM) (14).

1.2. Mechanisms of insulin action in health and disease

1.2.1. The intricacies of insulin signaling

Insulin is an important hormone regulating glucose homeostasis through glucose uptake and glycolysis and glycogenesis promotion, while down-regulating gluconeogenesis and glycogenolysis. Its anabolic effects apply to lipid and protein metabolism as well. It is a polypeptide consisting of two chains (A and B) connected with disulfide bonds synthesized in β-cells of pancreatic Langerhans islets. The final form of insulin is created by multiple posttranslational modifications, which include cleavage of its precursors, preproinsulin and proinsulin. All of its effects are achieved through its binding to the insulin receptor (IR). IR is a heterotetrameric transmembrane receptor with tyrosine kinase activity. It consists of two extracellular α-subunits that bind insulin and two transmembrane β-subunits with kinase activity. Once insulin is bound to IR, it initiates complex intracellular signaling pathways with both metabolic and mitogenic effects. It is multifaceted partly due to the existence of insulin-like peptides such as insulin-like growth factors (IGF-1 and IGF-2). These peptides bind to both their own receptors as well as IR and show overlap in signaling functions with insulin. Furthermore, there are two isoforms of IR, IR-A and IR-B, synthesized through alternative splicing that are not equally expressed in all tissues and that have different binding affinities to proinsulin, insulin, IGF-1 and IGF-2. IR-A and IR-B are not exposed to the same

circulating levels of the aforementioned peptides. For example, there is a higher concentration of insulin in the portal circulation and hepatocytes mostly express the more insulin-specific IR-B in their membrane, which is why its metabolic effects are more prominent in the liver than the mitogenic effects of IGF-1 and IGF-2. Even though these complex signaling pathways differ from tissue to tissue, especially in tissues tasked with maintaining tight metabolic homeostasis (white adipose tissue, skeletal muscle tissue, liver), the proximal signaling cascades maintain a degree of similarity (15, 16).

Once the pancreas is stimulated and insulin is secreted into the bloodstream, it binds to the α-subunit of the IR. This induces a conformational change in the β-subunits, allowing the receptor to become active by triphosphorylation of its activation loop, which consists of tyrosine residues (Tyr^{1162}, Tyr^{1158} and Tyr^{1163}), followed by phosphorylation of an additional residue (Tyr^{972}). IR is specific in that it does not directly activate cytoplasmic signaling molecules – it undergoes an additional step using so-called adaptor molecules that recruit necessary downstream molecules needed to specify and amplify the insulin cellular response (17). A best-understood group of these proteins are insulin receptor substrates (IRS). Research has shown that while there are similiarities between six known isoforms of IRS, there is a difference in tissue distribution and function (18, 19). The autophosphorylation of the IR allows for the binding of IRS, which are themselves then phosphorylated and activated by the IR, allowing for the main signaling cascades to be initiated.

As previously mentioned, there are metabolic and mitogenic signaling pathways. The metabolic signaling pathway, through which insulin accomplishes its effects on carbohydrate, protein and lipid metabolism starts proximally with the PI3K/PKB (Akt) pathway (20). Phosphoinositide-3-kinase (PI3K) is a tetrameric protein with a regulatory (p85) and catalytic (p110) subunit that binds to the IRS with its SH2 (Src homology-2) domain. It phosphorylates phosphatidylinositol-4,5-bisphosphate, a membrane phospholipid, giving rise to phosphatidylinositol-3,4,5-trisphosphate (PIP3). PIP3 recruits the phosphoinositide-dependent kinase-1 (PDK-1) to the membrane and activates it. PDK-1 substrates are a protein family – AGC protein kinases. When phosphorylated and activated, they carry out most of the metabolic effects of this signaling pathway, which can be tissue specific. They not only include isoforms of Akt/protein kinase B (PKB) that is mentioned in the commonly used name of this pathway, but also isoforms of protein kinase C (PKC), p70 ribosomal S6 kinase and serum- and glucocorticoid-induced protein kinase. The Akt/PKB isoform involved in insulin-stimulated signaling is Akt2. When talking about PKC, there are three isoform groups: conventional PKC isoforms (PKC-α, PKC-β1, PKC-β2 and PKC-γ) that are activated by

calcium, phosphatidylserine and diacylglycerols (DAG) or phorbol esters, novel PKC isoforms (PKC-δ, PKC-ε, PKC-θ and PKC-η) that do not require calcium and atypical PKC isoforms (PKC-ζ and PKC-ι/λ) that require neither calcium nor the aforementioned molecules for activation (21). The isoform expression differs from tissue to tissue.

In terms of carbohydrate metabolism, AGC protein kinases mobilize and transport glucose transporter (GLUT) storage vesicles to the cell membrane and facilitate their fusion, allowing glucose to enter the cell. In hepatic tissue, for example, they activate glucokinase to promote glycolysis. Additionally, they phosphorylate glycogen-synthase kinase, rendering it inactive and allowing glycogen synthase to remain active, therefore promoting glycogenesis (22, 23). The anabolic effects of insulin concerning protein and lipid metabolism through the Akt/PKB node are achieved by a kinase called the mechanistic target of rapamycin (mTOR, previously referred to as the mammalian target of rapamycin), activated by phosphorylation. It is a serine/threonine protein kinase from the PI3K related protein kinase family, consisting of two subunits – mTORC1 and mTORC2 (24). The PI3K/PKB pathway has been shown to regulate gene expression responsible for cell survival and apoptosis through FoxO proteins, a subgroup of the Forkhead transcription factor family (25), in addition to regulating the activity of proteins involved in cell growth, apoptosis and cell cycle regulation, such as Mdm2, P21Cip1, p27Kip1, Bax, Bad, caspase-9, etc. PKB also promotes nitric oxide synthesis and vasodilatation (26).

Nuclear effects, i.e. gene expression regulatory effects of insulin regarding cell proliferation, growth and differentiation are controlled by the second major arm of the insulin signaling pathway, the Grb2-SOS-Ras-MAPK pathway (Ras-MAPK, simplified, where MAPK stands from mitogen-activated protein kinase), an evolutionarily conserved pathway that is observed in all eukaryotic cells (27). It is based on a phosphorylation cascade that activates transcription factors and it begins with the growth factor receptor-bound protein 2 (Grb2). Grb2 is to this pathway what PI3K is to the PI3K/Akt pathway. It acts as a loading dock on IRS, binding to it with its SH2 domain. Once bound, it recruits a Son of Sevenless (SOS) protein to the submembrane region where it binds to the SH3 domain of Grb2. SOS acts as a guanine nucleotide exchange factor, so it activates its target protein, the membrane-bound Ras protein, by dissociating a GDP molecule and binding GTP to it. The inhibitory effects on Ras are carried out and amplified by the GTPase-activating protein, which increases the activity of the Ras intrinsic GTPase, rendering it inactive. This represents a typical interaction for so-called G-proteins that require GTP to activate and carry out their functions. Once activated, Raf, a serine/threonine kinase, is mobilized to the submembrane

region, bound to Ras and activated through an intricate process that includes phosphorylation (28). The cascade continues by activating the mitogen-activated protein kinase kinase (MEK, MAP2K, or MAPKK). Unlike the previously mentioned kinase proteins, MEK has a dual function – it acts both as a tyrosine kinase and a serine/threonine kinase. The final piece of the cascade before entering the nucleus to interact with the DNA is the extracellular signal-regulated kinase (ERK), becoming active when phosphorylated by MEK. Once in the nucleus, ERK activates numerous transcriptional factors responsible for cell proliferation, growth, differentiation and survival.

Negative feedback and inhibition of the insulin signaling pathways are of great importance because of the numerous effects the aforementioned effectors have. Inhibitory regulators include enzymes like lipid phosphatases and phosphoprotein phosphatases (PTEN, SHIP2) and adaptor proteins like Grb and SOCS. Signaling inhibition can also be achieved through inhibitory serine/threonine phosphorylation of the IRS (27).

1.2.2. Pathophysiological basis of InR

It is known that InR can be present years before signs and symptoms of T2DM appear. It affects multiple organs and organ systems, not just those heavily involved in metabolic homeostasis. Among them are the gastrointestinal tract, kidneys and the central nervous system (CNS) (29). The key tissues initially and primarily affected by InR are muscle tissue, white adipose tissue and the liver. Each of them has certain specifics in terms of a response to the initial effects of InR relating to metabolic changes as a compensatory mechanism to try and override the nosogenic effects brought on to them. Just as is the case with each pathological process exerting its nosogenic effects on a cell, tissue, organ, organ system and ultimately, the organism as a whole, the activated compensatory mechanisms can maintain this "fake" homeostasis only for a certain amount of time. Once they have worn out, the deleterious effects take over and begin to manifest clinically.

By definition, InR is the body's inability to use insulin for glucose uptake, be it endogenous or exogenous insulin. (30). In a clinical setting, InR can be quantified using the HOMA-IR (homeostasis model assessment of insulin resistance) index. This value can easily be calculated using fasting serum insulin and fasting serum glucose levels (31, 32). It is also a useful tool for detecting InR before clinical manifestation occurs in patients that have a risk of developing MetS, e.g. those with a positive family history. HOMA-IR index has also been

identified as a predictor for the development of several clinical entities related to MetS, including cardiovascular disease (33).

The complexities of MetS and InR and their consequences do not strictly relate to chronic hyperglycemia, changes in body weight and microvascular damage leading to atherosclerosis and consequently tissue hypoperfusion, small infarctions or large vascular incidents. There is a vast shift in metabolism that is brought on by rapid and large intracellular lipid accumulation. These lipids primarily disrupt intracellular signaling homeostasis mediated by insulin. By doing so, not only do they disable proper and prompt mobilization of GLUT to the cell surface leading to hyperglycemia, but they also block all the essential effects of insulin relating to lipid, carbohydrate and protein metabolism, as well as proper organelle function that relates to the Ras/MAPK arm of the insulin signaling pathway. This extends to damage to the ER, mitochondria and the cell membrane, which is brought on not only by intracellular lipids but also by an activated proinflammatory response. Several lipids have been identified as the main disruptors of insulin signaling – ceramides, DAGs and long-chain fatty acyl-CoAs (34 - 37). Overnutrition and chronic increase in caloric intake are initially reflected in hypertrophy and hyperplasia of adipose tissue. Adipose tissue cannot take on an infinite amount of lipids, also leading to adipocytokine dysfunction. Such excessive concentrations of lipids slowly begin to affect and trickle into other cells and tissues, mainly myocytes and hepatocytes. As they start overwhelming these tissues, they exert their lipotoxicity. The proinflammatory environment that begins to develop itself plays a large part in the development of InR. Gregor and Hotamisligil wrote a review paper in 2011 (38) focusing on obesity-driven inflammation. These inflammatory processes do have the same nature as the typically observed inflammatory processes – a certain nosogenic effect leading to activation of immune cells and proinflammatory mediator molecules, followed by antiinflammatory mediator dominance, resolution and tissue restitution in both the morphological and functional context. Gregor and Hotamisligil concluded that there are four characteristics of obesity-driven inflammation: it is metabolic, it is low-grade, it alters the cellular environment and it is chronic and maintained.

Back in 1999, a nuclear magnetic resonance spectroscopic study demonstrated a link between intramyocellular triglyceride content and InR (39). The three aforementioned groups of lipids have been extensively researched since the last decade of the past century in order to identify the specific mechanisms that trigger InR. While a proinflammatory environment helps promote and maintain InR, it is their role in blocking insulin signaling pathways that ultimately leads to resistance of peripheral tissues. The effects of these lipids on blocking

insulin signaling are shown in Figure 1.1. Ceramides belong to a group of lipids called sphingolipids. They are synthesized through a process that begins with a molecule of serine and palmitoyl-CoA. They are normally found in cell membranes, specifically in lipid rafts – specialized microdomains whose functions go much further than simple maintaining of cellular integrity and structure (40). Accumulation of intracellular ceramide leads to their increased interaction with PKC isoforms which then interfere with PKB and CD36 (34). PKB, as was mentioned in 1.2.1., is a major part of one of the two main signaling arms of insulin and its inhibition leads to dysregulation of GLUT transporter mobilization, as well as impairment of gene expression related to cell growth, differentiation and survival. CD36, on the other hand, is a membrane protein that imports free fatty acids (FFA) into the cell (41). This is just one of the many examples of closed vicious cycles seen in MetS. CD36 has been found in caveolae, a type of lipid rafts that contain IRs, i.e. they are important sites that regulate insulin signaling. They are rich in sphingomyelins that can be synthesized from ceramides (42, 43). Ceramide and DAG accumulation also leads to increased serine phosphorylation of IRS-1 (44). Ceramides shift metabolic pathways in favor of using FFAs as energy fuel by inhibiting glucose and amino acid uptake (45, 46) and disrupting the synthesis of nitrous oxide because it employs proteins in the same signaling pathways as insulin, which eventually leads to vascular endothelial damage and progression of atherosclerosis (47). FFA and fatty acyl-CoA accumulation in cells additionally favors using lipid metabolites as the main energy fuel instead of glucose. This has numerous consequences across all tissue types, specifically in hepatic and muscle tissue. These changes are in close correlation with mitochondrial dysfunction which has been another relevant factor in elucidating all the issues seen in cells that are resistant to insulin. Mitochondria are the "power plants" of the cell and the production of adenosine triphosphate (ATP) is absolutely essential for the cell. One of the reasons why mitochondrial function is diminished is a deficiency of an enzyme called N-acetyltransferase 2 (48). It is one of the few identified culprits related to InR that is not a direct reflection of dietary-related changes, but rather a matter of genetic predisposition. It has, however, been identified as an insulin-sensitivity gene (49). When taking N-acetyltransferase 2 out of the equation, it is still not fully understood whether mitochondrial dysfunction is one of the causes of InR, whether it is a secondary consequence of InR or whether the correct answer is, in fact, a combination of both. When using the term mitochondrial dysfunction, it primarily means that there is a decrease in the number of mitochondria coupled with their inability to properly produce ATP (50, 51). Their dysfunction leads to an increase in production of reactive oxygen species, i.e. free radicals (hydrogen

peroxide, superoxide). They represent a grave threat to the structural and functional integrity of the cell with the possibility of apoptosis if they are not properly dealt with. This introduces oxidative stress and lipid peroxidation as two nosogenic entities that add further complications to an already dysfunctional cell. A reversal of these changes, at least to a certain degree, has been observed, suggesting that while InR might not be fully irreversible, there are options to help slow down this deterioration. Exercise has been found to help with insulin sensitivity (52), mitochondrial function (53) and inflammation in skeletal muscle (54). Finally, another organelle showing impaired function in the context of InR is the endoplasmic reticulum (ER). This organelle is the site of protein and lipid synthesis and its dysfunction, often referred to as ER stress, can contribute to InR via a mechanism called the unfolded protein response (55). ER stress has been linked to MetS, T2DM and InR in both animal and clinical studies (56, 57).

Even though T2DM is not an autoimmune disorder like type 1 diabetes mellitus, where destruction of β-cells within the pancreatic Langerhans islets is observed and there is no InR, the pancreas should not be completely ignored in the context of T2DM. The overwhelming majority of consequences of InR, be it on a cellular level or clearly manifested clinically, are a reflection of the aforementioned processes. InR does, however, put a strain on the pancreas. Chronic hyperglycemia triggers the pancreas to overreact and produce high levels of insulin to try and compensate for a lack of glucose uptake. However, the overwhelming influx of lipids does not spare Langerhans islets, as they are also forced to face difficulties in maintaining homeostasis. These include mitochondrial dysfunction, ER stress, a proinflammatory environment and a specific nosogenic effect relating to the hyperproduction of amylin which can form amyloid fibrils (58 - 60). All of these eventually lead to β-cell death, creating yet another point of dysfunction worsening glucose homeostasis. Ultimately, InR is accompanied by hypoinsulinemia in chronic T2DM patients. Rahier et al. (61) undertook an analysis of pancreatic β-cell mass during autopsies of T2DM patients and concluded that β-cell mass in diabetics was approximately 39% lower than in non-diabetic controls, including a 30% lower insulin concentration.
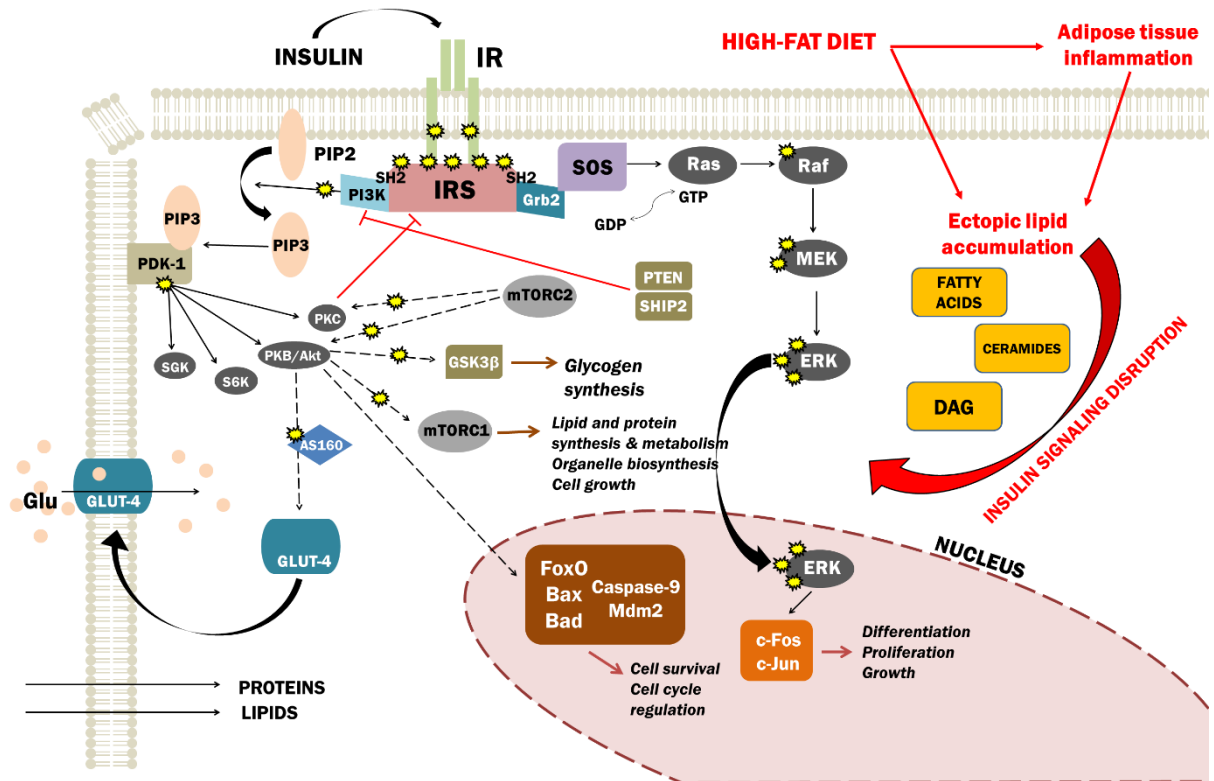
Figure 1.1. A simplified schematic of insulin signaling pathways and the basis of insulin resistance-related signaling disruption.

The figure was created by the author based on references (20 - 28, 34 - 40).

AS160 = Akt substrate of 160 kDa; Bad = Bcl-2-associated death promoter; Bax = Bcl-2-associated X protein; DAG = diacylglycerol; ERK = extracellular signal-regulated kinase; FoxO = Forkhead box O; GLUT-4 = glucose transporter 4; GDP = guanosine diphosphate; Glu = glucose; Grb2 = growth factor receptor-bound protein 2; GSK-3β = glycogen synthase kinase-3β; GTP = guanosine triphosphate; IR = insulin receptor; IRS = insulin receptor substrate; Mdm2 = mouse double minute 2 homolog; MEK = mitogen-activated protein kinase kinase; mTORC = mechanistic target of rapamycin complex 1; PDK-1 = 3-phosphoinositide-dependent protein kinase-1; PI3K = phosphatidylinositol 3-kinase; PIP2 = phosphatidylinositol 4,5-bisphosphate; PIP3 = phosphatidylinositol 3,4,5-trisphosphate; PKB = protein kinase B; PKC = protein kinase C; PTEN = phosphatase and tensin homolog; S6K = ribosomal protein S6 kinase β-1; SGK = serum and glucocorticoid-regulated kinase; SHIP2 = SH2 domain-containing inositol phosphate 5-phosphatase 2; SOS = Son of Sevenless protein

1.3. Glucose, insulin and InR in the CNS

Glucose is the principal energy source for the brain. Even though it is not the largest organ in the body, the brain requires an uninterrupted supply of fuel and approximately 20% of all energy produced is consumed by it. This consumption is not universal, both in the context of macroscopic regions of the brain, which depends on their state of activity, and on the cellular level. Most energy is consumed at the neuronal synaptic level, which comes as no surprise considering the complex processes occurring at these neuronal junctions (62, 63). Besides providing energy for synaptic transmission, there is a multitude of other neuronal functions where glucose is utilized, one of the most important being neurotransmitter synthesis (64 - 66). Several forms of GLUT are responsible for delivering glucose from the blood through the BBB into CNS, the most abundant types being the insulin-independent GLUT-1 and GLUT-3, regulating glucose uptake in neurons and glial cells. GLUT-2, on the other hand, is mainly found in the hypothalamus, while GLUT-4 is an insulin-dependent isoform found in many regions of the brain, including the hippocampus (67). While neurons do not exclusively depend on insulin for glucose uptake, the effects of insulin on the CNS go much further than just glucose uptake regulation.

Just over half a century after the initial discovery of insulin in 1921 (68), 1978 was the year that marked a paradigm shift in insulin research, specifically in the context of CNS, because it was believed up to that point that insulin had no role in the brain as glucose uptake was a process that required no hormonal regulation. In 1978, Havrankova et al. published results of their research that indicated the presence of both insulin and IRs in the CNS (69). In 1979, Woods et al. built on this finding in a research study in a baboon model that demonstrated a reduction in food intake and weight following intraventricular administration of insulin (70). What remained unknown following those findings was the question of the blood-brain barrier (BBB) – could insulin cross it or not? Do neurons produce their own insulin? These were questions on the minds of many researchers over the course of several decades and a clear answer has still not been uncovered. There has, however, been plenty of research published over the years that has provided a lot of insight into this matter and all the results point to insulin being both transported across the BBB as well as being synthesized within the CNS in a small percentage. In the 1980s, several research groups showed that insulin can indeed cross the BBB by focusing on insulin levels in the cerebrospinal fluid (CSF) in both animal and human studies. Strubbe et al. (71) demonstrated a positive correlation between plasma insulin levels and CSF insulin levels, while Wallum et al. (72)

similarly showed that intravenous insulin administration in humans also causes an increase in CSF insulin levels. These findings did not suggest that insulin could freely cross the BBB. There was a large gradient between plasma and CSF insulin levels that was found to be even greater in the obese (73). The presence of a gradient was suggestive of a saturable transport system that takes the insulin from systemic capillaries, across the choroid plexus, through Virchow-Robin spaces (neuronal perivascular spaces) into glia and neurons (74). This gradient system seems to be a protein similar to, if not identical to, IR itself, which allows for the transport of insulin via a vesicle-mediated system in the brain endothelial cells (75). There are exceptions to this rule, as certain parts of the CNS have fenestrated capillaries that are permeable to compounds of a larger molecular weight – so-called circumventricular organs that include structures such as the pituitary gland, the pineal gland, median eminence and preoptic recess (76). On the other hand, insulin does seem to be synthesized in the brain, at least in small concentrations. This was proven by detecting genes that code insulin precursors within the cortex, subcortical areas, hippocampus, etc. (77) Despite all these findings, there a new questions regarding this topic are still raised in more recent research. Rhea et al. performed an experiment that showed insulin transport is not impaired even when the BBB-related IR is inhibited or deleted (78). Similar to the aforementioned effects of exercise on insulin sensitivity in skeletal muscle, exercise also increases the transport of insulin through the BBB and its binding to cerebral vasculature (79).

The predominant isoform of IR in the CNS is IR-A. The difference between the two isoforms lies in the morphology of the α-subunits. IR can be found throughout the brain, with the highest concentrations seen in the olfactory bulb, cerebellum, cerebral cortex, hypothalamus and hippocampus (80). Similarly, insulin-like growth factor-1 receptor (IGF-1R) is also expressed in numerous areas of the CNS, but mostly in those involved with growth hormone release and regulation (81).

1.3.1. The many roles of insulin in the CNS

One of the most elucidated findings in neuroscientific research into the links between obesity/T2DM/MetS and CNS impairment is the hypothalamic dysregulation of food intake. The key nucleus responsible for food intake regulation is the arcuate nucleus which consists of two antagonistic types of neurons that communicate with neurons in different hypothalamic nuclei (paraventricular, dorsomedial, lateral, ventromedial) where a central reaction to stimuli

from the periphery is integrated into a response to maintain energy and metabolic homeostasis. These arcuate nucleus neurons are orexigenic ones that express neuropeptide Y and agouti-related peptide and anorexigenic ones that express proopiomelanocortin (82). Because of its proximity to the median eminence and fenestrated blood vessels, the activity of the arcuate nucleus is modulated both by insulin and leptin. Development of InR leads to a food intake dysregulation in the hypothalamus, leading to an increase in caloric intake that creates a vicious cycle of InR progression and further hypothalamic dysfunction, therefore potentiating many negative effects InR has not only on peripheral tissues but the CNS as well. As an anorexigenic hormone, insulin's interactions with the hypothalamus contribute to the down-regulation of hepatic glucose production as well, so hypothalamic insulin hyposensitivity might contribute to hyperglycemia in patients with T2DM (83).

As previously mentioned, due to the complexities of its signaling pathways, insulin's effects on many peripheral tissues go beyond the scope of simple glucose uptake through GLUT mobilization. Therefore, neuronal effects of insulin extend to proliferation, differentiation and neuroprotection/neuronal survival. The same has also been observed in glial cells (84). A research study in an oxygen-glucose deprivation model by Mielke JG et al. (85) suggested that neurons maintain levels of membrane IR to prevent ischemia-related cell death. Xu QG et al. showed that even peripheral injured axons had IR "preferentially and intensely expressed (…) just beyond a peripheral nerve crush injury zone" (86). Promotion of brain growth by insulin was noted in several studies (87, 88). Neurotrophic effects have been noted in the hippocampus as well. Lee CC et al. suggested that insulin promotes the translation of an important postsynaptic scaffolding protein through the PI3K/PKB signaling pathway in the CA1 region (89). Finally, insulin protects neurons from oxidative stress and organelle dysfunction, the same factors linked to the development of InR (90, 91).

Since IRs are most densely packed in the synaptic areas, it comes as no surprise that insulin modulates the effects of synaptic transmission, including regulation of neurotransmitter reuptake, ion channel activity and neurotransmitter receptor density (92 – 94). Through the hypothalamus-pituitary gland-peripheral tissue hormonal regulatory axis, insulin also exerts its effects on the secretion of reproductive hormones (95, 96).

1.3.2. The link between InR and neurodegeneration

At the turn of the century, a new term began circulating in the scientific community. It pertained to neurodegenerative processes leading to Alzheimer's disease (AD) following discoveries that typical InR-related dysfunction was present in neurons of AD patients. The scientific community named this type 3 diabetes mellitus (97). AD is a progressive, irreversible, degenerative and metabolic disease affecting the CNS that, broadly speaking, clinically manifests itself with memory impairment and cognitive decline (98). AD biomarkers have also been identified to help make its diagnosis, including amyloid-β (Aβ) and tau protein concentration in the CSF, as well as morphological changes evaluated by positron emission tomography or magnetic resonance imaging (neuronal injury, brain atrophy – volumetric analysis) (99). Similarly to MetS and T2DM, AD represents a large economic burden on healthcare systems worldwide.

As is the case with InR, the process of neurodegeneration is present in cells well before clinical manifestation occurs. On a macroscopic level, patients suffering from AD have varied levels of brain atrophy. This is often accompanied by microvascular and macrovascular ischemic changes (100). AD affects both gray and white matter, which includes medial temporal structures such as the hippocampus (101). On a microscopic level, however, there is an incredibly complex web of dysfunction and structural change, where nosogenic effects such as those observed in InR are coupled with CNS-specific effects, such as amyloid plaque deposition. No part of brain tissue is spared – dendritic spines, synapses, glial cells, brain microvasculature, myelin, etc. The exact trigger that brings about neurodegenerative processes has not been uncovered yet. While there is evidence that certain exogenous factors like chemicals act like neurotoxins (102), and that there is some genetic predisposition (103) that can lead to AD dementia, their involvement does not account for all AD cases. Impaired CNS metabolism is the key factor in the majority of AD cases and all the aforementioned effects seen in InR cells (intracellular lipid accumulation, mitochondrial dysfunction, lipid peroxidation, proinflammatory environment, ER stress) have been observed in neurons. These changes are coupled with an unregulated production of amyloid plaques and their intracellular and extracellular deposition, leading to additional functional impairment and, ultimately, neuronal death.

Amyloid deposits arise from the amyloid precursor protein (APP). It is a transmembrane protein expressed throughout many tissue types, but it has particular relevance in the CNS, where it regulates synaptic function (104), iron metabolism (105), neuronal

plasticity (106), etc. The proteolytic cleavage of APP is performed by a group of secretases. The difference between them is the end product of their action. While α-secretase action leads to a non-amyloidogenic cleavage of APP, β-secretase cleavage represents the initial step in creating neurotoxic Aβ deposits. There is also γ-secretase that further cleaves the protein in both pathways. The final product, Aβ, is a peptide that consists of 38 to 43 amino acids (107). These peptides can exist in a number of different shapes, structures and sizes – as monomers, oligomers, protofibrils and insoluble amyloid fibrils (that aggregate into plaques) (108). They are all seen, in various amounts, throughout the brains of AD patients and the reason for this variety is not fully understood. Initial research into AD pathophysiology suggested that large fibrillary Aβ plaques were the key culprit in neuronal dysfunction and death. This has since been debunked (at least to a certain degree), with the Aβ oligomers now under the magnifying glass. Research suggests that the toxicity of Aβ formations grows larger as the size of the molecule decreases once it reaches critical mass (109). The critical mass theory is further backed by findings that there is an age-dependent increase in Aβ plaques even in patients who do not meet the criteria for neurodegenerative clinical entities such as AD (110). Aβ dimers, specifically, have been found to aggregate into neurotoxic protofibrils (111 - 113). The toxicity of Aβ peptides is multifaceted. It causes synaptic dysfunction due to its ability to bind to several groups of neurotransmitter receptors (glutamate receptors, acetylcholine receptors, β_2-adrenergic receptors), affecting processes such as long-term potentiation (LTP) and depression (LTD) and synaptic vesicle formation (114). It can bind to a number of other proteins involved in crucial signaling pathways, including the IR (115). Aβ peptides have a significant impact on neuronal membrane structure and integrity, as studies have shown that they promote lipid peroxidation, resulting in an increase in reactive oxygen species (116), and that they can directly insert themselves into the membrane and create pores (117), as well as interact with other molecules within the membrane, such as gangliosides (118). This is also associated with mitochondrial dysfunction (119). The process of amyloidogenesis and its effects is depicted in a simplified schematic in Figure 1.2.

Aβ peptides are not the only pathological protein found in neurodegenerative entities. Another crucial protein involved in the disruption of neuronal homeostasis is tau protein. It is created by alternative splicing of the microtubule-associated protein tau. Its pathological form is created following post-translational phosphorylation, creating phosphorylated tau (pTau). This modification is not automatically pathological, as pTau plays an important part in the neuronal cytoskeleton (120). Hyperphosphorylation of tau is seen in pathological states when cytoskeletal proteins' affinity for it begins to decrease, which leads to an accumulation of

pTau, creating so-called neurofibrillary tangles that have been found in patients suffering from multiple neurodegenerative diseases (tauopathies), including AD (120, 121). PTau has a specific, prion-like ability to move from one cell to another, which is something not seen in Aβ peptides. This suggests that a previously healthy neuron can be "infected" with pTau tangles (122). Even though Aβ peptides and pTau do not completely overlap when it comes to the location and timing of appearance, i.e. they do not appear in the same regions of the brain at the same time, which would suggest that the accumulation of these proteins represents two independent processes (123), there is evidence suggesting that the interplay between these two proteins is based on a positive feedback loop (124). That is why Aβ and pTau represent two fundamental biomarkers for AD.

The theory that Aβ peptides, in any form, are the sole driving force behind neurodegeneration in AD patients is not fully accepted. The initial "amyloid cascade hypothesis", first presented in 1992 (125), has recently been questioned. Some are suggesting the possibility that there are other factors that could serve as triggers for AD pathogenesis other than Aβ peptides (126). This is where neuroinflammation and other nosogenic factors come into play, some which are closely related to InR as well. The link between InR and AD has not been fully uncovered yet, specifically whether or not InR can serve as a trigger for Aβ formation or if it simply creates an environment that accelerates the process. An insulin-resistant state has been shown to increase the expression of APP and Aβ peptides, which creates another positive feedback loop, or in other words, another vicious cycle in which Aβ peptide further reduces sensitivity to insulin.
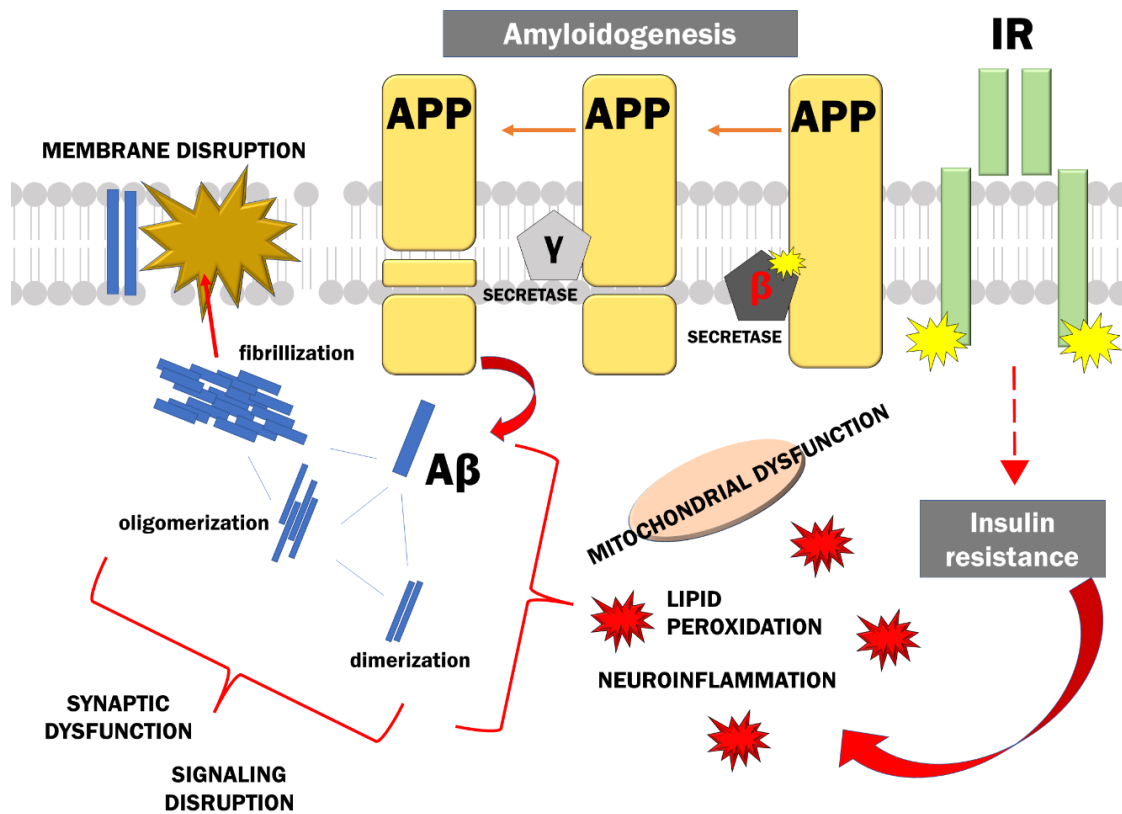
Figure 1.2. A simplified schematic of the pathogenesis and effects of neuronal amyloidogenesis in combination with insulin resistance.

The figure was created by the author based on references (107 - 119).

Aβ = amyloid beta; APP = amyloid precursor protein; IR = insulin receptor.

1.4. The hippocampus

1.4.1. Hippocampal anatomy and physiological properties

Hippocampal circuitry represents one of the most unique neuronal "webs" that is preserved all across the animal kingdom. While the function of this paired structure remains the same, its anatomic location and shape varies from species to species – the same can be said for humans and rodents. The human hippocampus is a C-shaped structure that is located deep within the medial temporal lobe (127). In rodents, even though it is also shaped similarly to the letter C, its location is different. The rodent hippocampus is located more superiorly and posteriorly (taking into account large differences in the brain as a whole), adjacent to the cerebral cortex superiorly and the thalamus inferiorly. The size of the rodent hippocampus compared to its total brain volume is much larger than in humans (128, 129).

There are several distinct regions of the hippocampus: the dentate gyrus (DG), the Cornu Ammonis (CA), that is separated into three unique regions (CA1, CA2 and CA3), and the subiculum. The CA is also often referred to as "hippocampus proper". The entorhinal cortex sends its projections to the DG, which connects to the CA3 region and then the CA3 region connects to the CA1 region. This is the trisynaptic hippocampal pathway. The subiculum then serves as the outgoing connection to the cortex. Entorhinal projections can also enter the hippocampus directly into the CA1 region. Incoming projections also come from other areas in the brain (127). In humans, it is known that the prefrontal cortex, reticular formation, anterior cingulate gyrus and others send projecting neurons to the hippocampus, while outgoing projections can reach areas such as the cingulate cortex, thalamic nuclei and even the contralateral hippocampus (130). In the rat brain, there is a specific differentiation in terms of projections along its dorsoventral axis. A functional study into the rat hippocampus connectivity showed that perirhinal projections are more prominent in the ventral hippocampus, while postrhinal projections are more prominent in the dorsal hippocampus (131). The complexity and relevance of this axis are reflected not only in functional, but also in structural differences – the hippocampal lipidomic profile shows many differences between its ventral and dorsal pole (132). There are also connections between hippocampal regions, such as recurrent (Schaffer) collaterals that run from the CA3 region back to the CA1 region (127). When looking at the fine structure of the hippocampus, it has several layers, the most prominent of those being pyramidal neurons that play the largest role in carrying out the multitude of its functions.

Two features of the hippocampus that are crucial for its physiological functioning are synaptic plasticity and neurogenesis. Synaptic plasticity is the basis of learning, memory and cognition, key functions of the hippocampus that are achieved through LTP and LTD (133). The hippocampus is one of three regions in the CNS with the ability of adult neurogenesis, with the other two being the amygdala and the subventricular zone, which represents cells lining the lateral walls of the lateral ventricles. Adult neurogenesis in the hippocampus is observed in the subgranular zone of the DG (134).

1.4.2. The effects of neurodegeneration and InR on the hippocampus

Neurodegenerative processes affecting the hippocampus manifest themselves clinically as memory impairment and cognitive decline. Amyloid plaques and neurofibrillary tangles appearing in the hippocampus affect its proper functioning and these changes have been well documented over decades of research investigating AD (135 - 137). As was previously mentioned in 1.3.2., an important interplay between InR and neurodegeneration in the context of AD exists, with a vicious cycle present where both components further accelerate each other's progression and exacerbate their consequences. Since the turn of the century, effects of InR on the CNS, including the hippocampus, have become an emerging topic of interest and a slew of research investigating this pathology has been published, especially in rodent models. Results of those studies overwhelmingly confirm that InR affects synaptic plasticity by impairing LTP and LTD and reducing dendritic spine density (138 - 142). InR also affects the integrity of the BBB in the hippocampus (143, 144), impairs adult neurogenesis (145 - 147) and promotes a chronic neuroinflammatory state (148, 149). There is a specific group of research papers describing investigations into locally induced InR. These studies eliminate any effects of systemic metabolic changes indirectly affecting the CNS and they also unequivocally show significant synaptic degeneration and dysfunction, leading to memory impairment and cognitive decline (150 - 153). Part of the reason why the hippocampus is affected by InR and why this state further aggravates the effects of pathological deposits lies in the fact that it is rich in IRs and that insulin represents a crucial regulatory protein that promotes a wide array of functions, including adult neurogenesis (154, 155).

1.5. T2DM pharmacotherapy

A universal pharmacotherapeutic agent for T2DM treatment that successfully regulates plasma glucose levels while ameliorating unwanted consequences of InR and MetS, unfortunately, does not exist. Frederick G. Banting and John J. R. Macleod, who worked in the Institute of Physiology at the University of Toronto first discovered insulin in 1921, for which they received a Nobel Prize in Physiology or Medicine in 1923 (156). Ever since, for over a century now, treatment of T2DM has been evolving. With T2DM prevalence reaching global pandemic levels and the introduction and rise of personalized medicine, T2DM treatment has been focused on an individualized approach that takes into account patients' comorbidities and carefully examines the effectiveness of each pharmacological agent and its side effects (157). The complex nature of finding optimal pharmacotherapy for any individual patient and maintaining satisfactory glycemia is based on balancing the patient's cooperation, their comorbidities (arterial hypertension, underlying kidney disease, micro- and macrovascular complications of atherosclerosis, etc.), temporal dynamics (progression) of the disease and precise monitoring of certain parameters (HbA1C levels, plasma glucose levels, etc.)

Even though T2DM pathogenesis is rooted in the development of receptor resistance to insulin, there are certain indications when insulin can be prescribed to help treat T2DM, usually in patients with newly diagnosed T2DM where compensatory hyperinsulinemia might help correct their glycemic status and in patients that are unable to reach euglycemia with different combinations of oral agents (158).

There are several classes of pharmacological agents used for treating T2DM. Prior to starting treatment with any oral antidiabetic agent, it is necessary to emphasize the importance of conservative treatment methods to get patients to adhere to them (physical exercise, dietary changes, etc.) Once conservative methods are insufficient in maintaining euglycemia, the focus shifts to pharmacotherapy. Metformin is the first treatment of choice in T2DM patients unless contraindicated (severe heart failure, renal failure, hypersensitivity, etc.) (159). If metformin alone is unable to regulate plasma glucose levels and HbA1c levels, another oral antidiabetic agent can and should be added to the treatment plan. All these classes of agents differ based on their mechanism of action and the tissue they primarily act on. Metformin, for example, belongs to the group of biguanides that acts on many organs by causing a metabolic shift – among other effects, it reduces hepatic gluconeogenesis and adipose tissue lipolysis, while inhibiting glucose reabsorption from the gastrointestinal tract (160). Sulfonylureas and

meglitinides are insulin secretagogues, which means that they enhance pancreatic insulin secretion (161). Thiazolidinediones, also known as glitazones, modulate the peroxisome proliferator-activated receptor γ (PPAR-γ) signaling that has a large role in regulating metabolism (162). There are agents that primarily affect the intestinal absorption of carbohydrates, such as α-glucosidase inhibitors (161). A somewhat newer group of pharmacological agents that includes dipeptidyl peptidase-4 (DPP-4) inhibitors and glucagon-like peptide-1 (GLP-1) receptor agonists are related to a group of endogenously secreted proteins called incretins. GLP-1 is one of two incretins that can still be modulated in T2DM in order to achieve insulin secretion stimulation. Common GLP-1 receptor agonists include liraglutide, exenatide and dulaglutide. DPP-4 inhibitors, on the other hand, block the deactivation of incretins by an enzyme of the same name (163). Finally, sodium-glucose co-transporter 2 (SGLT-2) inhibitors act on the kidneys, promoting the secretion of glucose into the urine by blocking its tubular reabsorption (164).

1.5.1. Metformin action in the CNS

As mentioned earlier, metformin is a biguanide that most prominently exerts its effects by changing metabolic pathways in the skeletal muscle, liver and adipose tissue (160). It has been used as a first-line treatment for T2DM for over half a century (165). Not everyone responds to metformin treatment optimally, as lactic acidosis, besides hypoglycemia, is a common and one of the most severe side effects. It occurs because metformin inhibits hepatic mitochondrial respiration which subsequently increases plasma lactate levels (166). A key feature of metformin action is its effect on 5'-AMP-activated protein kinase (AMPK) – it inhibits mitochondrial respiration, therefore decreasing levels of ATP in cells which is a trigger for AMPK activation. Activated AMPK then triggers a shift in metabolism that inhibits gluconeogenesis and increases sensitivity to insulin, among other effects (167, 168).

Metformin can cross the BBB, which is why there have been many research studies to find out if it has positive or negative effects on brain function. In terms of neurodegenerative entities, such as AD, several animal model studies showed positive effects. In a C57/129J mice model, Wang et al. demonstrated that metformin enhances neurogenesis in several investigated areas of the brain, including the hippocampus, which translated to an enhancement in spatial memory (169). Correia et al. investigated oxidative stress in diabetic GK rats and showed significant decreases in several oxidative stress-related compounds, as

well as significant increases in several antioxidants following metformin treatment (170). When observing the hippocampus specifically, Hwang et al. used obese Zucker rats to demonstrate that metformin ameliorates T2DM effects of halted cell proliferation and neuroblast differentiation (171). Metformin effects extend to Aβ and pTau deposits – studies using mice models treated with metformin showed a reduction in Aβ plaques (172), while tau phosphorylation was inhibited and transmission of pTau halted by means of autophagy (172, 173). Clinical studies correlate well with findings from animal studies. A Taiwanese study conducted by Hsu CC et al. concluded that metformin therapy (in combination with sulfonylureas) decreases non-vascular dementias in T2DM patients (174), with several other clinical studies backing this finding (175, 176). These findings, while valid, still do not place metformin in the driver's seat for AD prevention. Imfeld et al. and Kuan et al. published results of clinical studies that suggested an increased risk of AD following chronic metformin treatment (177, 178).

1.5.2. Liraglutide action in the CNS

Similarly to metformin, liraglutide's mechanism of action is based on modulating signaling pathways that somewhat overlap with insulin signaling, affecting proteins such as PKB, PKC, MAPK and PI3K (179). It is a GLP-1 analogue and by stimulating insulin secretion in such a manner, there is little risk of hypoglycemic events. It has also been shown to affect the gastrointestinal system by delaying gastric emptying and reducing appetite (180). There has recently been growing interest in the usage of liraglutide as a weight-loss agent as well (181).

An important benefit of liraglutide is that it can cross the BBB and is not affected by DPP-4 (182). GLP-1 receptors are distributed throughout the brain, including the hippocampus (183). AD research showed that liraglutide has numerous positive effects on neuronal homeostasis, both in animal and clinical studies. A study using a mixed murine model of AD and T2DM, focusing on the brain as a whole with a specific interest in the hippocampus, showed that liraglutide treatment ameliorated metabolic changes in the brain due to T2DM, limited neuronal loss, decreased neuroinflammation and positively affected Aβ and pTau accumulation, which ultimately translated to an improvement in cognitive function (184). Similar findings were observed in another study, where β-amyloid plaque count in the mouse cortex was cut almost in half. This study also demonstrated a positive effect of

liraglutide on synaptic integrity and neurogenesis (185). Edison et al. performed a large clinical trial and concluded that liraglutide treatment improves cognitive function and total brain volume in AD patients (186).

Since multiple studies overwhelmingly show favorable implications of metformin and liraglutide in the CNS in both models of InR and AD, a lipidomic analysis of rat hippocampi fed with a diet enriched with fats and carbohydrates and treated with these two pharmacotherapeutics can give a more specific insight into structural and functional changes of this incredibly important structure that is arguably the epicenter of neurodegenerative changes.

2. HYPOTHESIS

A diet enriched with fats and carbohydrates, as well as early metformin and liraglutide treatment, cause sex-specific changes in the hippocampal lipidome of adult Sprague Dawley rats.

3. AIMS

The research aims were:

- To perform a sex-specific immunohistochemical analysis of all animal group hippocampi to determine expression levels of common neuronal gangliosides and InR-related proteins and to determine spatial differences in their expression.

- To carry out a sex-specific analysis of the hippocampal lipidome in all animal groups using MALDI-TOF (matrix-assisted laser desorption/ionization time-of-flight) mass spectrometry and to identify the differences in lipid expression between all groups.

4. MATERIALS AND METHODS

4.1. Research design

The research was structured as a paired research, comparing the following groups of adult Sprague Dawley rats:

- rats on a standard diet (SD) with rats on a high-fat high-sugar diet (HFHSD);
- rats on a HFHSD with rats on a HFHSD treated with metformin (HFHSD-M);
- rats on a HFHSD with rats on a HFHSD treated with liraglutide (HFHSD-L);
- males of all groups with females of all groups.

4.2. Materials

The research was carried out on hippocampal tissue of Sprague Dawley rats (*Rattus norvegicus*), commonly used as an animal model for investigations into InR and MetS (187). Rats included in this research are part of the research project "*The role of oxidative stress in development of impaired vascular response in obese pre-diabetic elderly rats of both sexes treated with metformin or liraglutide",* which was approved by the Ethics committee of the Faculty of Medicine, J. J. Strossmayer University of Osijek on Dec 16th, 2016, class: 602-04/16-08/15, no: 2158-61-07-16-143. It was carried out at the Department for Medical Biology and Genetics at the Faculty of Medicine, J. J. Strossmayer University of Osijek and the Department for Clinical Chemistry at Clinical Hospital Centre Osijek.

4.2.1. Animal model

64 Sprague Dawley rats (32 males, 32 females), 45 weeks of age, were separated into four sex-specific groups of 16 (eight males and eight females per group):

1. control group on a SD;
2. HFHSD group;
3. HFHSD-M group;
4. HFHSD-L group.

The experiment design was replicated from project RECOOP #029 2015-2021: "Obesity & Diabetes". The experiment lasted for 20 weeks. It was initiated once the rats reached 45 weeks of age. Firstly, a six-week change in diet was introduced to groups 2, 3 and 4 to induce obesity and InR. Pertinent changes in diet included an increase in carbohydrate share from 51% to 61.5%, an increase in unprocessed fat share from 4% to 12.06% and a decrease in raw protein share from 20% to 9.25%, while the overall energy value increased from 2842.266 kcal/kg to 3879.495 kcal/kg. The detailed composition of these diets is shown in Figure 4.1 and Figure 4.2. Following the six-week change in diet, a 14-week period of antidiabetic drug treatment began, with rats in group 3 treated with metformin (s.c., 50 mg/kg/day, manufacturer: Sigma-Aldrich, St. Louis, MO, USA) and rats in group 4 treated with liraglutide (s.c., 0.3 mg/kg/day; manufacturer: Creative Peptides, Shirley, NY, USA).

In order to confirm hyperglycemia and the development of T2DM/InR, all rats were subjected to oral glucose tolerance tests (OGTT) performed at three separate points during the experiment. The first OGTT was performed before the start of the experiment, the second one was performed five weeks into the experiment and the third and final OGTT was performed at the end of the experiment. Food was removed from the cages the night before the test. The following morning, fasting plasma glucose level was measured by sampling blood from a rat tail vein. A 25% glucose solution was then prepared and administered intraperitoneally (2 mg of glucose solution/grams of body mass). The second blood sampling was performed 2 hours after administering the glucose solution.

A total of 14 rats expired prior to the end of the experiment. The number of rats per group that reached the end of the experiment whose hippocampal tissue was used for immunohistochemical and spectrometric analysis were, as follows: 8 males and 7 females in the SD group, 7 males and 5 females in the HFHSD group, 7 males and 8 females in the HFHSD-M group, and 5 males and 3 females in the HFHSD-L group. All rats included in the experiment were terminated after reaching 65 weeks of age (Figure 4.3.)
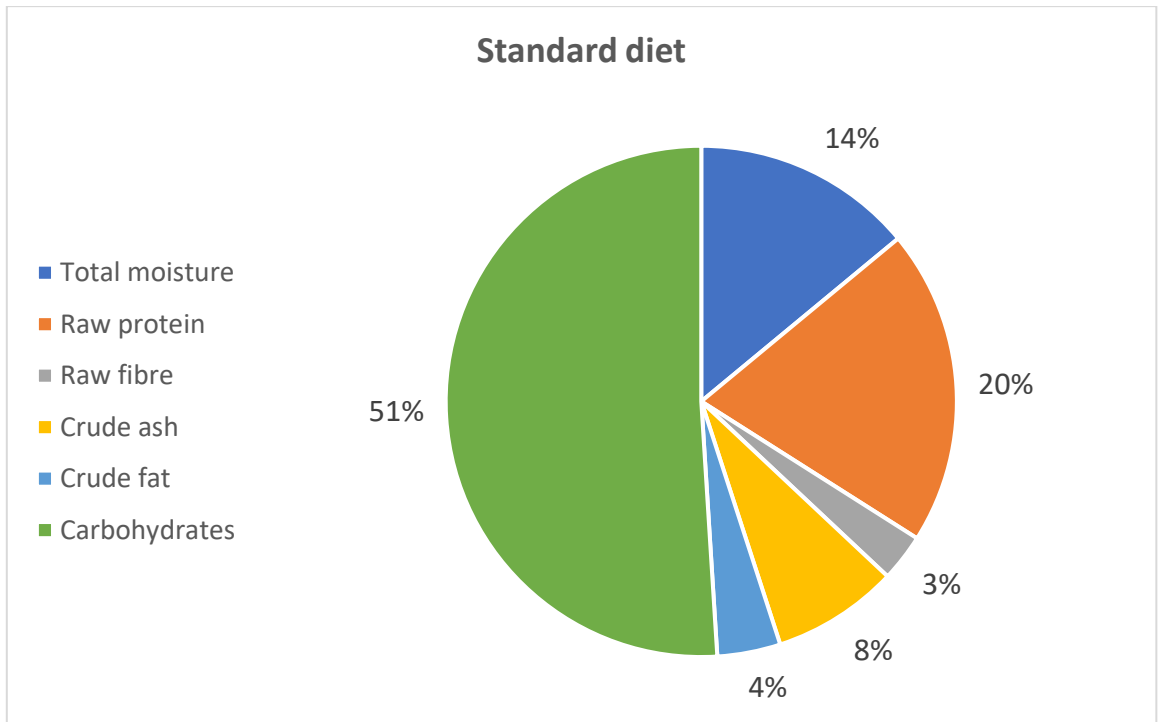
Figure 4.1. Composition of the standard diet.
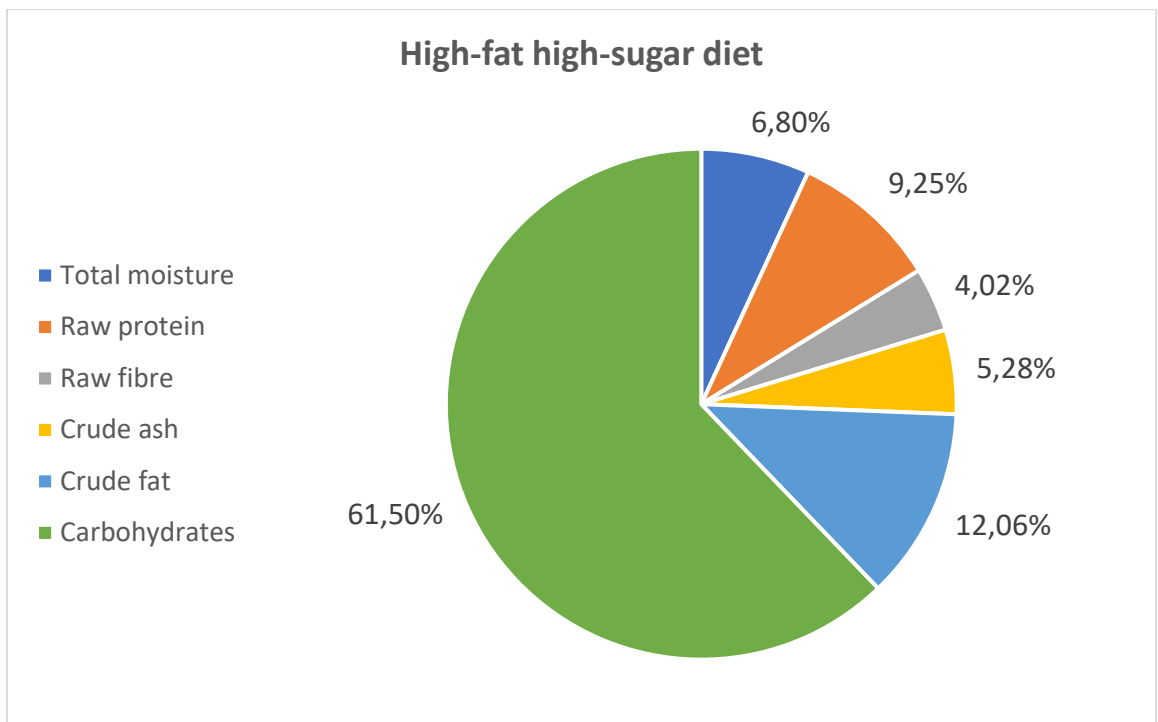
Figure 4.2. Composition of the high-fat high-sugar diet.
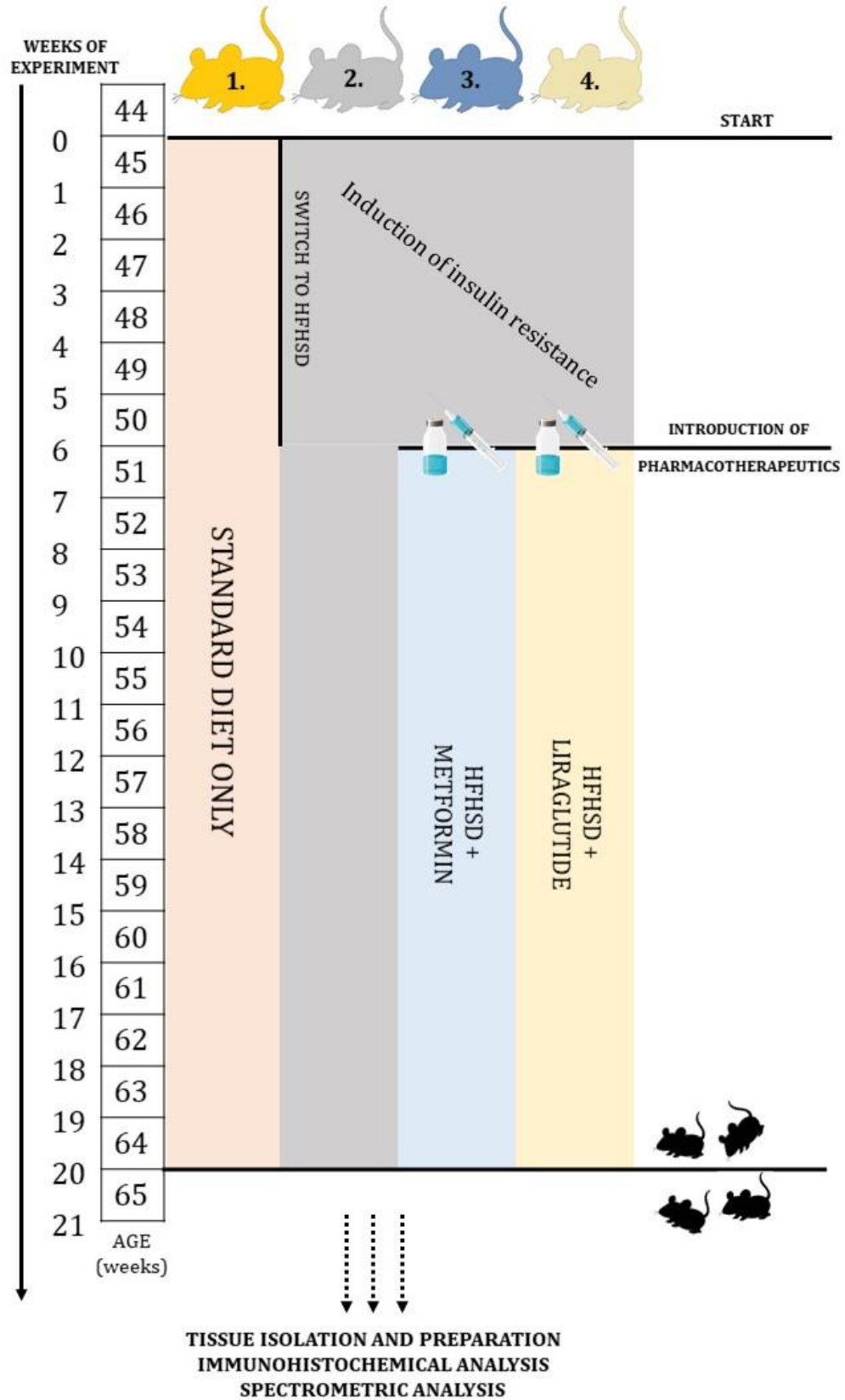
Figure 4.3. A schematic of the experiment design and chronology.

HFHSD = high-fat high-sugar diet.

4.3. Methods

Once the rats were terminated, brain tissue was isolated and halved in the sagittal plane in order to perform free-floating immunohistochemical analysis and spectrometric analysis using MALDI-TOF technology.

4.3.1. Immunohistochemistry

A group-specific and sex-specific immunohistochemical analysis of the hippocampi was performed to analyse and compare the expression of the four commonly expressed gangliosides in neuronal membranes and myelin sheaths (GM1, GD1a, GD1b and GT1b) and proteins relevant to the pathogenesis of InR (IR, IGF-1R, APP and pTau).

Tissue halves used for immunohistochemical analysis were fixed in a 4% paraformaldehyde solution for a 48-hour period, then cryoprotected using 10%, then 20%, and finally 30% sucrose solutions. This was followed by freezing of tissue samples, briefly dipping them in cooled isopentane. Samples were then stored at -80°C until analysis. Once added to a tissue freezing medium (Tissue Freezing Medium; Leica, Nussloch, Germany), samples were cut by cryostat (Cryostat CM3050S; Leica, Nussloch, Germany) in the coronal plane to 25 μm thick slices.

Free-floating method of immunohistochemical analysis was used to stain the slices using specific primary antibodies for the epitopes of the aforementioned gangliosides and proteins, detailed in Tables 4.1. and 4.2. Primary antibodies for the included gangliosides were kindly provided as a donation from Professor Ronald L. Schnaar, Ph.D. from Johns Hopkins University School of Medicine in Baltimore, MD, USA, manufactured at the Department of Pharmacology and Molecular Sciences. Visualization of selected antigen-antibody complexes was accomplished using avidin-biotin complex (ABC) conjugated with horseradish peroxidase (HRP) (Vector Laboratories, Burlingame, CA, USA, cat. no. PK-6100) and 3, 3'-diaminobenzidine (DAB) (Vector Laboratories, Burlingame, CA, USA, cat. no. SK-4100) as the HRP substrate, which results in a change of color.

Table 4.1. Primary antibodies used in free-floating immunohistochemical analysis of gangliosides in rat hippocampi.

Primary antibody	Antibody Class	Origin animal	Manufacturer	Dilution
GM1 ganglioside	IgG	Mouse	The Department of Pharmacology and Molecular Sciences, The Johns Hopkins University School of Medicine, Baltimore, USA	1:1,000
GD1a ganglioside	IgG	Mouse		1:10,000
GD1b ganglioside	IgG	Mouse		1:1,000
GT1b ganglioside	IgG	Mouse		1:4,000

Table 4.2. Primary antibodies used in free-floating immunohistochemical analysis of proteins in rat hippocampi.

Primary antibody abbreviation	Primary antibody	Antibody class	Origin animal	Manufacturer	Dilution
IR	Anti-Insulin receptor alpha	IgG, polyclonal	rabbit	Santa Cruz Biotechnology, Dallas, TX, USA, SC-710	1:500
IGF-R1	Anti-Insulin-like growth factor-receptor 1 beta	IgG, polyclonal	rabbit	Santa Cruz Biotechnology, Dallas, TX, USA, SC-713	1:250
APP	Anti-Amyloid-beta precursor protein	IgG, polyclonal	rabbit	Abcam, Cambridge, MA, USA, ab32136	1:1,000
pTau	Anti-Phosphorylated tau protein	IgG, polyclonal	rabbit	Abcam, Cambridge, MA, USA, ab131354	1:500

The protocol for immunohistochemical staining of hippocampal tissue slices was, as follows:

- Pre-treatment with 1% solution of hydrogen peroxide for 30 minutes at 4°C on a shaker in order to saturate endogenous peroxidases;

- Incubation of slices with a blocking buffer (5% goat serum and 1% bovine serum albumin (BSA) prepared in phosphate buffered saline (PBS), 1 × PBS: 137 mM NaCl, 2.7 mM KCl, 10 mM NaH_2PO_4, 1.8 mM KH_2PO_4) for 2 hours on a shaker to prevent non-specific secondary antibody binding;

- Slice transfer into primary antibody solutions that were prepared with a blocking buffer;

- Overnight incubation at 4°C;

- Slice washing using 1× PBS for 10 minutes;

- Incubation in a solution containing appropriate, biotin-conjugated secondary antibodies for 4 hours at 4°C on a shaker (biotinylated goat anti-mouse IgG (Jackson Immunoresearch Laboratories, Philadelphia, PA, USA, cat. no. 115-065-166) or biotinylated goat anti-rabbit IgG (Jackson Immunoresearch Laboratories, Philadelphia, PA, USA, cat. no. 111-065-144));

- Slice washing using 1× PBS for 10 minutes;

- Slice incubation with ABC conjugated with HRP for 2 hours at 4°C on a shaker;

- Slice washing using 1× PBS for 10 minutes;

- Adding slices to a solution containing DAB at room temperature for 4 minutes, allowing for the visualization of proteins detected by specific antibodies;

- Transfer of slices to a solution of 1× PBS to stop the reaction between HRP and DAB.

The next steps were microscopy, photography and analysis. The slices were slide-mounted and coverslipped using Vectamount (Vector Laboratories, Burlingame, CA, USA, cat. no. H-5000). Using a digital camera (Olympus D70; Olympus, Hamburg, Germany) set up on a microscope (Zeiss Axioskop 2 MOT; Carl Zeiss Microscopy, Thornwood, NY, USA), the slices were photographed under a 40× objective and uploaded (DP Manager, v. 1.2.1.107., DP Controller v. 1.2.1.108). Analysis of the acquired digital micrographs for expression of aforementioned gangliosides and proteins was performed using the computer software Fiji (188).

Using a rat brain atlas (189), the anatomical regions of interest (ROI) were identified – the DG, the CA1 region and the CA3 region, as shown in Figure 4.4. Due to the inability to precisely delineate and identify the CA2 region to confidently interpret results, it was excluded from the analysis.
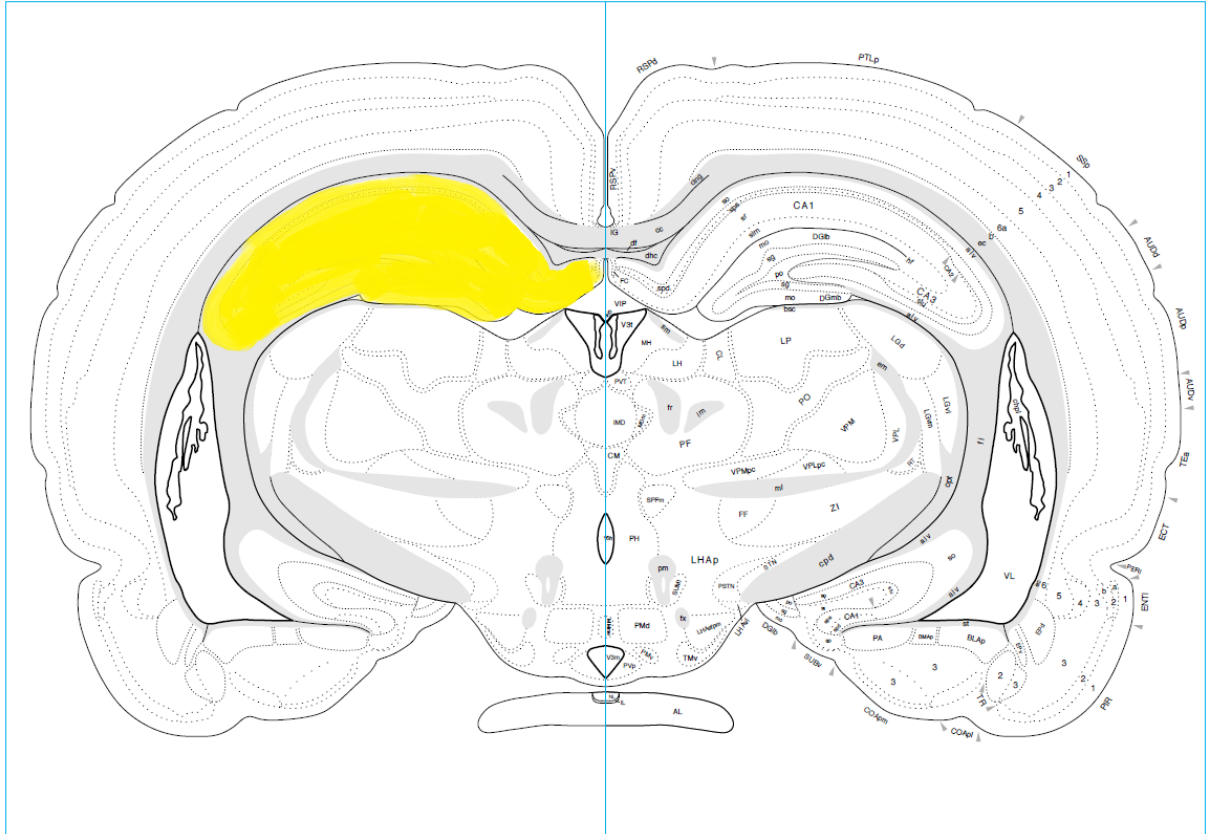
Figure 4.4. Location of the hippocampus (in yellow) within the rat brain, coronal plane. *Modified image from an open-access Sprague Dawley rat brain atlas (available at http://www.larryswanson.com)*

The image analysis protocol for tissue samples specifically immunostained for aforementioned gangliosides and proteins using the computer software Fiji was, as follows:
- micrographs were converted to 8-bit images;
- using ROI Manager, an area of 22 500 µm2 (correspondent to 2,073,600 pixel^2) was selected for analysis (ROI) and Raw Integrated Density Value (IDV) was measured;

- the value of immunopositive reaction was presented as positively correlated integrated colour density (measured Raw IDV was subtracted from maximal IDV, which corresponds to the total pixel number of a ROI multiplied with 255), minus the average IDV value of negative controls.

4.3.2. MALDI-TOF spectrometry

In order to perform the spectrometric analysis, hippocampal tissue was homogenized, followed by lipid extraction. The two-phase extraction of lipids was performed using the Bligh and Dyer method (190). The protocol for spectrometric analysis sample preparation was, as follows:

- Tissue homogenization in a 20 mM ammonium acetate buffer (pH = 8,1), using an ultrasonic homogenizer (Bandelin Sonopuls 2070) for 15 seconds per sample at 100 % amplitude;
- Centrifugation of homogenates for 12 minutes at 1000 g at 4°C;
- Extraction of 160 µL of the supernatant for the two-phase extraction of lipids;
- Adding 400 µL of methanol and 200 µL of chloroform to the 160 µL of samples;
- Solution vortexing and resting for 10 minutes at room temperature;
- Adding an additional 200 µL of chloroform and 200 µL of distilled water to the solutions;
- Solution vortexing for 5 seconds;
- Centrifugation of solutions for 20 minutes at 14000 g at 4°C, allowing for the differentiation of the upper, polar phase and lower, non-polar phase;
- Separation of the polar and non-polar phases in respective amber glass vials;
- Solution evaporation, performed using Techne Dri-Block DB 200/3 heater with nitrogen stream at 45°C;
- Upon solvent evaporation samples were stored at -80 °C until usage;
- Samples were redissolved in 50 ul of methanol prior to use.

All solvents used in extraction and imaging protocol were minimum HPLC grade.

Spectrometric analysis was performed using the Bruker ultrafleXtreme MALDI-TOF/TOF mass spectrometer (Bruker Corporation, Billerica, Massachusetts, USA). In order to perform the analysis, 5 µL of sample solutions were mixed with 5 µL of a matrix solution –

10 mg/mL 2,5-dihydroxybenzoic acid (Sigma-Aldrich, St. Louis, MO, USA) for the positive phase and 10 mg/mL 9-aminoacridine (Merck) for the negative phase. 3 µL of the sample/matrix solutions were then placed on ground steel sample. Samples were imaged in the positive and negative mode in the range of 500 Da - 2500 Da.

Machine settings for imaging at Bruker UltrafleXtreme MALDI-TOF/TOF MS (Bruker, Billerica, MA, USA) were identical for positive and negative modes. The sample rate and digitizer were set at 5.00 GS/s, Smartbeam (laser) set to medium, laser frequency 2000 Hz, laser power 90%, 200 shots/pixel, and every measurement was a sum of 15000 shots.

Calibration in positive mode was done with Leucine-Enkephalin (Sigma-Aldrich, Saint Louis, MO, USA) and Bruker Peptide calibration mix (Bruker, Billerica, MA, USA). Calibration in negative mode was done with red phosphorus clusters (Sigma-Aldrich, Saint Louis, MO, USA).

The analysis and data extraction were performed in Bruker Flex Analysis software (Bruker, Billerica, MA, USA) with the following adjustments: Peak detection algorithm was *Snap; s/n threshold* was 6, Smoothing Algorithm was *SavitzkyGolay* (width 0.2 m/z, cycles 1), Baseline subtraction was done with *TopHat.* m/z ratios with an intensity < 1% compared to the signal with highest intensity were not used in further analysis.

R statistical software (Vienna, Austria) was used for the statistical analysis of the spectrum data with the following libraries: *matrixTests, roperators, FELLA, KEGGREST, igraph, magrittr, resample* (191, 192). Affected metabolic pathways were identified through the aforementioned software using the Human Metabolome Database (193) and the Kyoto Encyclopaedia of Genes and Genomes (KEGG) (194) and compared between analyzed groups.

4.4. Statistical analysis

Statistical analysis was performed using the software IBM SPSS Statistics (release 26.0.0.0, SPSS Inc., Chicago, IL, USA). Statistical significance level was set at $P < 0.05$.

Presented numerical variables showed normal distribution and were expressed as means and standard deviations. Paired samples t test and repeated measures ANOVA were used for variable comparisons between different groups and measurements. For significance analysis of between-group comparisons in the immunohistochemical analysis to determine the

influence of sex, intervention or their interaction, two-way ANOVA was applied. Post hoc analysis was performed following Levene's test for variance equality assessment. Because equal variances were not assumed, Tukey's post hoc test was used for the analysis.

5. RESULTS

5.1. Plasma glucose levels

In order to validate the animal model of the study, an OGTT was performed at three separate points during the experiment for analysis of each group's glycemic status. Female rats in the HFHSD-L group were not subjected to the third and final OGTT due to the fact that their general physical status was very poor.

The results of the three OGTTs, presented in Table 5.1, show increases in plasma glucose levels at the 2-hour mark in all groups on a HFHSD when compared to the SD group. The third OGTT showed decreases in plasma glucose levels at the 2-hour mark in rats of both sexes treated with metformin and male rats treated with liraglutide. Using the repeated measures ANOVA test (sphericity not assumed, Greenhouse-Geisser estimate), specific pairwise comparisons were made in order to demonstrate the biggest changes in plasma glucose levels following administration of the glucose solution (Table 5.2). There were no significant changes in plasma glucose levels in the SD groups of both sexes, with the exception being the comparison of the first and third OGTT in female rats. Comparison of the second and third OGTT, relevant to determine the effects of pharmacotherapy, showed statistically significant reductions in plasma glucose levels at the 2-hour mark in HFHSD-M and HFHSD-L groups of male rats, while significance was not reached in the comparison of the aforementioned tests in HFHSD-M female rats.

Table 5.1. Results of oral glucose tolerance tests measured at three points during the experiment and differences between measured plasma glucose levels ($P < 0.05$)

Sex	Group	OGTT 1 Fasting	OGTT 1 At 2 hours	t[†] (P)	OGTT 2 Fasting	OGTT 2 At 2 hours	t (P)	OGTT 3 Fasting	OGTT 3 At 2 hours	t (P)
		Plasma glucose, mmol/L*			Plasma glucose, mmol/L			Plasma glucose, mmol/L		
male	SD	5.8 (0.4)	9.1 (5)	-1.706 (0.14)	6.3 (1.1)	15 (4)	-4.848 (0.003)	5.2 (0.8)	15.3 (4.3)	-5.392 (0.002)
	HFHSD	4.3 (0.4)	10.3 (4.6)	-3.372 (0.02)	6 (0.6)	27 (7.9)	-6.807 (0.001)	7 (0.8)	12 (4.4)	-2.534 (0.05)
	HFHSD-M	3.3 (0.4)	8.6 (5.7)	-2.543 (0.04)	6 (0.9)	20.9 (5.6)	-8.045 (< 0.001)	4.5 (0.8)	12 (3.1)	-7.821 (< 0.001)
	HFHSD-L	4.2 (1.3)	11.5 (4.4)	-3.703 (0.01)	5.5 (1.1)	24.5 (7.6)	-5.672 (0.002)	5.2 (0.4)	14.4 (5.7)	-3.85 (0.01)
female	SD	5.1 (0.6)	7.3 (1.2)	-4.651 (0.004)	4.6 (0.6)	10.1 (5.9)	-2.475 (0.05)	6.4 (0.4)	14.9 (4.5)	-4.867 (0.003)
	HFHSD	5 (0.6)	7.1 (1)	-3.728 (0.01)	5 (0.8)	9.6 (3)	-2.98 (0.03)	5.6 (1)	15 (9.7)	-2.437 (0.06)
	HFHSD-M	4.6 (3.9)	6.2 (2)	-1.592 (0.15)	5.1 (1.6)	16.2 (7.9)	-4.563 (0.003)	4.8 (0.6)	11.1 (3.6)	-4.483 (0.003)
	HFHSD-L	6.2 (0.9)	21.9 (11.4)	-3.424 (0.02)	4.9 (0.6)	18.8 (9.1)	-3.789 (0.01)	/	/	/

HFHSD = high fat high sugar diet; HFHSD-L = high fat high sugar diet treated with liraglutide; HFHSD-M = high fat high sugar diet treated with metformin; OGTT = oral glucose tolerance test; SD = standard diet. * mean (standard deviation); [†] paired samples t test.

Table 5.2. Pairwise comparisons of plasma glucose level means from three oral glucose torelance tests ($P < 0.05$)

Sex	Group	Repeated measures ANOVA		Mean difference[†] (P)		
		F value (df)	P*	OGTT 1 vs OGTT 2	OGTT 2 vs OGTT 3	OGTT 1 vs OGTT 3
				Plasma glucose (mmol/L) at 2 hours		
male	SD	4.383 (2, 12)	0.04	-5.9 (0.1)	-0.3 (> 0.9)	-6.2 (0.19)
	HFHSD	25.7 (2, 10)	0.003	-16.7 (0.003)	14.9 (0.02)	-1.7 (0.78)
	HFHSD-M	22.539 (2, 14)	0.001	-12.3 (< 0.001)	8.8 (0.01)	-3.4 (0.56)
	HFHSD-L	14.016 (2, 10)	0.002	-13 (0.01)	10.1 (0.05)	-2.9 (0.76)
female	SD	10.594 (2, 12)	0.003	-2.8 (0.54)	-4.8 (0.1)	-7.6 (0.005)
	HFHSD	4.565 (2, 10)	0.08	-2.5 (0.13)	-5.5 (0.31)	-7.9 (0.24)
	HFHSD-M	7.16 (2, 14)	0.02	-10 (0.03)	5.1 (0.49)	-4.9 (0.03)
	HFHSD-L	/	/	/	/	/

df = degrees of freedom; HFHSD = high fat high sugar diet; HFHSD-L = high fat high sugar diet treated with liraglutide; HFHSD-M = high fat high sugar diet treated with metformin; OGTT = oral glucose tolerance test; SD = standard diet. *Greenhouse-Geisser estimate; †Bonferroni correction.

5.2. Immunohistochemical analysis

A sex-specific immunohistochemical analysis of selected gangliosides and proteins was performed for all animal groups in the three ROIs. Results are presented for each analyzed epitope separately, with presented images of acquired stains, each individually sized 150 μm x 150 μm, organized by ROI, sex and group.

5.2.1. Expression of common gangliosides

A two-way ANOVA analysis revealed that sex, animal group and their interaction all had statistically significant differences in IDV means for GM1 in all three ROI (Table 5.3, 5.6 and 5.9). Male rats overall had higher IDV means than females, more notably in the DG and CA3 region.

The CA1 region, however, showed little immunoreactivity. There was no immunoreactivity in the HFHSD and HFHSD-M groups of both sexes, with very little immunoreactivity in the SD group. The largest difference in immunoreactivity was in the HFHSD-L group in male rats, suggesting an effect of liraglutide on the expression of GM1 in this specific ROI (Table 5.7, 5.8).

The effects of liraglutide on the expression of GM1 in male rats were further observed in the DG and CA3 region. While there was no significant difference in IDV mean values between the SD group and HFHSD group, there were sex-specific differences between the two HFHSD-L groups as well as differences between the male HFHSD and HFHSD-L groups in both ROI, demonstrating an increase in GM1 expression following liraglutide treatment (Table 5.4, 5.5, 5.10, 5.11).

Metformin, on the other hand, did not significantly alter the expression of GM1 in any of the groups.

Images of the acquired stains are shown in Figure 5.1.
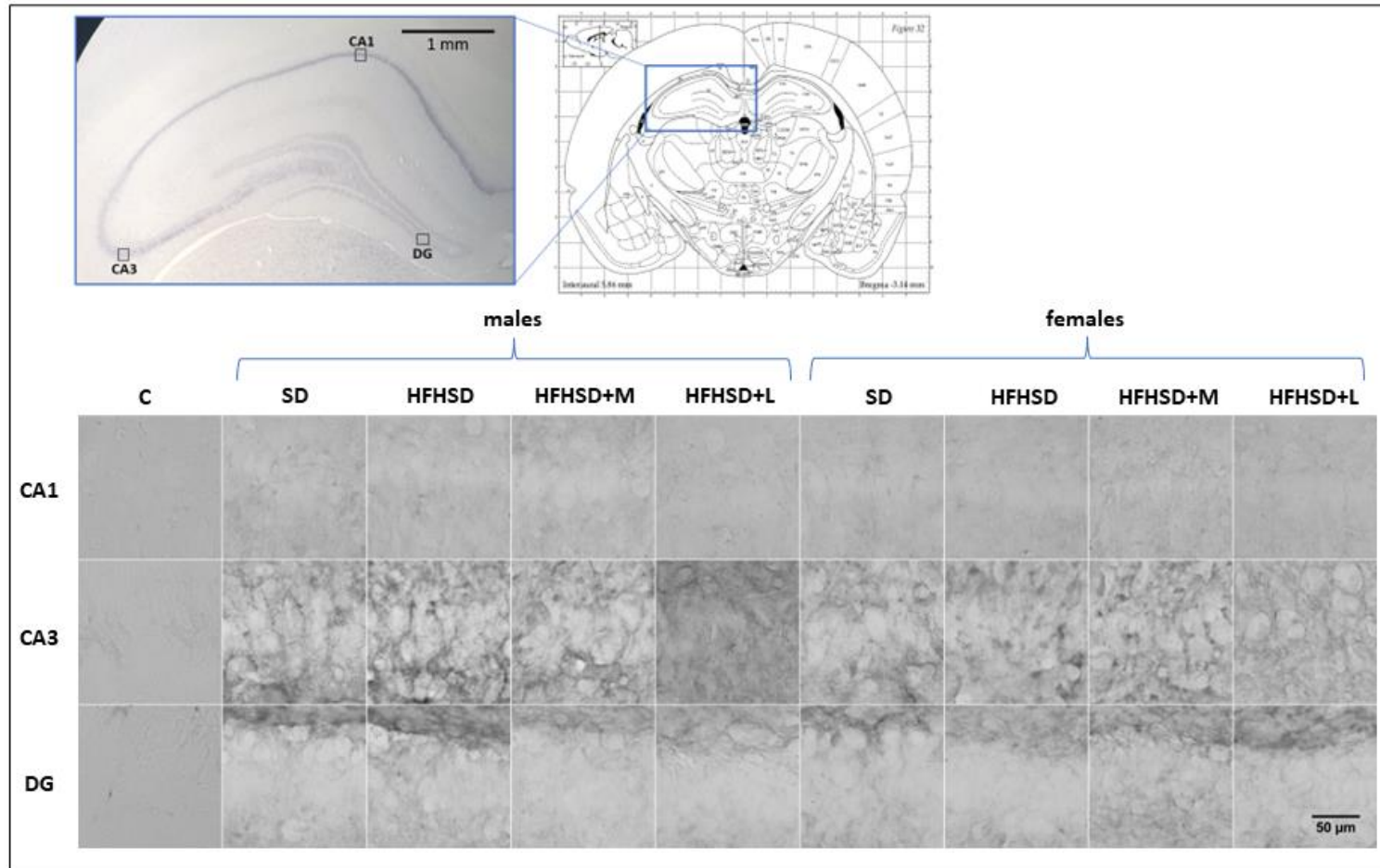
Figure 5.1. Expression of ganglioside GM1 in all animal group hippocampi, organized by region of interest, sex and group. C – negative control; CA1 – Cornu Ammonis region 1; CA3 – Cornu Ammonis region 3; DG – dentate gyrus; HFHSD – high-fat high-sugar diet; HFHSD+L – HFHSD treated with liraglutide; HFHSD+M – HFHSD treated with metformin; SD – standard diet.

Table 5.3. Integrated density values for the GM1 ganglioside in the dentate gyrus

Variable	IDV mean	Two-way ANOVA	
		F value (df)	*P*
Sex			
Male	2.18×10^7	51.708 (1, 116)	**< 0.001**
Female	3.74×10^6		
Group			
SD	1.33×10^7		
HFHSD	9.05×10^6	14.806 (3, 116)	**< 0.001**
HFHSD+M	3.18×10^5		
HFHSD+L	2.55×10^7		
Interaction	-	11.261 (3, 116)	**< 0.001**

df = degrees of freedom; HFHSD = high-fat high-sugar diet; HFHSD+L = high-fat high-sugar diet treated with liraglutide; HFHSD+M = high-fat high-sugar diet treated with metformin; IDV = integrated density value; SD = standard diet.

Table 5.4. Group-specific pairwise comparisons of integrated density values for the GM1 ganglioside in the dentate gyrus

Compared groups	IDV difference mean[*]	*P*[†]
SD vs HFHSD	3.68×10^6	0.73
SD vs HFHSD+M	9.29×10^6	**0.005**
SD vs HFHSD+L	-1.37×10^7	**< 0.001**
HFHSD vs HFHSD+M	5.61×10^6	0.41
HFHSD vs HFHSD+L	-1.74×10^7	**< 0.001**
HFHSD+M vs HFHSD+L	-2.3×10^7	**< 0.001**

HFHSD = high-fat high-sugar diet; HFHSD+L = high-fat high-sugar diet treated with liraglutide; HFHSD+M = high-fat high-sugar diet treated with metformin; IDV = integrated density value; SD = standard diet; *estimated marginal means; †Tukey's post hoc HSD.

Table 5.5. Relevant group-specific and sex-specific pairwise comparisons of integrated density values for the GM1 ganglioside in the dentate gyrus

Compared groups	IDV difference mean[*]	$P^{\dagger}$
M - SD vs M - HFHSD	5.33×10^6	0.97
M - SD vs F - SD	1.61×10^7	**0.03**
M - HFHSD vs M - HFHSD+M	1.22×10^7	0.26
M - HFHSD vs M - HFHSD+L	-2.99×10^7	**< 0.001**
M - HFHSD vs F - HFHSD	1.39×10^7	0.13
M - HFHSD+M vs F - HFHSD+M	1.32×10^6	> 0.9
M - HFHSD+L vs F - HFHSD+L	4.08×10^7	**< 0.001**
F - SD vs F - HFHSD	3.11×10^6	> 0.9
F - HFHSD vs F - HFHSD+M	-4.47×10^5	> 0.9
F - HFHSD vs F - HFHSD+L	-3.09×10^6	> 0.9

F = female; HFHSD = high-fat high-sugar diet; HFHSD+L = high-fat high-sugar diet treated with liraglutide; HFHSD+M = high-fat high-sugar diet treated with metformin; IDV = integrated density value; M = male; SD = standard diet; [*]estimated marginal means; [†]Tukey's post hoc HSD.

Table 5.6. Integrated density values for the GM1 ganglioside in the Cornu Ammonis 1 region

Variable	IDV mean	Two-way ANOVA	
		F value (df)	P
Sex			
Male	5.31×10^6	16.822 (1, 114)	**< 0.001**
Female	8.56×10^4		
Group			
SD	3.13×10^5		
HFHSD	2.23×10^3	17.942 (3, 114)	**< 0.001**
HFHSD+M	7.858×10^{-7}		
HFHSD+L	1.05×10^7		
Interaction	-	17.219 (3, 114)	**< 0.001**

df = degrees of freedom; HFHSD = high-fat high-sugar diet; HFHSD+L = high-fat high-sugar diet treated with liraglutide; HFHSD+M = high-fat high-sugar diet treated with metformin; IDV = integrated density value; SD = standard diet.

Table 5.7. Group-specific pairwise comparisons of integrated density values for the GM1 ganglioside in the Cornu Ammonis 1 region

Compared groups	IDV difference mean[*]	P[†]
SD vs HFHSD	3.18×10^4	> 0.9
SD vs HFHSD+M	3.2×10^5	> 0.9
SD vs HFHSD+L	-9.55×10^6	**< 0.001**
HFHSD vs HFHSD+M	2.48×10^3	> 0.9
HFHSD vs HFHSD+L	-9.87×10^6	**< 0.001**
HFHSD+M vs HFHSD+L	-9.87×10^6	**< 0.001**

HFHSD = high-fat high-sugar diet; HFHSD+L = high-fat high-sugar diet treated with liraglutide; HFHSD+M = high-fat high-sugar diet treated with metformin; IDV = integrated density value; SD = standard diet; *estimated marginal means; †Tukey's post hoc HSD.

Table 5.8. Relevant group-specific and sex-specific pairwise comparisons of integrated density values for the GM1 ganglioside in the Cornu Ammonis 1 region

Compared groups	IDV difference mean[*]	P[†]
M - SD vs M - HFHSD	5.24×10^5	> 0.9
M - SD vs F - SD	4.3×10^5	> 0.9
M - HFHSD vs M - HFHSD+M	4.47×10^3	> 0.9
M - HFHSD vs M - HFHSD+L	-2.07×10^7	**< 0.001**
M - HFHSD vs F - HFHSD	4.47×10^3	> 0.9
M - HFHSD+M vs F - HFHSD+M	0	> 0.9
M - HFHSD+L vs F - HFHSD+L	2.05×10^7	**< 0.001**
F - SD vs F - HFHSD	9.83×10^4	> 0.9
F - HFHSD vs F - HFHSD+M	0	> 0.9
F - HFHSD vs F - HFHSD+L	-2.44×10^5	> 0.9

F = female; HFHSD = high-fat high-sugar diet; HFHSD+L = high-fat high-sugar diet treated with liraglutide; HFHSD+M = high-fat high-sugar diet treated with metformin; IDV = integrated density value; M = male; SD = standard diet; *estimated marginal means; †Tukey's post hoc HSD.

Table 5.9. Integrated density values for the GM1 ganglioside in the Cornu Ammonis 3 region

Variable	IDV mean	Two-way ANOVA	
		F value (df)	*P*
Sex			
Male	2.16×10^7	54.824 (1, 77)	**< 0.001**
Female	7.47×10^6		
Group			
SD	6.35×10^6		
HFHSD	6.51×10^6	87.446 (3, 77)	**< 0.001**
HFHSD+M	5.42×10^6		
HFHSD+L	3.99×10^7		
Interaction	-	77.720 (3, 77)	**< 0.001**

df = degrees of freedom; HFHSD = high-fat high-sugar diet; HFHSD+L = high-fat high-sugar diet treated with liraglutide; HFHSD+M = high-fat high-sugar diet treated with metformin; IDV = integrated density value; SD = standard diet.

Table 5.10. Group-specific pairwise comparisons of integrated density values for the GM1 ganglioside in the Cornu Ammonis 3 region

Compared groups	IDV difference mean[*]	*P*[†]
SD vs HFHSD	8.82×10^4	> 0.9
SD vs HFHSD+M	1.9×10^6	> 0.9
SD vs HFHSD+L	-2.71×10^7	**< 0.001**
HFHSD vs HFHSD+M	1.81×10^6	> 0.9
HFHSD vs HFHSD+L	-2.72×10^7	**< 0.001**
HFHSD+M vs HFHSD+L	-2.9×10^7	**< 0.001**

HFHSD = high-fat high-sugar diet; HFHSD+L = high-fat high-sugar diet treated with liraglutide; HFHSD+M = high-fat high-sugar diet treated with metformin; IDV = integrated density value; SD = standard diet; *estimated marginal means; †Tukey's post hoc HSD.

Table 5.11. Relevant group-specific and sex-specific pairwise comparisons of integrated density values for the GM1 ganglioside in the Cornu Ammonis 3 region

Compared groups	IDV difference mean[*]	P[†]
M - SD vs M - HFHSD	1.11×10^6	> 0.9
M - SD vs F - SD	2.72×10^6	> 0.9
M - HFHSD vs M - HFHSD+M	5.28×10^6	0.85
M - HFHSD vs M - HFHSD+L	-6.42×10^7	**< 0.001**
M - HFHSD vs F - HFHSD	1.93×10^5	> 0.9
M - HFHSD+M vs F - HFHSD+M	-8.21×10^6	0.53
M - HFHSD+L vs F - HFHSD+L	6.18×10^7	**< 0.001**
F - SD vs F - HFHSD	-1.42×10^6	> 0.9
F - HFHSD vs F - HFHSD+M	-3.11×10^6	> 0.9
F - HFHSD vs F - HFHSD+L	-2.55×10^6	> 0.9

F = female; HFHSD = high-fat high-sugar diet; HFHSD+L = high-fat high-sugar diet treated with liraglutide; HFHSD+M = high-fat high-sugar diet treated with metformin; IDV = integrated density value; M = male; SD = standard diet; *estimated marginal means; [†]Tukey's post hoc HSD.

GD1a IDV means between male and female rats in the SD group were similar in the DG and vastly different in the CA3 region, with female rats showing a much larger expression of the ganglioside. The CA1 region (Table 5.15, 5.16, 5.17) showed nearly no immunoreactivity whatsoever, therefore no significant comparisons could be observed and conclusions drawn from the data.

Following the HFHSD regimen and the metformin and liraglutide treatment, IDV mean changes between sexes showed different trajectories in the other two ROIs. In female rats, HFHSD caused a large decrease in GD1a expression in the DG (Table 5.12, 5.13, 5.14) and CA3 region (Table 5.18, 5.19, 5.20), where the decrease was significant in comparison with the SD group. While metformin did not cause any significant changes in GD1a expression in both the DG and CA3 region, there was a significant difference between IDV mean values of the HFHSD group and HFHSD-L group, where liraglutide treatment showed an increase in GD1a expression in the CA3 region.

In male rats, no significant differences in IDV means were found between groups to suggest any changes in GD1a expression.

Images of the acquired stains are shown in Figure 5.2.
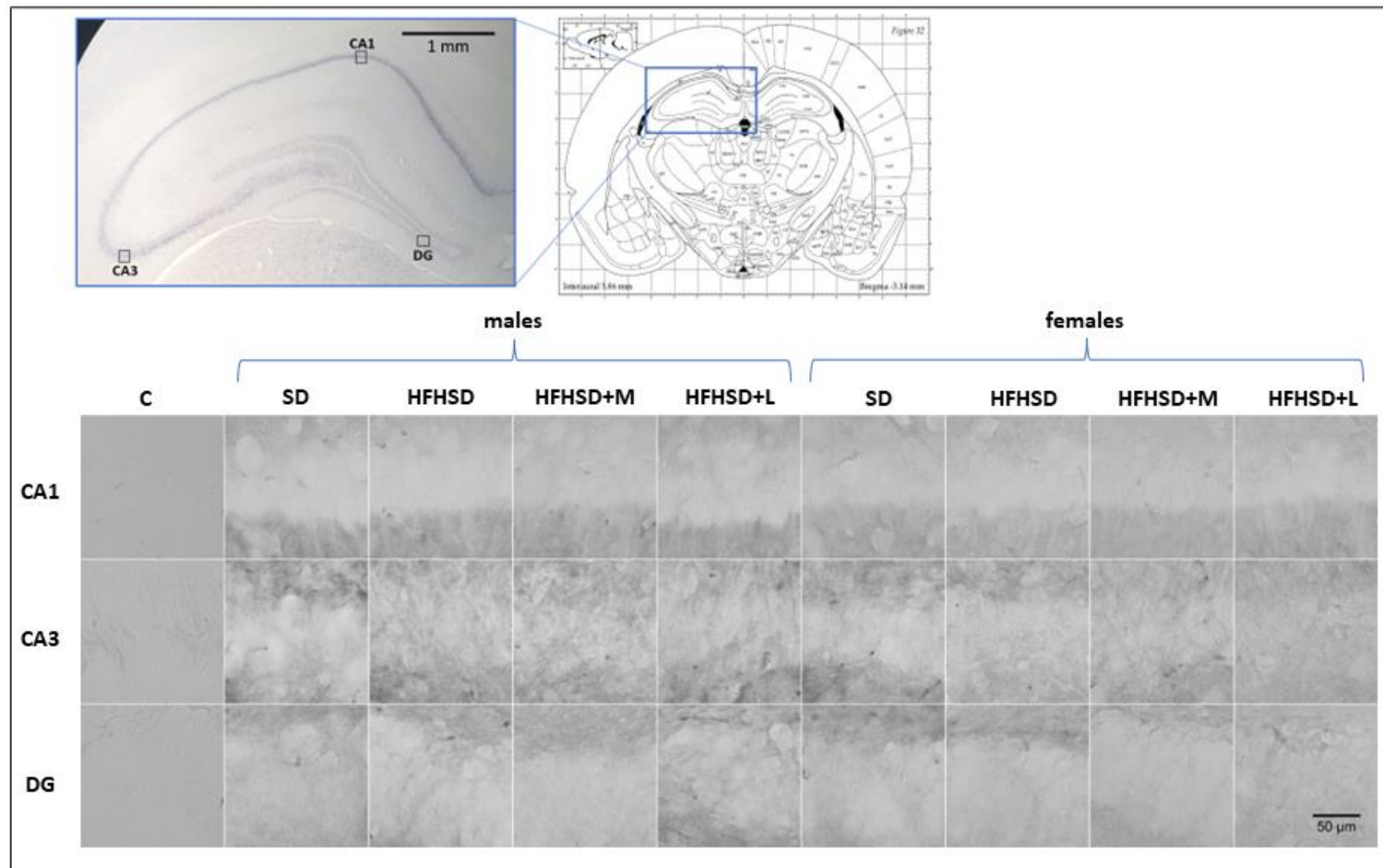
Figure 5.2. Expression of ganglioside GD1a in all animal group hippocampi, organized by ROI, sex and group.

C – negative control; CA1 – Cornu Ammonis region 1; CA3 – Cornu Ammonis region 3; DG – dentate gyrus; HFHSD – high-fat high sugar diet; HFHSD+L – HFHSD treated with liraglutide; HFHSD+M – HFHSD treated with metformin; SD – standard diet.

Table 5.12. Integrated density values for the GD1a ganglioside in the dentate gyrus

Variable	IDV mean	Two-way ANOVA	
		F value (df)	*P*
Sex			
Male	4.24×10^6	11.070 (1, 113)	**0.001**
Female	1.45×10^6		
Group			
SD	4.29×10^6		
HFHSD	2.42×10^6	3.223 (3, 113)	**0.02**
HFHSD+M	9.37×10^5		
HFHSD+L	3.73×10^6		
Interaction	-	2.211 (3, 113)	0.09

df = degrees of freedom; HFHSD = high-fat high-sugar diet; HFHSD+L = high-fat high-sugar diet treated with liraglutide; HFHSD+M = high-fat high-sugar diet treated with metformin; IDV = integrated density value; SD = standard diet.

Table 5.13. Group-specific pairwise comparisons of integrated density values for the GD1a ganglioside in the dentate gyrus

Compared groups	IDV difference mean[*]	*P*[†]
SD vs HFHSD	1.86×10^6	0.38
SD vs HFHSD+M	3.29×10^6	**0.03**
SD vs HFHSD+L	4.56×10^5	> 0.9
HFHSD vs HFHSD+M	1.43×10^6	0.64
HFHSD vs HFHSD+L	-1.4×10^6	0.66
HFHSD+M vs HFHSD+L	-2.83×10^6	0.09

HFHSD = high-fat high-sugar diet; HFHSD+L = high-fat high-sugar diet treated with liraglutide; HFHSD+M = high-fat high-sugar diet treated with metformin; IDV = integrated density value; SD = standard diet; *estimated marginal means; [†]Tukey's post hoc HSD.

Table 5.14. Relevant group-specific and sex-specific pairwise comparisons of integrated density values for the GD1a ganglioside in the dentate gyrus

Compared groups	IDV difference mean*	$P^\dagger$
M - SD vs M - HFHSD	2.25×10^5	> 0.9
M - SD vs F - SD	4.93×10^5	> 0.9
M - HFHSD vs M - HFHSD+M	2.83×10^6	0.7
M - HFHSD vs M - HFHSD+L	-2.33×10^6	0.87
M - HFHSD vs F - HFHSD	3.78×10^6	0.37
M - HFHSD+M vs F - HFHSD+M	1.09×10^6	> 0.9
M - HFHSD+L vs F - HFHSD+L	5.83×10^6	**0.02**
F - SD vs F - HFHSD	3.51×10^6	0.39
F - HFHSD vs F - HFHSD+M	1.42×10^5	> 0.9
F - HFHSD vs F - HFHSD+L	-2.79×10^5	> 0.9

F = female; HFHSD = high-fat high-sugar diet; HFHSD+L = high-fat high-sugar diet treated with liraglutide; HFHSD+M = high-fat high-sugar diet treated with metformin; IDV = integrated density value; M = male; SD = standard diet; *estimated marginal means; †Tukey's post hoc HSD.

Table 5 15. Integrated density values for the GD1a ganglioside in the Cornu Ammonis 1 region

Variable	IDV mean	Two-way ANOVA	
		F value (df)	P
Sex			
Male	6.33×10^{-12}	1.919 (1, 113)	**0.02**
Female	5.93×10^4		
Group			
SD	107883.1		
HFHSD	0	1.493 (3, 113)	**0.04**
HFHSD+M	-3.68×10^{-12}		
HFHSD+L	1.07×10^4		
Interaction	-	1.493 (3, 113)	**0.04**

df = degrees of freedom; HFHSD = high-fat high-sugar diet; HFHSD+L = high-fat high-sugar diet treated with liraglutide; HFHSD+M = high-fat high-sugar diet treated with metformin; IDV = integrated density value; SD = standard diet.

Table 5.16. Group-specific pairwise comparisons of integrated density values for the GD1a ganglioside in the Cornu Ammonis 1 region

Compared groups	IDV difference mean[*]	P[†]
SD vs HFHSD	1.08×10^5	0.3
SD vs HFHSD+M	1.08×10^5	0.29
SD vs HFHSD+L	9.62×10^4	0.37
HFHSD vs HFHSD+M	0	> 0.9
HFHSD vs HFHSD+L	-1.17×10^4	> 0.9
HFHSD+M vs HFHSD+L	-1.17×10^4	> 0.9

HFHSD = high-fat high-sugar diet; HFHSD+L = high-fat high-sugar diet treated with liraglutide; HFHSD+M = high-fat high-sugar diet treated with metformin; IDV = integrated density value; SD = standard diet; *estimated marginal means; [†]Tukey's post hoc HSD.

Table 5.17. Relevant group-specific and sex-specific pairwise comparisons of integrated density values for the GD1a ganglioside in the Cornu Ammonis 1 region

Compared groups	IDV difference mean[*]	P[†]
M - SD vs M - HFHSD	0	> 0.9
M - SD vs F - SD	-2.16×10^5	0.197
M - HFHSD vs M - HFHSD+M	0	> 0.9
M - HFHSD vs M - HFHSD+L	0	> 0.9
M - HFHSD vs F - HFHSD	0	> 0.9
M - HFHSD+M vs F - HFHSD+M	0	> 0.9
M - HFHSD+L vs F - HFHSD+L	-2.14×10^4	> 0.9
F - SD vs F - HFHSD	2.16×10^5	0.216
F - HFHSD vs F - HFHSD+M	0	> 0.9
F - HFHSD vs F - HFHSD+L	-2.14×10^4	> 0.9

F = female; HFHSD = high-fat high-sugar diet; HFHSD+L = high-fat high-sugar diet treated with liraglutide; HFHSD+M = high-fat high-sugar diet treated with metformin; IDV = integrated density value; M = male; SD = standard diet; *estimated marginal means; [†]Tukey's post hoc HSD.

Table 5.18. Integrated density values for the GD1a ganglioside in the Cornu Ammonis 3 region

Variable	IDV mean	Two-way ANOVA	
		F value (df)	*P*
Sex			
Male	3.86×10^5	21.119 (1, 103)	**< 0.001**
Female	2.48×10^6		
Group			
SD	2.97×10^6		
HFHSD	8.51×10^4	9.238 (3, 103)	**< 0.001**
HFHSD+M	6.03×10^5		
HFHSD+L	2.08×10^6		
Interaction	-	7.018 (3, 103)	**< 0.001**

df = degrees of freedom; HFHSD = high-fat high-sugar diet; HFHSD+L = high-fat high-sugar diet treated with liraglutide; HFHSD+M = high-fat high-sugar diet treated with metformin; IDV = integrated density value; SD = standard diet.

Table 5.19. Group-specific pairwise comparisons of integrated density values for the GD1a ganglioside in the Cornu Ammonis 3 region

Compared groups	IDV difference mean[*]	*P*[†]
SD vs HFHSD	2.79×10^6	**< 0.001**
SD vs HFHSD+M	2.4×10^6	**0.003**
SD vs HFHSD+L	6.63×10^5	0.7
HFHSD vs HFHSD+M	-3.92×10^5	0.94
HFHSD vs HFHSD+L	-2.13×10^6	**0.003**
HFHSD+M vs HFHSD+L	-1.74×10^6	0.05

HFHSD = high-fat high-sugar diet; HFHSD+L = high-fat high-sugar diet treated with liraglutide; HFHSD+M = high-fat high-sugar diet treated with metformin; IDV = integrated density value; SD = standard diet; *estimated marginal means; [†]Tukey's post hoc HSD.

Table 5.20. Relevant group-specific and sex-specific pairwise comparisons of integrated density values for the GD1a ganglioside in the Cornu Ammonis 3 region

Compared groups	IDV difference mean[*]	P[†]
M - SD vs M - HFHSD	1.93×10^5	> 0.9
M - SD vs F - SD	-5.22×10^6	**< 0.001**
M - HFHSD vs M - HFHSD+M	1.7×10^5	> 0.9
M - HFHSD vs M - HFHSD+L	-8.41×10^5	> 0.9
M - HFHSD vs F - HFHSD	1.7×10^5	> 0.9
M - HFHSD+M vs F - HFHSD+M	-1.2×10^6	> 0.9
M - HFHSD+L vs F - HFHSD+L	-2.13×10^6	0.22
F - SD vs F - HFHSD	5.58×10^6	**< 0.001**
F - HFHSD vs F - HFHSD+M	-1.2×10^6	> 0.9
F - HFHSD vs F - HFHSD+L	-3.14×10^6	**0.006**

F = female; HFHSD = high-fat high-sugar diet; HFHSD+L = high-fat high-sugar diet treated with liraglutide; HFHSD+M = high-fat high-sugar diet treated with metformin; IDV = integrated density value; M = male; SD = standard diet; [*]estimated marginal means; [†]Tukey's post hoc HSD.

Out of the four analyzed gangliosides, GD1b had the largest number of significant differences in expression between observed groups in all three ROIs. In SD groups, there was a large difference in IDV means between sexes, with the female rats showing a much higher level of expression of GD1b than male rats, as was similarly observed for the GD1a ganglioside. These IDV mean differences between sexes were significant in all three ROIs.

Following the HFHSD regimen and compared with their respective SD group, sex-specific changes were observed in opposite trajectories – the diet increased the expression of GD1b in male rats and decreased it in female rats. The sex-specific IDV mean value differences between the SD and the HFHSD group were significant in all three ROIs.

The difference between IDV mean values of male and female rats was reduced once metformin and liraglutide were introduced. In the DG, male rats had significant decreases in IDV mean values compared to the HFHSD group following both metformin and liraglutide treatment, while female rats showed significant decreases in IDV mean values following only liraglutide treatment (Table 5.21, 5.22, 5.23). GD1b was one of only two gangliosides (GT1b) that showed consistently high immunoreactivity in all three ROIs in the CA1 region (Table

5.24). In the CA1 and CA3 region (Table 5.27), both sexes had significant decreases in IDV means following both metformin and liraglutide expression (Table 5.25, 5.26, 5.28, 5.29).

Images of the acquired stains are shown in Figure 5.3.
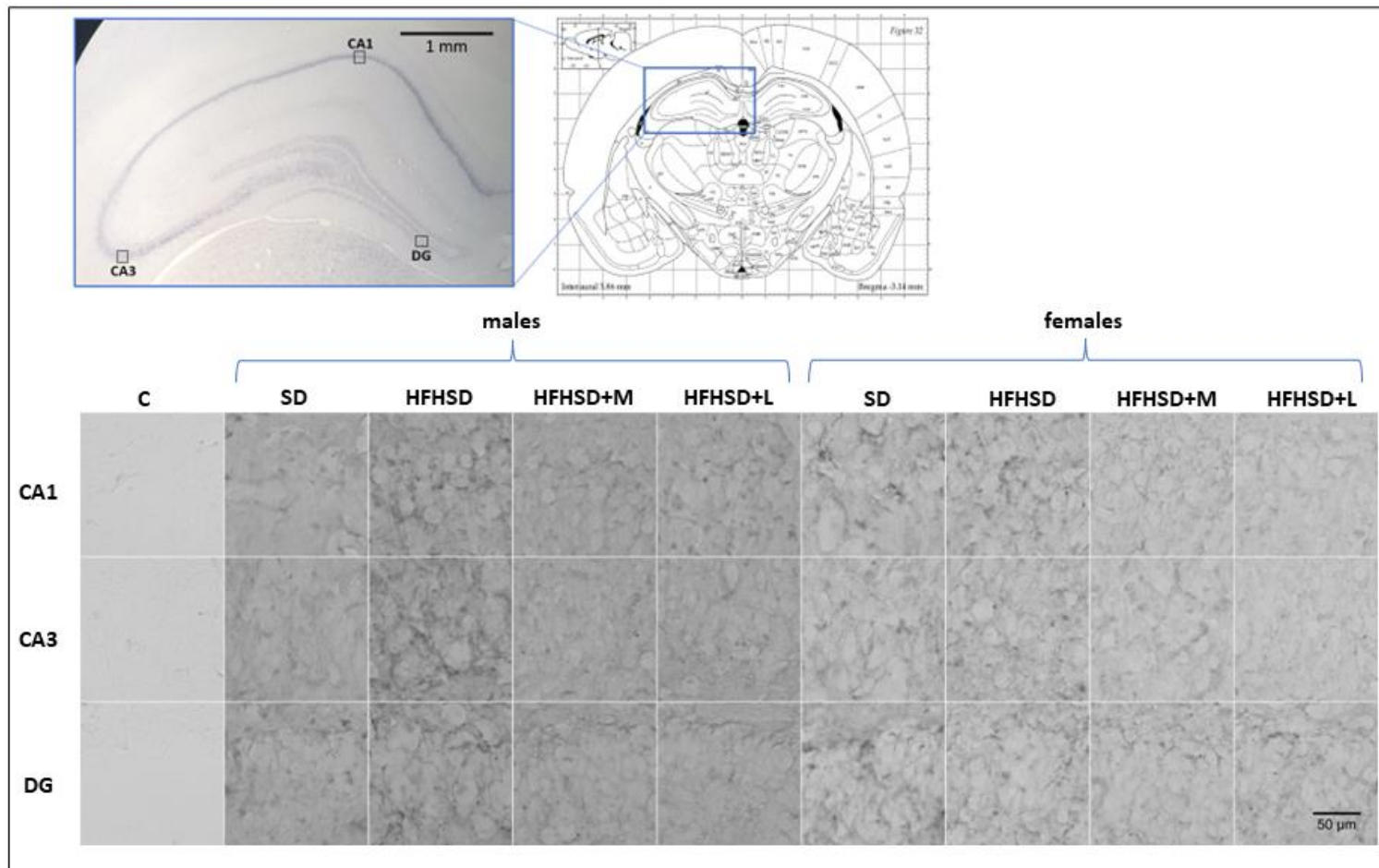
Figure 5.3. Expression of ganglioside GD1b in all animal group hippocampi, organized by region of interest, sex and group. C – negative control; CA1 – Cornu Ammonis region 1; CA3 – Cornu Ammonis region 3; DG – dentate gyrus; HFHSD – high-fat high-sugar diet; HFHSD+L – HFHSD treated with liraglutide; HFHSD+M – HFHSD treated with metformin; SD – standard diet.

Table 5.21. Integrated density values for the GD1b ganglioside in the dentate gyrus

Variable	IDV mean	Two-way ANOVA	
		F value (df)	*P*
Sex			
Male	4.4×10^7	13.880 (1, 86)	**< 0.001**
Female	4.93×10^7		
Group			
SD	4.91×10^7		
HFHSD	5.51×10^7	26.518 (3, 86)	**< 0.001**
HFHSD+M	4.4×10^7		
HFHSD+L	3.85×10^7		
Interaction	-	38.843 (3, 86)	**< 0.001**

df = degrees of freedom; HFHSD = high-fat high-sugar diet; HFHSD+L = high-fat high-sugar diet treated with liraglutide; HFHSD+M = high-fat high-sugar diet treated with metformin; IDV = integrated density value; SD = standard diet.

Table 5.22. Group-specific pairwise comparisons of integrated density values for the GD1b ganglioside in the dentate gyrus

Compared groups	IDV difference mean[*]	*P*[†]
SD vs HFHSD	-7.56×10^6	**0.001**
SD vs HFHSD+M	3.81×10^6	0.25
SD vs HFHSD+L	9.2×10^6	**< 0.001**
HFHSD vs HFHSD+M	1.14×10^7	**< 0.001**
HFHSD vs HFHSD+L	1.68×10^7	**< 0.001**
HFHSD+M vs HFHSD+L	5.4×10^6	**0.04**

HFHSD = high-fat high-sugar diet; HFHSD+L = high-fat high-sugar diet treated with liraglutide; HFHSD+M = high-fat high-sugar diet treated with metformin; IDV = integrated density value; SD = standard diet; *estimated marginal means; †Tukey's post hoc HSD.

Table 5.23. Relevant group-specific and sex-specific pairwise comparisons of integrated density values for the GD1b ganglioside in the dentate gyrus

Compared groups	IDV difference mean[*]	P[†]
M - SD vs M - HFHSD	-2.66×10^7	**< 0.001**
M - SD vs F - SD	-3.08×10^7	**< 0.001**
M - HFHSD vs M - HFHSD+M	1.69×10^7	**< 0.001**
M - HFHSD vs M - HFHSD+L	2.16×10^7	**< 0.001**
M - HFHSD vs F - HFHSD	1.05×10^7	**< 0.001**
M - HFHSD+M vs F - HFHSD+M	-1.14×10^6	> 0.9
M - HFHSD+L vs F - HFHSD+L	3.47×10^5	> 0.9
F - SD vs F - HFHSD	1.47×10^7	**< 0.001**
F - HFHSD vs F - HFHSD+M	5.26×10^6	0.62
F - HFHSD vs F - HFHSD+L	1.14×10^7	**0.001**

F = female; HFHSD = high-fat high-sugar diet; HFHSD+L = high-fat high-sugar diet treated with liraglutide; HFHSD+M = high-fat high-sugar diet treated with metformin; IDV = integrated density value; M = male; SD = standard diet; [*]estimated marginal means; [†]Tukey's post hoc HSD.

Table 5.24. Integrated density values for the GD1b ganglioside in the Cornu Ammonis 1 region

Variable	IDV mean	Two-way ANOVA	
		F value (df)	P
Sex			
Male	4.16×10^7	15.292 (1, 85)	**< 0.001**
Female	4.77×10^7		
Group			
SD	5×10^7	31.982 (3, 85)	**< 0.001**
HFHSD	5.33×10^7		
HFHSD+M	4×10^7		
HFHSD+L	3.53×10^7		
Interaction	-	12.430 (3, 85)	**< 0.001**

df = degrees of freedom; HFHSD = high-fat high-sugar diet; HFHSD+L = high-fat high-sugar diet treated with liraglutide; HFHSD+M = high-fat high-sugar diet treated with metformin; IDV = integrated density value; SD = standard diet.

Table 5.25. Group-specific pairwise comparisons of integrated density values for the GD1b ganglioside in the Cornu Ammonis 1 region

Compared groups	IDV difference mean[*]	P[†]
SD vs HFHSD	-1.34×10^6	0.93
SD vs HFHSD+M	1.17×10^7	**< 0.001**
SD vs HFHSD+L	1.65×10^7	**< 0.001**
HFHSD vs HFHSD+M	1.31×10^7	**< 0.001**
HFHSD vs HFHSD+L	1.78×10^7	**< 0.001**
HFHSD+M vs HFHSD+L	4.72×10^6	0.11

HFHSD = high-fat high-sugar diet; HFHSD+L = high-fat high-sugar diet treated with liraglutide; HFHSD+M = high-fat high-sugar diet treated with metformin; IDV = integrated density value; SD = standard diet; *estimated marginal means; †Tukey's post hoc HSD.

Table 5.26. Relevant group-specific and sex-specific pairwise comparisons of integrated density values for the GD1b ganglioside in the Cornu Ammonis 1 region

Compared groups	IDV difference mean[*]	P[†]
M - SD vs M - HFHSD	-1.6×10^7	**< 0.001**
M - SD vs F - SD	-2.32×10^7	**< 0.001**
M - HFHSD vs M - HFHSD+M	1.41×10^7	**0.001**
M - HFHSD vs M - HFHSD+L	2.09×10^7	**< 0.001**
M - HFHSD vs F - HFHSD	2.21×10^6	> 0.9
M - HFHSD+M vs F - HFHSD+M	4.17×10^5	> 0.9
M - HFHSD+L vs F - HFHSD+L	-3.63×10^6	0.88
F - SD vs F - HFHSD	9.39×10^6	0.05
F - HFHSD vs F - HFHSD+M	1.23×10^7	**0.002**
F - HFHSD vs F - HFHSD+L	1.51×10^7	**< 0.001**

F = female; HFHSD = high-fat high-sugar diet; HFHSD+L = high-fat high-sugar diet treated with liraglutide; HFHSD+M = high-fat high-sugar diet treated with metformin; IDV = integrated density value; M = male; SD = standard diet; *estimated marginal means; †Tukey's post hoc HSD.

Table 5.27. Integrated density values for the GD1b ganglioside in the Cornu Ammonis 3 region

| Variable	IDV mean	Two-way ANOVA	
		F value (df)	P
Sex			
Male	4.65×10^7	0.504 (1, 86)	0.48
Female	4.53×10^7		
Group			
SD	5.19×10^7		
HFHSD	5.54×10^7	40.780 (3, 86)	**< 0.001**
HFHSD+M	4.22×10^7		
HFHSD+L	3.41×10^7		
Interaction	-	22.267 (3, 86)	**< 0.001**

df = degrees of freedom; HFHSD = high-fat high-sugar diet; HFHSD+L = high-fat high-sugar diet treated with liraglutide; HFHSD+M = high-fat high-sugar diet treated with metformin; IDV = integrated density value; SD = standard diet.

Table 5.28. Group-specific pairwise comparisons of integrated density values for the GD1b ganglioside in the Cornu Ammonis 3 region

Compared groups	IDV difference mean[*]	P[†]
SD vs HFHSD	-1.03×10^6	0.96
SD vs HFHSD+M	1.24×10^7	**< 0.001**
SD vs HFHSD+L	2.1×10^7	**< 0.001**
HFHSD vs HFHSD+M	1.34×10^7	**< 0.001**
HFHSD vs HFHSD+L	2.2×10^7	**< 0.001**
HFHSD+M vs HFHSD+L	8.6×10^6	**0.001**

HFHSD = high-fat high-sugar diet; HFHSD+L = high-fat high-sugar diet treated with liraglutide; HFHSD+M = high-fat high-sugar diet treated with metformin; IDV = integrated density value; SD = standard diet; *estimated marginal means; [†]Tukey's post hoc HSD.

Table 5.29. Relevant group-specific and sex-specific pairwise comparisons of integrated density values for the GD1b ganglioside in the Cornu Ammonis 3 region

Compared groups	IDV difference mean*	$P^{\dagger}$
M - SD vs M - HFHSD	-1.82×10^7	**< 0.001**
M - SD vs F - SD	-2.09×10^7	**< 0.001**
M - HFHSD vs M - HFHSD+M	1.42×10^7	**0.001**
M - HFHSD vs M - HFHSD+L	2.05×10^7	**< 0.001**
M - HFHSD vs F - HFHSD	8.54×10^6	0.13
M - HFHSD+M vs F - HFHSD+M	6.68×10^6	0.49
M - HFHSD+L vs F - HFHSD+L	1.01×10^7	**0.02**
F - SD vs F - HFHSD	1.13×10^7	**0.006**
F - HFHSD vs F - HFHSD+M	1.23×10^7	**0.007**
F - HFHSD vs F - HFHSD+L	2.21×10^7	**< 0.001**

F = female; HFHSD = high-fat high-sugar diet; HFHSD+L = high-fat high-sugar diet treated with liraglutide; HFHSD+M = high-fat high-sugar diet treated with metformin; IDV = integrated density value; M = male; SD = standard diet; *estimated marginal means; †Tukey's post hoc HSD.

Even though the two-way ANOVA analysis showed significant effects of both sex and animal groups on GT1b expression in most ROI (Table 5.30, 5.33, 5.36), only a couple of pairwise comparisons were of significance to the research study.

In male rats, there was a significant increase in GT1b expression GT1b in the HFHSD group compared with the SD group in the CA1 region. However, neither metformin of liraglutide treatment showed any significant changes in IDV mean values to suggest any effect on GT1b expression (Table 5.34, 5.35). In female rats, there was a significant increase in GT1b expression in the HFHSD-L group compared with the HFHSD group in the CA1 region. In the DG (Table 5.31, 5.32) and the CA3 region (Table 5.37, 5.38), the observed significant differences in IDV mean values did not provide any relevant information in relation to the effects of metformin and liraglutide treatment on GT1b expression.

Images of the acquired stains are shown in Figure 5.4.
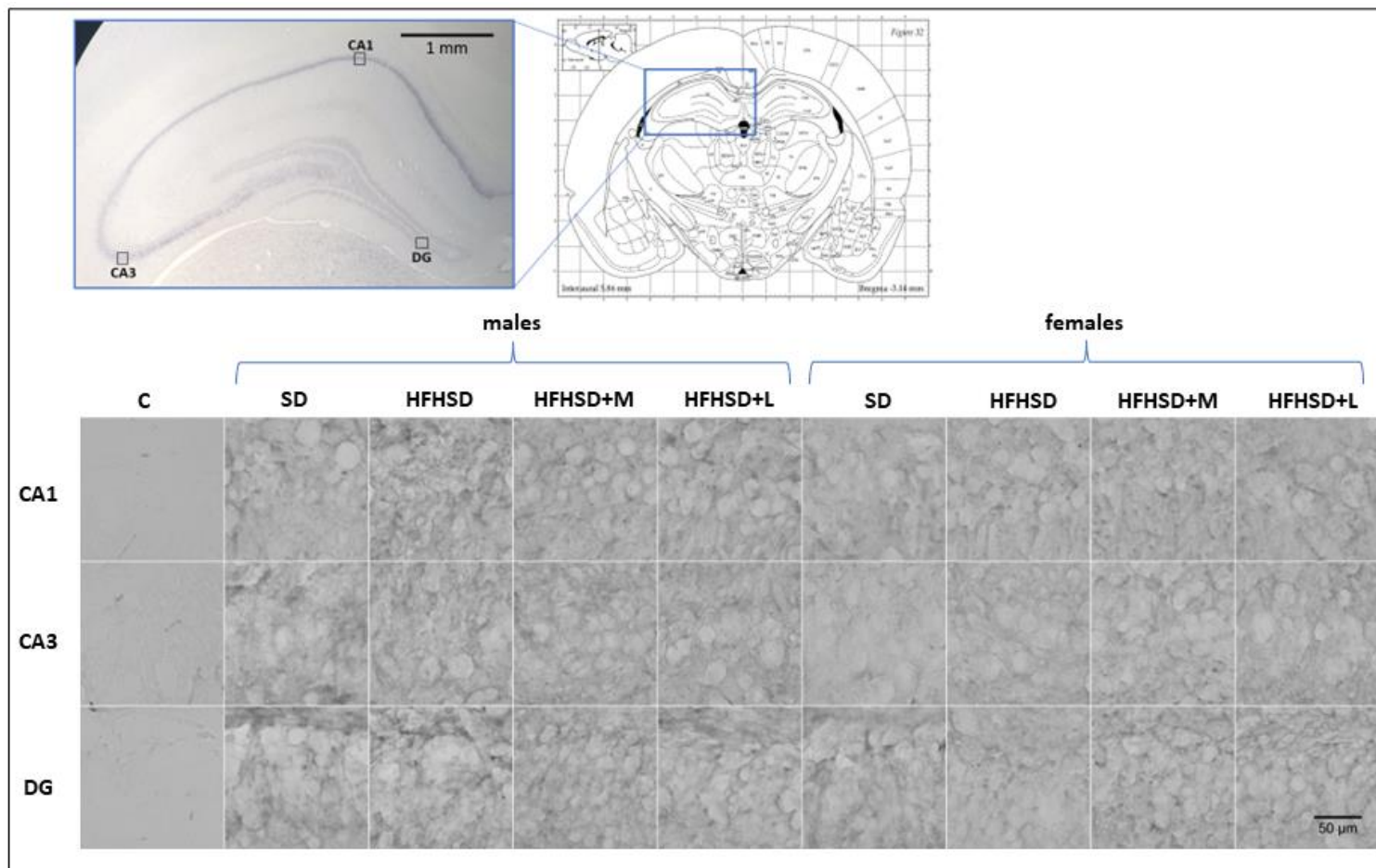
Figure 5.4. Expression of ganglioside GT1b in all animal group hippocampi, organized by region of interest, sex and group. C – negative control; CA1 – Cornu Ammonis region 1; CA3 – Cornu Ammonis region 3; DG – dentate gyrus; HFHSD – high-fat high-sugar diet; HFHSD+L – HFHSD treated with liraglutide; HFHSD+M – HFHSD treated with metformin; SD – standard diet.

Table 5.30. Integrated density values for the GT1b ganglioside in the dentate gyrus

Variable	IDV mean	Two-way ANOVA	
		F value (df)	*P*
Sex			
Male	2.22×10^7	49.890 (1, 98)	**< 0.001**
Female	1.51×10^7		
Group			
SD	1.58×10^7		
HFHSD	1.81×10^7	4.764 (3, 98)	**0.004**
HFHSD+M	2.1×10^7		
HFHSD+L	1.96×10^7		
Interaction	-	3.293 (3, 98)	**0.02**

df = degrees of freedom; HFHSD = high-fat high-sugar diet; HFHSD+L = high-fat high-sugar diet treated with liraglutide; HFHSD+M = high-fat high-sugar diet treated with metformin; IDV = integrated density value; SD = standard diet.

Table 5.31. Group-specific pairwise comparisons of integrated density values for the GT1b ganglioside in the dentate gyrus

Compared groups	IDV difference mean[*]	*P*[†]
SD vs HFHSD	-2.33×10^6	0.37
SD vs HFHSD+M	-5.79×10^6	**0.001**
SD vs HFHSD+L	-4.21×10^6	**0.02**
HFHSD vs HFHSD+M	-3.46×10^6	0.08
HFHSD vs HFHSD+L	-1.88×10^6	0.55
HFHSD+M vs HFHSD+L	1.58×10^6	0.68

HFHSD = high-fat high-sugar diet; HFHSD+L = high-fat high-sugar diet treated with liraglutide; HFHSD+M = high-fat high-sugar diet treated with metformin; IDV = integrated density value; SD = standard diet; *estimated marginal means; †Tukey's post hoc HSD.

Table 5.32. Relevant group-specific and sex-specific pairwise comparisons of integrated density values for the GT1b ganglioside in the dentate gyrus

Compared groups	IDV difference mean[*]	P[†]
M - SD vs M - HFHSD	-5.01×10^6	0.3
M - SD vs F - SD	5.78×10^6	0.11
M - HFHSD vs M - HFHSD+M	-1.75×10^6	> 0.9
M - HFHSD vs M - HFHSD+L	2.69×10^6	> 0.9
M - HFHSD vs F - HFHSD	1.12×10^7	**< 0.001**
M - HFHSD+M vs F - HFHSD+M	8.92×10^6	**0.001**
M - HFHSD+L vs F - HFHSD+L	2.77×10^6	0.86
F - SD vs F - HFHSD	3.78×10^5	> 0.9
F - HFHSD vs F - HFHSD+M	-3.99×10^6	0.49
F - HFHSD vs F - HFHSD+L	-5.7×10^6	0.08

F = female; HFHSD = high-fat high-sugar diet; HFHSD+L = high-fat high-sugar diet treated with liraglutide; HFHSD+M = high-fat high-sugar diet treated with metformin; IDV = integrated density value; M = male; SD = standard diet; [*]estimated marginal means; [†]Tukey's post hoc HSD.

Table 5.33. Integrated density values for the GT1b ganglioside in the Cornu Ammonis 1 region

Variable	IDV mean	Two-way ANOVA	
		F value (df)	P
Sex			
Male	1.58×10^7	0.081 (1, 89)	0.78
Female	1.56×10^7		
Group			
SD	1.28×10^7		
HFHSD	1.51×10^7	10.838 (3, 89)	**< 0.001**
HFHSD+M	1.69×10^7		
HFHSD+L	1.81×10^7		
Interaction	-	8.390 (3, 89)	**< 0.001**

df = degrees of freedom; HFHSD = high-fat high-sugar diet; HFHSD+L = high-fat high-sugar diet treated with liraglutide; HFHSD+M = high-fat high-sugar diet treated with metformin; IDV = integrated density value; SD = standard diet.

Table 5.34. Group-specific pairwise comparisons of integrated density values for the GT1b ganglioside in the Cornu Ammonis 1 region

Compared groups	IDV difference mean[*]	P[†]
SD vs HFHSD	-2.59×10^6	0.06
SD vs HFHSD+M	-4.16×10^6	**< 0.001**
SD vs HFHSD+L	-5.31×10^6	**< 0.001**
HFHSD vs HFHSD+M	-1.54×10^6	0.39
HFHSD vs HFHSD+L	-2.73×10^6	**0.03**
HFHSD+M vs HFHSD+L	-1.18×10^6	0.6

HFHSD = high-fat high-sugar diet; HFHSD+L = high-fat high-sugar diet treated with liraglutide; HFHSD+M = high-fat high-sugar diet treated with metformin; IDV = integrated density value; SD = standard diet; *estimated marginal means; †Tukey's post hoc HSD.

Table 5.35. Relevant group-specific and sex-specific pairwise comparisons of integrated density values for the GT1b ganglioside in the Cornu Ammonis 1 region

Compared groups	IDV difference mean[*]	P[†]
M - SD vs M - HFHSD	-6.41×10^5	**< 0.001**
M - SD vs F - SD	-2.63×10^6	0.61
M - HFHSD vs M - HFHSD+M	4.12×10^5	> 0.9
M - HFHSD vs M - HFHSD+L	1.39×10^6	0.97
M - HFHSD vs F - HFHSD	5.48×10^6	**0.004**
M - HFHSD+M vs F - HFHSD+M	1.16×10^6	> 0.9
M - HFHSD+L vs F - HFHSD+L	-3.22×10^6	0.25
F - SD vs F - HFHSD	1.7×10^6	> 0.9
F - HFHSD vs F - HFHSD+M	-3.91×10^6	0.12
F - HFHSD vs F - HFHSD+L	-7.3×10^6	**< 0.001**

F = female; HFHSD = high-fat high-sugar diet; HFHSD+L = high-fat high-sugar diet treated with liraglutide; HFHSD+M = high-fat high-sugar diet treated with metformin; IDV = integrated density value; M = male; SD = standard diet; *estimated marginal means; †Tukey's post hoc HSD.

Table 5.36. Integrated density values for the GT1b ganglioside in the Cornu Ammonis 3 region

Variable	IDV mean	Two-way ANOVA	
		F value (df)	P
Sex			
Male	1.64×10^7	21.520 (1, 103)	**< 0.001**
Female	2.08×10^7		
Group			
SD	1.82×10^7		
HFHSD	1.8×10^7	0.525 (3, 103)	0.67
HFHSD+M	1.96×10^7		
HFHSD+L	1.84×10^7		
Interaction	-	3.023 (3, 103)	**0.03**

df = degrees of freedom; HFHSD = high-fat high-sugar diet; HFHSD+L = high-fat high-sugar diet treated with liraglutide; HFHSD+M = high-fat high-sugar diet treated with metformin; IDV = integrated density value; SD = standard diet.

Table 5.37. Group-specific pairwise comparisons of integrated density values for the GT1b ganglioside in the Cornu Ammonis 3 region

Compared groups	IDV difference mean[*]	P[†]
SD vs HFHSD	6.78×10^5	> 0.9
SD vs HFHSD+M	-9.11×10^5	> 0.9
SD vs HFHSD+L	1.39×10^4	> 0.9
HFHSD vs HFHSD+M	-1.59×10^6	0.64
HFHSD vs HFHSD+L	-6.64×10^5	> 0.9
HFHSD+M vs HFHSD+L	9.25×10^5	> 0.9

HFHSD = high-fat high-sugar diet; HFHSD+L = high-fat high-sugar diet treated with liraglutide; HFHSD+M = high-fat high-sugar diet treated with metformin; IDV = integrated density value; SD = standard diet; *estimated marginal means; [†]Tukey's post hoc HSD.

Table 5.38. Relevant group-specific and sex-specific pairwise comparisons of integrated density values for the GT1b ganglioside in the Cornu Ammonis 3 region

Compared groups	IDV difference mean[*]	P[†]
M - SD vs M - HFHSD	1.13×10^6	> 0.9
M - SD vs F - SD	-6.03×10^6	0.05
M - HFHSD vs M - HFHSD+M	-5.48×10^6	0.09
M - HFHSD vs M - HFHSD+L	-2.49×10^6	0.89
M - HFHSD vs F - HFHSD	-7.87×10^6	**0.001**
M - HFHSD+M vs F - HFHSD+M	-9.36×10^4	> 0.9
M - HFHSD+L vs F - HFHSD+L	-3.64×10^6	0.47
F - SD vs F - HFHSD	-7.05×10^5	> 0.9
F - HFHSD vs F - HFHSD+M	2.3×10^6	> 0.9
F - HFHSD vs F - HFHSD+L	1.75×10^6	> 0.9

F = female; HFHSD = high-fat high-sugar diet; HFHSD+L = high-fat high-sugar diet treated with liraglutide; HFHSD+M = high-fat high-sugar diet treated with metformin; IDV = integrated density value; M = male; SD = standard diet; [*]estimated marginal means; [†]Tukey's post hoc HSD.

5.2.2. Expression of proteins involved in the pathophysiology of InR

A two-way ANOVA test showed significant differences in IDV mean values based on sex, animal group and their interaction in all three ROIs (Table 5.39, 5.42, 5.45). When observing the absolute values of IDV mean values between sexes, male groups showed much larger immunoreactivity compared to female groups, suggesting that HFHSD and treatment with both metformin and liraglutide affect the expression of IR in the hippocampus predominantly in male rats.

In the DG, there was a small increase in IDV mean values in HFHSD male rats compared with the SD group. Further, significant increases were observed following metformin and liraglutide treatment in male rats compared with the HFHSD group (Table 5.40, 5.41). Similarly, significant increases in the HFHSD-M and HFHSD-L male rats were observed in the CA3 region compared with the HFHSD group. There was, however, a decrease in IDV mean values in HFHSD male rats compared with their respective SD group (Table 5.46, 5.47). The CA1 region showed an increase in IDV mean values in HFHSD male

rats compared with their respective SD group, while metformin and liraglutide treatment caused a significant decrease in IDV mean values (Table 5.43, 5.44).

Female groups, on the other hand, besides the lesser immunoreactivity, showed no significant differences in IDV mean values.

Images of the acquired stains are shown in Figure 5.5.
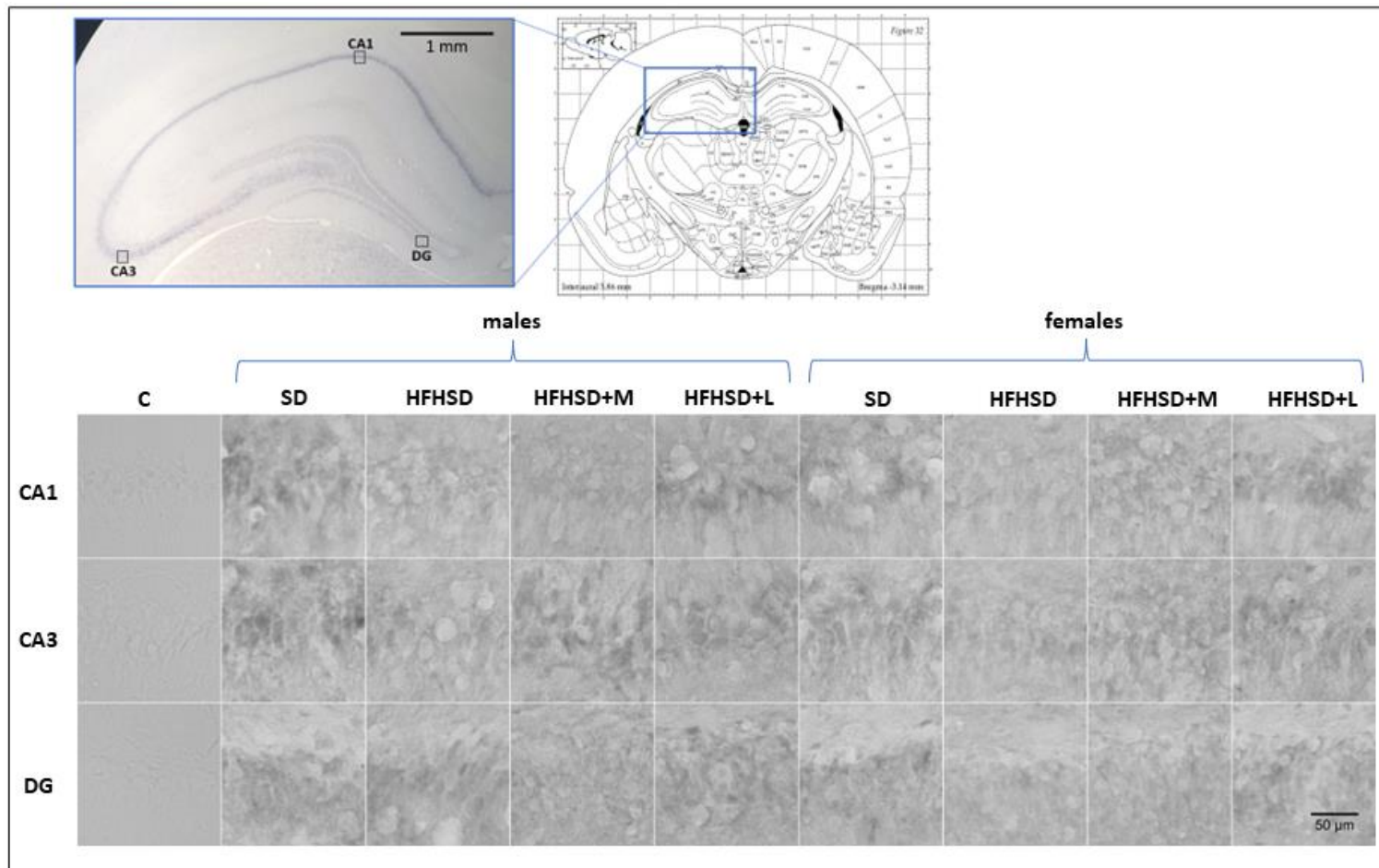
Figure 5.5. Expression of the insulin receptor in all animal group hippocampi, organized by region of interest, sex and group. C – negative control; CA1 – Cornu Ammonis region 1; CA3 – Cornu Ammonis region 3; DG – dentate gyrus; HFHSD – high-fat high-sugar diet; HFHSD+L – HFHSD treated with liraglutide; HFHSD+M – HFHSD treated with metformin; SD – standard diet.

Table 5.39. Integrated density values for the insulin receptor in the dentate gyrus

Variable	IDV mean	Two-way ANOVA	
		F value (df)	*P*
Sex			
Male	10^7	31.465 (1, 128)	**< 0.001**
Female	3.24×10^6		
Group			
SD	3.45×10^6		
HFHSD	3.07×10^6	10.621 (3, 128)	**< 0.001**
HFHSD+M	9.52×10^6		
HFHSD+L	1.04×10^7		
Interaction	-	12.807 (3, 128)	**< 0.001**

df = degrees of freedom; HFHSD = high-fat high-sugar diet; HFHSD+L = high-fat high-sugar diet treated with liraglutide; HFHSD+M = high-fat high-sugar diet treated with metformin; IDV = integrated density value; SD = standard diet.

Table 5.40. Group-specific pairwise comparisons of integrated density values for the insulin receptor in the dentate gyrus

Compared groups	IDV difference mean[*]	*P*[†]
SD vs HFHSD	4.98×10^5	> 0.9
SD vs HFHSD+M	-5.96×10^6	**0.005**
SD vs HFHSD+L	-7.46×10^6	**< 0.001**
HFHSD vs HFHSD+M	-6.46×10^6	**0.001**
HFHSD vs HFHSD+L	-7.96×10^6	**< 0.001**
HFHSD+M vs HFHSD+L	-1.5×10^6	0.8

HFHSD = high-fat high-sugar diet; HFHSD+L = high-fat high-sugar diet treated with liraglutide; HFHSD+M = high-fat high-sugar diet treated with metformin; IDV = integrated density value; SD = standard diet; *estimated marginal means; †Tukey's post hoc HSD.

Table 5.41. Relevant group-specific and sex-specific pairwise comparisons of integrated density values for the insulin receptor in the dentate gyrus

Compared groups	IDV difference mean[*]	P[†]
M - SD vs M - HFHSD	-9.25×10^5	> 0.9
M - SD vs F - SD	-1.93×10^6	> 0.9
M - HFHSD vs M - HFHSD+M	-1.39×10^7	**< 0.001**
M - HFHSD vs M - HFHSD+L	-1.34×10^7	**< 0.001**
M - HFHSD vs F - HFHSD	6.76×10^5	> 0.9
M - HFHSD+M vs F - HFHSD+M	1.55×10^7	**< 0.001**
M - HFHSD+L vs F - HFHSD+L	1.28×10^7	**< 0.001**
F - SD vs F - HFHSD	1.69×10^6	> 0.9
F - HFHSD vs F - HFHSD+M	9.7×10^5	> 0.9
F - HFHSD vs F - HFHSD+L	-1.31×10^6	> 0.9

F = female; HFHSD = high-fat high-sugar diet; HFHSD+L = high-fat high-sugar diet treated with liraglutide; HFHSD+M = high-fat high-sugar diet treated with metformin; IDV = integrated density value; M = male; SD = standard diet; [*]estimated marginal means; [†]Tukey's post hoc HSD.

Table 5.42. Integrated density values for the insulin receptor in the Cornu Ammonis 1 region

Variable	IDV mean	Two-way ANOVA	
		F value (df)	P
Sex			
Male	4.69×10^7	37.747 (1, 127)	**< 0.001**
Female	1.27×10^7		
Group			
SD	2.02×10^7		
HFHSD	8.31×10^7	44.130 (3, 127)	**< 0.001**
HFHSD+M	7.96×10^6		
HFHSD+L	7.96×10^6		
Interaction	-	57.626 (3, 127)	**< 0.001**

df = degrees of freedom; HFHSD = high-fat high-sugar diet; HFHSD+L = high-fat high-sugar diet treated with liraglutide; HFHSD+M = high-fat high-sugar diet treated with metformin; IDV = integrated density value; SD = standard diet.

Table 5.43. Group-specific pairwise comparisons of integrated density values for the insulin receptor in the Cornu Ammonis 1 region

Compared groups	IDV difference mean[*]	$P^{\dagger}$
SD vs HFHSD	-6.29×10^{7}	**< 0.001**
SD vs HFHSD+M	1.22×10^{7}	0.44
SD vs HFHSD+L	1.22×10^{7}	0.42
HFHSD vs HFHSD+M	7.51×10^{7}	**< 0.001**
HFHSD vs HFHSD+L	7.51×10^{7}	**< 0.001**
HFHSD+M vs HFHSD+L	-7.6×10^{3}	> 0.9

HFHSD = high-fat high-sugar diet; HFHSD+L = high-fat high-sugar diet treated with liraglutide; HFHSD+M = high-fat high-sugar diet treated with metformin; IDV = integrated density value; SD = standard diet; *estimated marginal means; †Tukey's post hoc HSD.

Table 5.44. Relevant group-specific and sex-specific pairwise comparisons of integrated density values for the insulin receptor in the Cornu Ammonis 1 region

Compared groups	IDV difference mean[*]	$P^{\dagger}$
M - SD vs M - HFHSD	-1.54×10^{8}	**< 0.001**
M - SD vs F - SD	-2.62×10^{7}	0.34
M - HFHSD vs M - HFHSD+M	1.53×10^{8}	**< 0.001**
M - HFHSD vs M - HFHSD+L	1.51×10^{8}	**< 0.001**
M - HFHSD vs F - HFHSD	1.57×10^{8}	**< 0.001**
M - HFHSD+M vs F - HFHSD+M	6.78×10^{5}	> 0.9
M - HFHSD+L vs F - HFHSD+L	5.21×10^{6}	> 0.9
F - SD vs F - HFHSD	2.88×10^{7}	0.18
F - HFHSD vs F - HFHSD+M	-3.13×10^{6}	> 0.9
F - HFHSD vs F - HFHSD+L	-8.55×10^{5}	> 0.9

F = female; HFHSD = high-fat high-sugar diet; HFHSD+L = high-fat high-sugar diet treated with liraglutide; HFHSD+M = high-fat high-sugar diet treated with metformin; IDV = integrated density value; M = male; SD = standard diet; *estimated marginal means; †Tukey's post hoc HSD.

Table 5.45. Integrated density values for the insulin receptor in the Cornu Ammonis 3 region

Variable	IDV mean	Two-way ANOVA	
		F value (df)	*P*
Sex			
Male	7.64×10^6	21.135 (1, 121)	**< 0.001**
Female	4.2×10^6		
Group			
SD	5.14×10^6	14.814 (3, 121)	**< 0.001**
HFHSD	2.26×10^6		
HFHSD+M	7.92×10^6		
HFHSD+L	8.36×10^6		
Interaction	-	4.115 (3, 121)	**0.008**

df = degrees of freedom; HFHSD = high-fat high-sugar diet; HFHSD+L = high-fat high-sugar diet treated with liraglutide; HFHSD+M = high-fat high-sugar diet treated with metformin; IDV = integrated density value; SD = standard diet.

Table 5.46. Group-specific pairwise comparisons of integrated density values for the insulin receptor in the Cornu Ammonis 3 region

Compared groups	IDV difference mean[*]	*P*[†]
SD vs HFHSD	2.87×10^6	**0.03**
SD vs HFHSD+M	-3.36×10^6	**0.01**
SD vs HFHSD+L	-2.94×10^6	**0.03**
HFHSD vs HFHSD+M	-6.23×10^6	**< 0.001**
HFHSD vs HFHSD+L	-5.81×10^6	**< 0.001**
HFHSD+M vs HFHSD+L	4.19×10^5	> 0.9

HFHSD = high-fat high-sugar diet; HFHSD+L = high-fat high-sugar diet treated with liraglutide; HFHSD+M = high-fat high-sugar diet treated with metformin; IDV = integrated density value; SD = standard diet; *estimated marginal means; [†]Tukey's post hoc HSD.

Table 5.47. Relevant group-specific and sex-specific pairwise comparisons of integrated density values for the insulin receptor in the Cornu Ammonis 3 region

Compared groups	IDV difference mean*	$P^\dagger$
M - SD vs M - HFHSD	5.59×10^6	**0.005**
M - SD vs F - SD	4.5×10^6	0.06
M - HFHSD vs M - HFHSD+M	-8.99×10^6	**< 0.001**
M - HFHSD vs M - HFHSD+L	-8.75×10^6	**< 0.001**
M - HFHSD vs F - HFHSD	-9.03×10^5	> 0.9
M - HFHSD+M vs F - HFHSD+M	5.74×10^6	**0.009**
M - HFHSD+L vs F - HFHSD+L	4.41×10^6	0.07
F - SD vs F - HFHSD	1.77×10^5	> 0.9
F - HFHSD vs F - HFHSD+M	-2.34×10^6	0.81
F - HFHSD vs F - HFHSD+L	-3.44×10^6	0.23

F = female; HFHSD = high-fat high-sugar diet; HFHSD+L = high-fat high-sugar diet treated with liraglutide; HFHSD+M = high-fat high-sugar diet treated with metformin; IDV = integrated density value; M = male; SD = standard diet; *estimated marginal means; †Tukey's post hoc HSD.

The two-way ANOVA analysis showed significant effects of sex, animal group and their interaction in the DG (Table 5.48) on the expression of IGF-1R, significant effects of animal group and interaction of sex and animal group in the CA1 region (Table 5.51) and a significant effect of sex and animal group in the CA3 region (Table 5.54).

When analyzing the expression of IGF-1R by sex, male rats showed similar dynamics to IDV mean values in all three ROIs. The analysis showed strong immunoreactivity in SD rats, which was much lower in HFHSD rats, with significant differences in IDV mean values in all three ROIs. Following treatment with metformin, there was a significant increase in IGF-1R expression in the CA3 region (Table 5.55, 5.56). Following treatment with liraglutide, there was a significant increase in IGF-1R expression in both the DG (Table 5.49, 5.50) and the CA3 region. In the CA1 region, however, treatment with liraglutide showed a decrease in expression in comparison with their respective HFHSD group, however with no significance (Table 5.52, 5.53).

There were no significant differences in pairwise comparisons of IDV mean values between female groups.

Images of the acquired stains are shown in Figure 5.6.
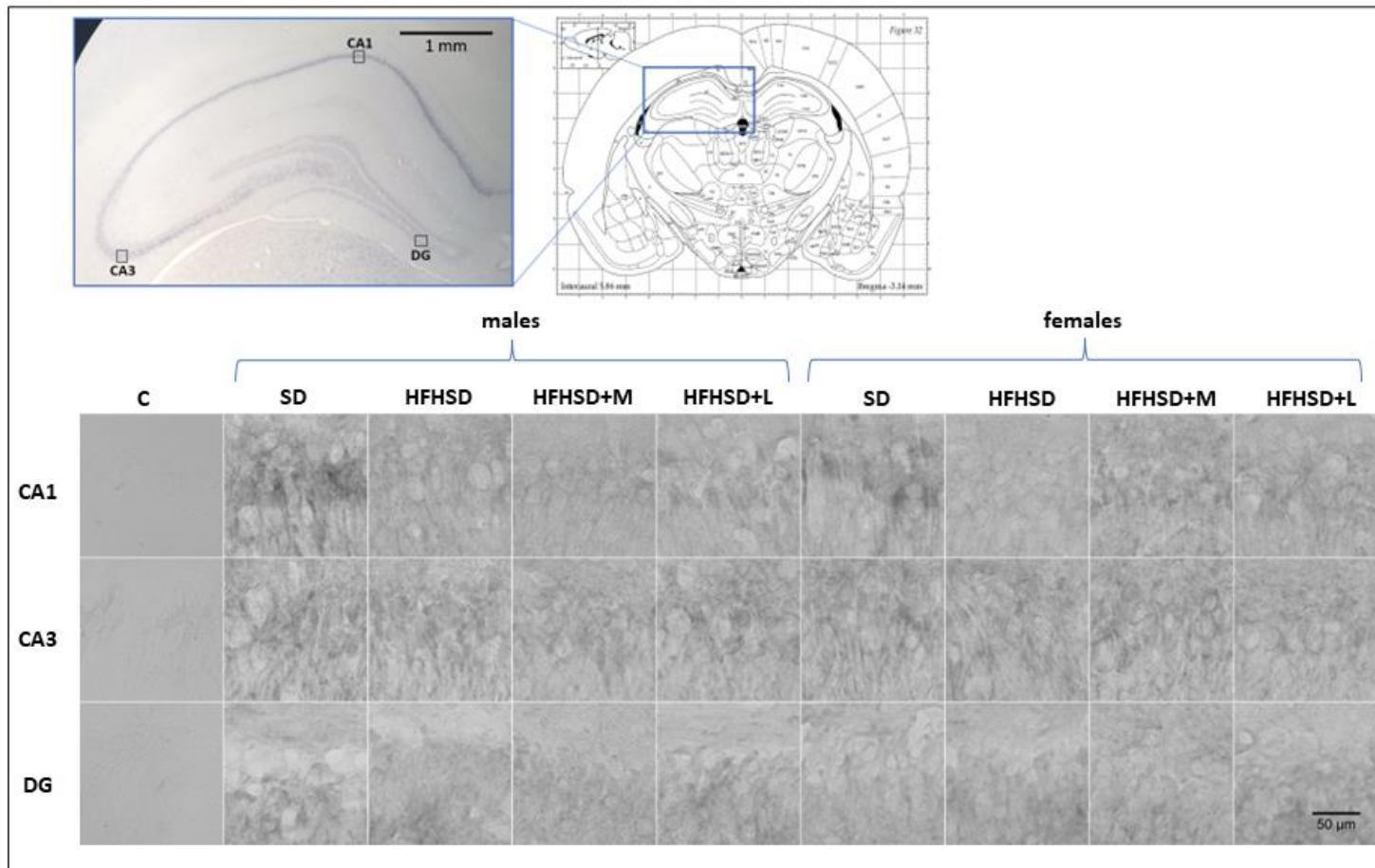
Figure 5.6. Expression of insulin-like growth factor-1 receptor in all animal group hippocampi, organized by region of interest, sex and group.

C – negative control; CA1 – Cornu Ammonis region 1; CA3 – Cornu Ammonis region 3; DG – dentate gyrus; HFHSD – high-fat high-sugar diet; HFHSD+L – HFHSD treated with liraglutide; HFHSD+M – HFHSD treated with metformin; SD – standard diet.

Table 5.48. Integrated density values for the insulin-like growth factor-1 receptor in the dentate gyrus

Variable	IDV mean	Two-way ANOVA	
		F value (df)	*P*
Sex			
Male	1.69×10^7	23.496 (1, 124)	**< 0.001**
Female	9.78×10^6		
Group			
SD	1.85×10^7		
HFHSD	10^7	6.100 (3, 124)	**0.001**
HFHSD+M	1.14×10^7		
HFHSD+L	1.33×10^7		
Interaction	-	5.051 (3, 124)	**0.002**

df = degrees of freedom; HFHSD = high-fat high-sugar diet; HFHSD+L = high-fat high-sugar diet treated with liraglutide; HFHSD+M = high-fat high-sugar diet treated with metformin; IDV = integrated density value; SD = standard diet.

Table 5.49. Group-specific pairwise comparisons of integrated density values for the insulin-like growth factor-1 receptor in the dentate gyrus

Compared groups	IDV difference mean[*]	*P*[†]
SD vs HFHSD	8.48×10^6	**0.001**
SD vs HFHSD+M	7.25×10^6	**0.004**
SD vs HFHSD+L	5.23×10^6	**0.06**
HFHSD vs HFHSD+M	-1.23×10^6	> 0.9
HFHSD vs HFHSD+L	-3.25×10^6	0.38
HFHSD+M vs HFHSD+L	-2.02×10^6	0.74

HFHSD = high-fat high-sugar diet; HFHSD+L = high-fat high-sugar diet treated with liraglutide; HFHSD+M = high-fat high-sugar diet treated with metformin; IDV = integrated density value; SD = standard diet; *estimated marginal means; [†]Tukey's post hoc HSD.

Table 5.50. Relevant group-specific and sex-specific pairwise comparisons of integrated density values for the insulin-like growth factor-1 receptor in the dentate gyrus

Compared groups	IDV difference mean[*]	P[†]
M - SD vs M - HFHSD	1.4×10^7	**< 0.001**
M - SD vs F - SD	1.12×10^7	**0.008**
M - HFHSD vs M - HFHSD+M	-2.72×10^6	> 0.9
M - HFHSD vs M - HFHSD+L	-1.01×10^7	**0.01**
M - HFHSD vs F - HFHSD	2.25×10^5	> 0.9
M - HFHSD+M vs F - HFHSD+M	3×10^6	> 0.9
M - HFHSD+L vs F - HFHSD+L	1.39×10^7	**< 0.001**
F - SD vs F - HFHSD	2.98×10^6	> 0.9
F - HFHSD vs F - HFHSD+M	5.45×10^4	> 0.9
F - HFHSD vs F - HFHSD+L	3.58×10^6	> 0.9

F = female; HFHSD = high-fat high-sugar diet; HFHSD+L = high-fat high-sugar diet treated with liraglutide; HFHSD+M = high-fat high-sugar diet treated with metformin; IDV = integrated density value; M = male; SD = standard diet; *estimated marginal means; †Tukey's post hoc HSD.

Table 5.51. Integrated density values for the insulin-like growth factor-1 receptor in the Cornu Ammonis 1 region

Variable	IDV mean	Two-way ANOVA	
		F value (df)	P
Sex			
Male	1.37×10^7	1.694 (1, 115)	0.2
Female	1.24×10^7		
Group			
SD	1.57×10^7		
HFHSD	1.14×10^7	3.625 (3, 115)	**0.01**
HFHSD+M	1.37×10^7		
HFHSD+L	1.15×10^7		
Interaction	-	3.913 (3, 115)	**0.01**

df = degrees of freedom; HFHSD = high-fat high-sugar diet; HFHSD+L = high-fat high-sugar diet treated with liraglutide; HFHSD+M = high-fat high-sugar diet treated with metformin; IDV = integrated density value; SD = standard diet.

Table 5.52. Group-specific pairwise comparisons of integrated density values for the insulin-like growth factor-1 receptor in the Cornu Ammonis 1 region

Compared groups	IDV difference mean*	$P^{\dagger}$
SD vs HFHSD	3.97×10^6	**0.04**
SD vs HFHSD+M	1.7×10^6	0.67
SD vs HFHSD+L	3.88×10^6	**0.05**
HFHSD vs HFHSD+M	-2.27×10^6	0.39
HFHSD vs HFHSD+L	-8.66×10^4	> 0.9
HFHSD+M vs HFHSD+L	2.18×10^6	0.42

HFHSD = high-fat high-sugar diet; HFHSD+L = high-fat high-sugar diet treated with liraglutide; HFHSD+M = high-fat high-sugar diet treated with metformin; IDV = integrated density value; SD = standard diet; *estimated marginal means; †Tukey's post hoc HSD.

Table 5.53. Relevant group-specific and sex-specific pairwise comparisons of integrated density values for the insulin-like growth factor-1 receptor in the Cornu Ammonis 1 region

Compared groups	IDV difference mean*	$P^{\dagger}$
M - SD vs M - HFHSD	8.93×10^6	**0.002**
M - SD vs F - SD	7.79×10^6	**0.02**
M - HFHSD vs M - HFHSD+M	-2.67×10^6	0.88
M - HFHSD vs M - HFHSD+L	-8.22×10^5	> 0.9
M - HFHSD vs F - HFHSD	-1.54×10^6	> 0.9
M - HFHSD+M vs F - HFHSD+M	-7.83×10^5	> 0.9
M - HFHSD+L vs F - HFHSD+L	-6.56×10^4	> 0.9
F - SD vs F - HFHSD	-3.96×10^5	> 0.9
F - HFHSD vs F - HFHSD+M	-1.91×10^6	> 0.9
F - HFHSD vs F - HFHSD+L	6.51×10^5	> 0.9

F = female; HFHSD = high-fat high-sugar diet; HFHSD+L = high-fat high-sugar diet treated with liraglutide; HFHSD+M = high-fat high-sugar diet treated with metformin; IDV = integrated density value; M = male; SD = standard diet; *estimated marginal means; †Tukey's post hoc HSD.

Table 5.54. Integrated density values for the insulin-like growth factor-1 receptor in the Cornu Ammonis 3 region

Variable	IDV mean	Two-way ANOVA	
		F value (df)	*P*
Sex			
Male	1.22×10^7	18.099 (1, 131)	**< 0.001**
Female	1.58×10^7		
Group			
SD	1.45×10^7		
HFHSD	1.12×10^7	5.536 (3, 131)	**0.001**
HFHSD+M	1.59×10^7		
HFHSD+L	1.42×10^7		
Interaction	-	2.604 (3, 131)	0.05

df = degrees of freedom; HFHSD = high-fat high-sugar diet; HFHSD+L = high-fat high-sugar diet treated with liraglutide; HFHSD+M = high-fat high-sugar diet treated with metformin; IDV = integrated density value; SD = standard diet.

Table 5.55. Group-specific pairwise comparisons of integrated density values for the insulin-like growth factor-1 receptor in the Cornu Ammonis 3 region

Compared groups	IDV difference mean[*]	*P*[†]
SD vs HFHSD	3.4×10^6	**0.03**
SD vs HFHSD+M	-1.41×10^6	0.64
SD vs HFHSD+L	2.6×10^5	> 0.9
HFHSD vs HFHSD+M	-4.81×10^6	**< 0.001**
HFHSD vs HFHSD+L	-3.14×10^6	**0.04**
HFHSD+M vs HFHSD+L	1.67×10^6	0.5

HFHSD = high-fat high-sugar diet; HFHSD+L = high-fat high-sugar diet treated with liraglutide; HFHSD+M = high-fat high-sugar diet treated with metformin; IDV = integrated density value; SD = standard diet; *estimated marginal means; †Tukey's post hoc HSD.

Table 5.56. Relevant group-specific and sex-specific pairwise comparisons of integrated density values for the insulin-like growth factor-1 receptor in the Cornu Ammonis 3 region

Compared groups	IDV difference mean[*]	P[†]
M - SD vs M - HFHSD	5.99×10^6	**0.01**
M - SD vs F - SD	-2.02×10^6	> 0.9
M - HFHSD vs M - HFHSD+M	-6.52×10^6	**0.004**
M - HFHSD vs M - HFHSD+L	-6.08×10^6	**0.01**
M - HFHSD vs F - HFHSD	-7.4×10^6	**0.001**
M - HFHSD+M vs F - HFHSD+M	-3.77×10^6	0.32
M - HFHSD+L vs F - HFHSD+L	-1.24×10^6	> 0.9
F - SD vs F - HFHSD	6.06×10^5	> 0.9
F - HFHSD vs F - HFHSD+M	-2.89×10^6	0.68
F - HFHSD vs F - HFHSD+L	7.7×10^4	> 0.9

F = female; HFHSD = high-fat high-sugar diet; HFHSD+L = high-fat high-sugar diet treated with liraglutide; HFHSD+M = high-fat high-sugar diet treated with metformin; IDV = integrated density value; M = male; SD = standard diet; *estimated marginal means; [†]Tukey's post hoc HSD.

For APP expression, there were significant effects of sex, animal group and their interaction following a two-way ANOVA analysis in all three ROI, except for the effect of sex in the DG, where P values were close to statistical significance, but did not achieve it (P = 0.08) (Table 5.57, 5.60, 5.63).

In the DG (Table 5.58, 5.59), sex-specific comparisons of IDV mean values between the SD and HFHSD groups showed significant differences in female rats only. There was a significant difference between the HFHSD group and the HFHSD-M group of both sexes, where metformin treatment increased the expression of APP. In HFHSD-L groups, there were no significant differences in IDV mean values compared with the HFHSD groups of both sexes.

In the CA1 region (Table 5.61, 5.62), significant differences in IDV mean values in male rats were found between the SD group and the HFHSD group, where a HFHSD decreased expression of APP, as well as between the HFHSD group and HFHSD-M group, where metformin treatment increased APP expression that was higher in IDV mean values than both the SD and HFHSD group. In female rats, significant differences in IDV mean

values were found between the HFHSD group and the HFHSD-M and HFHSD-L group. Compared with the HFHSD group, metformin treatment increased the expression of APP, while liraglutide treatment decreased it to IDV mean values lower than even the SD group.

In the CA3 region (Table 5.64, 5.65), there were no significant differences in IDV mean values between the SD and HFHSD group of both sexes. Metformin treatment significantly increased the expression of APP compared with the HFHSD group in both sexes, while liraglutide treatment significantly increased the expression of APP compared with the HFHSD group in male rats only.

Images of the acquired stains are shown in Figure 5.7.
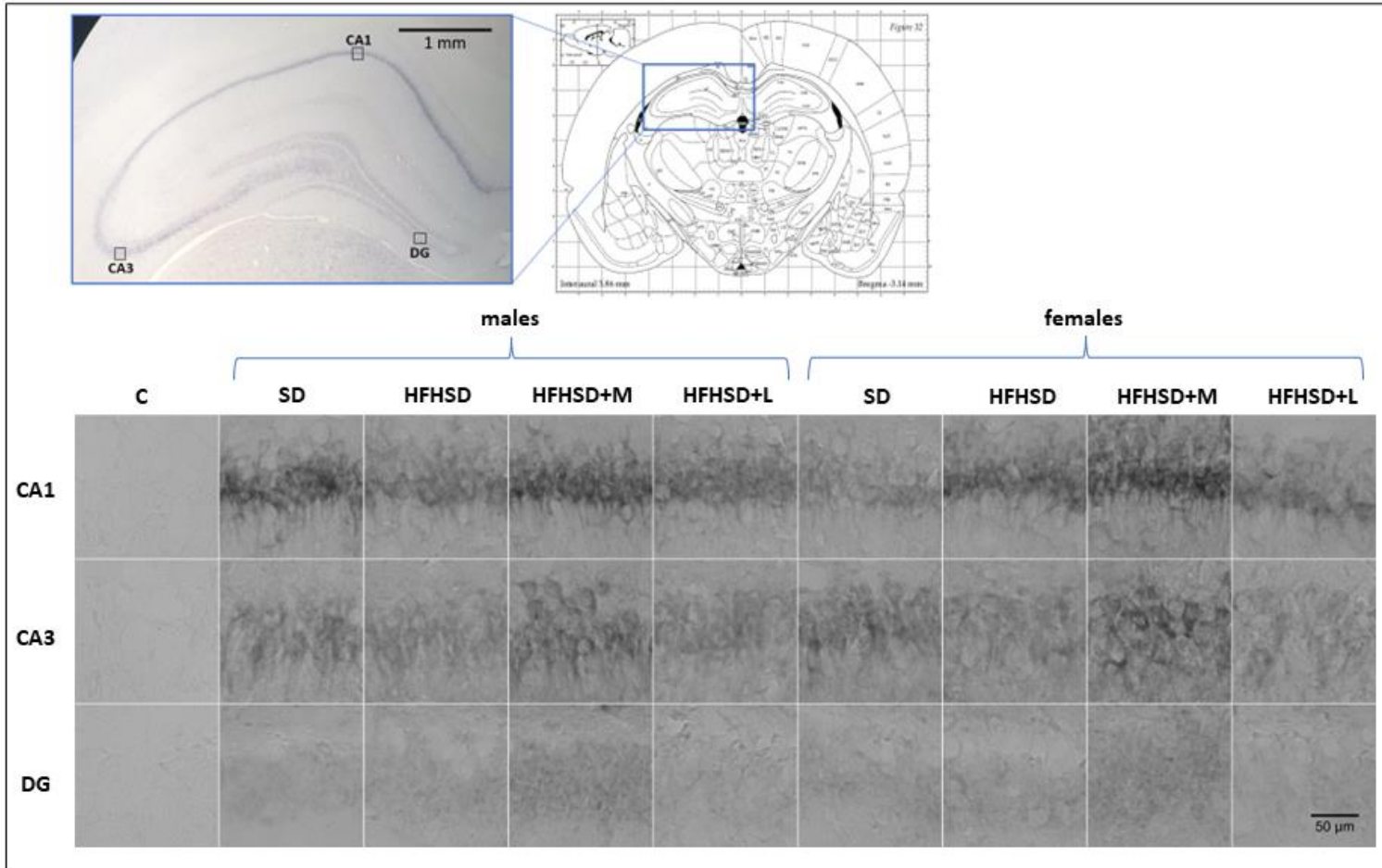
Figure 5.7. Expression of amyloid precursor protein in all animal group hippocampi, organized by region of interest, sex and group. C – negative control; CA1 – Cornu Ammonis region 1; CA3 – Cornu Ammonis region 3; DG – dentate gyrus; HFHSD – high-fat high-sugar diet; HFHSD+L – HFHSD treated with liraglutide; HFHSD+M – HFHSD treated with metformin; SD – standard diet.

Table 5.57. Integrated density values for the amyloid precursor protein in the dentate gyrus

Variable	IDV mean	Two-way ANOVA	
		F value (df)	*P*
Sex			
Male	3.99×10^7	3.123 (1, 108)	0.08
Female	4.2×10^7		
Group			
SD	3.34×10^7		
HFHSD	3.77×10^7	78.093 (3, 108)	**< 0.001**
HFHSD+M	5.63×10^7		
HFHSD+L	3.62×10^7		
Interaction	-	8.108 (3, 108)	**< 0.001**

df = degrees of freedom; HFHSD = high-fat high-sugar diet; HFHSD+L = high-fat high-sugar diet treated with liraglutide; HFHSD+M = high-fat high-sugar diet treated with metformin; IDV = integrated density value; SD = standard diet.

Table 5.58. Group-specific pairwise comparisons of integrated density values for the amyloid precursor protein in the dentate gyrus

| Compared groups	IDV difference mean[*]	*P*[†]
SD vs HFHSD	-3.68×10^6	0.12
SD vs HFHSD+M	-2.34×10^7	**< 0.001**
SD vs HFHSD+L	-2.57×10^6	0.42
HFHSD vs HFHSD+M	-1.97×10^7	**< 0.001**
HFHSD vs HFHSD+L	1.11×10^6	0.9
HFHSD+M vs HFHSD+L	2.08×10^7	**< 0.001**

HFHSD = high-fat high-sugar diet; HFHSD+L = high-fat high-sugar diet treated with liraglutide; HFHSD+M = high-fat high-sugar diet treated with metformin; IDV = integrated density value; SD = standard diet; *estimated marginal means; †Tukey's post hoc HSD.

Table 5.59. Relevant group-specific and sex-specific pairwise comparisons of integrated density values for the amyloid precursor protein in the dentate gyrus

Compared groups	IDV difference mean*	$P^{\dagger}$
M - SD vs M - HFHSD	7.88×10^3	> 0.9
M - SD vs F - SD	4.51×10^6	0.59
M - HFHSD vs M - HFHSD+M	-1.53×10^7	**< 0.001**
M - HFHSD vs M - HFHSD+L	-1.54×10^6	> 0.9
M - HFHSD vs F - HFHSD	-4.1×10^6	0.6
M - HFHSD+M vs F - HFHSD+M	-1.06×10^7	**< 0.001**
M - HFHSD+L vs F - HFHSD+L	1.94×10^6	> 0.9
F - SD vs F - HFHSD	-8.6×10^6	**0.02**
F - HFHSD vs F - HFHSD+M	-2.19×10^7	**< 0.001**
F - HFHSD vs F - HFHSD+L	4.5×10^6	0.6

F = female; HFHSD = high-fat high-sugar diet; HFHSD+L = high-fat high-sugar diet treated with liraglutide; HFHSD+M = high-fat high-sugar diet treated with metformin; IDV = integrated density value; M = male; SD = standard diet; *estimated marginal means; †Tukey's post hoc HSD.

Table 5.60. Integrated density values for the amyloid precursor protein in the Cornu Ammonis 1 region

Variable	IDV mean	Two-way ANOVA	
		F value (df)	P
Sex			
Male	7.12×10^7	31.841 (1, 130)	**< 0.001**
Female	6.2×10^7		
Group			
SD	6.54×10^7		
HFHSD	6.38×10^7	33.873 (3, 130)	**< 0.001**
HFHSD+M	7.99×10^7		
HFHSD+L	5.73×10^7		
Interaction	-	6.288 (3, 130)	**0.001**

df = degrees of freedom; HFHSD = high-fat high-sugar diet; HFHSD+L = high-fat high-sugar diet treated with liraglutide; HFHSD+M = high-fat high-sugar diet treated with metformin; IDV = integrated density value; SD = standard diet.

Table 5.61. Group-specific pairwise comparisons of integrated density values for the amyloid precursor protein in the Cornu Ammonis 1 region

Compared groups	IDV difference mean[*]	P[†]
SD vs HFHSD	1.78×10^6	0.86
SD vs HFHSD+M	-1.41×10^7	**< 0.001**
SD vs HFHSD+L	8.88×10^6	**0.001**
HFHSD vs HFHSD+M	-1.59×10^7	**< 0.001**
HFHSD vs HFHSD+L	7.1×10^6	**0.01**
HFHSD+M vs HFHSD+L	2.3×10^7	**< 0.001**

HFHSD = high-fat high-sugar diet; HFHSD+L = high-fat high-sugar diet treated with liraglutide; HFHSD+M = high-fat high-sugar diet treated with metformin; IDV = integrated density value; SD = standard diet; *estimated marginal means; †Tukey's post hoc HSD.

Table 5.62. Relevant group-specific and sex-specific pairwise comparisons of integrated density values for the amyloid precursor protein in the Cornu Ammonis 1 region

Compared groups	IDV difference mean[*]	P[†]
M - SD vs M - HFHSD	1.02×10^7	**0.03**
M - SD vs F - SD	1.9×10^7	**< 0.001**
M - HFHSD vs M - HFHSD+M	-1.71×10^7	**< 0.001**
M - HFHSD vs M - HFHSD+L	1.17×10^6	> 0.9
M - HFHSD vs F - HFHSD	1.51×10^6	> 0.9
M - HFHSD+M vs F - HFHSD+M	3.74×10^6	> 0.9
M - HFHSD+L vs F - HFHSD+L	1.23×10^7	**0.007**
F - SD vs F - HFHSD	-7.22×10^6	0.33
F - HFHSD vs F - HFHSD+M	-1.49×10^7	**< 0.001**
F - HFHSD vs F - HFHSD+L	1.19×10^7	**0.006**

F = female; HFHSD = high-fat high-sugar diet; HFHSD+L = high-fat high-sugar diet treated with liraglutide; HFHSD+M = high-fat high-sugar diet treated with metformin; IDV = integrated density value; M = male; SD = standard diet; *estimated marginal means; †Tukey's post hoc HSD.

Table 5.63. Integrated density values for the amyloid precursor protein in the Cornu Ammonis 3 region

Variable	IDV mean	Two-way ANOVA	
		F value (df)	*P*
Sex			
Male	6.63×10^7	20.631 (1, 125)	**< 0.001**
Female	5.92×10^7		
Group			
SD	5.97×10^7		
HFHSD	5.56×10^7	61.220 (3, 125)	**< 0.001**
HFHSD+M	8.06×10^7		
HFHSD+L	5.52×10^7		
Interaction	-	18.358 (3, 125)	**< 0.001**

df = degrees of freedom; HFHSD = high-fat high-sugar diet; HFHSD+L = high-fat high-sugar diet treated with liraglutide; HFHSD+M = high-fat high-sugar diet treated with metformin; IDV = integrated density value; SD = standard diet.

Table 5.64. Group-specific pairwise comparisons of integrated density values for the amyloid precursor protein in the Cornu Ammonis 3 region

Compared groups	IDV difference mean[*]	*P*[†]
SD vs HFHSD	5.11×10^6	0.11
SD vs HFHSD+M	-2.06×10^7	**< 0.001**
SD vs HFHSD+L	5.44×10^6	0.08
HFHSD vs HFHSD+M	-2.57×10^7	**< 0.001**
HFHSD vs HFHSD+L	3.31×10^5	> 0.9
HFHSD+M vs HFHSD+L	2.6×10^7	**< 0.001**

HFHSD = high-fat high-sugar diet; HFHSD+L = high-fat high-sugar diet treated with liraglutide; HFHSD+M = high-fat high-sugar diet treated with metformin; IDV = integrated density value; SD = standard diet; *estimated marginal means; †Tukey's post hoc HSD.

Table 5.65. Relevant group-specific and sex-specific pairwise comparisons of integrated density values for the amyloid precursor protein in the Cornu Ammonis 3 region

Compared groups	IDV difference mean[*]	$P^{\dagger}$
M - SD vs M - HFHSD	2.44×10^6	> 0.9
M - SD vs F - SD	8.85×10^6	0.14
M - HFHSD vs M - HFHSD+M	-1.31×10^7	**0.002**
M - HFHSD vs M - HFHSD+L	-2.9×10^6	> 0.9
M - HFHSD vs F - HFHSD	1.23×10^7	**0.003**
M - HFHSD+M vs F - HFHSD+M	-1.16×10^7	**0.006**
M - HFHSD+L vs F - HFHSD+L	1.89×10^7	**< 0.001**
F - SD vs F - HFHSD	5.88×10^6	0.62
F - HFHSD vs F - HFHSD+M	-3.7×10^7	**< 0.001**
F - HFHSD vs F - HFHSD+L	3.74×10^6	> 0.9

F = female; HFHSD = high-fat high-sugar diet; HFHSD+L = high-fat high-sugar diet treated with liraglutide; HFHSD+M = high-fat high-sugar diet treated with metformin; IDV = integrated density value; M = male; SD = standard diet; *estimated marginal means; [†]Tukey's post hoc HSD.

A two-way ANOVA analysis showed that sex was not a significant factor in pTau expression, while animal group and interaction of sex and group showed significance in all three ROI (Table 5.66, 5.69, 5.72). There were no significant differences in IDV mean values between the SD and HFHSD groups in male rats, while there was a significant decrease in IDV mean values of HFHSD female rats compared with their respective SD group in all three ROI.

In the DG (Table 5.67, 5.68), IDV mean values of both male and female rats showed significant decreases in pTau expression in the HFHSD groups compared with the SD group. Metformin treatment had no significant effect on both groups. Liraglutide treatment showed significant, yet opposite effects on animal groups of different sexes – male rats showed a decrease in pTau expression, while female rats showed an increase in pTau expression compared with their respective HFHSD group.

Similarly, IDV mean values in the CA1 region (Table 5.70, 5.71) showed a significant decrease in IDV mean values for HFHSD-L male rats compared with their respective HFHSD group, while HFHSD-L female rats saw an increase in IDV mean values, however, this

difference was not significant. There was, however, a significant decrease in IDV mean values in female HFHSD rats compared with their respective SD group.

Liraglutide treatment had significant effects in the CA3 region as well (Table 5.73, 5.74). Compared with their respective HFHSD groups, IDV mean values in male rats once again saw a significant decrease, while IDV mean values in female rats saw a significant increase.

Metformin treatment did not cause any significant changes in pTau expression in either of the three ROIs.

Images of the acquired stains are shown in Figure 5.8.
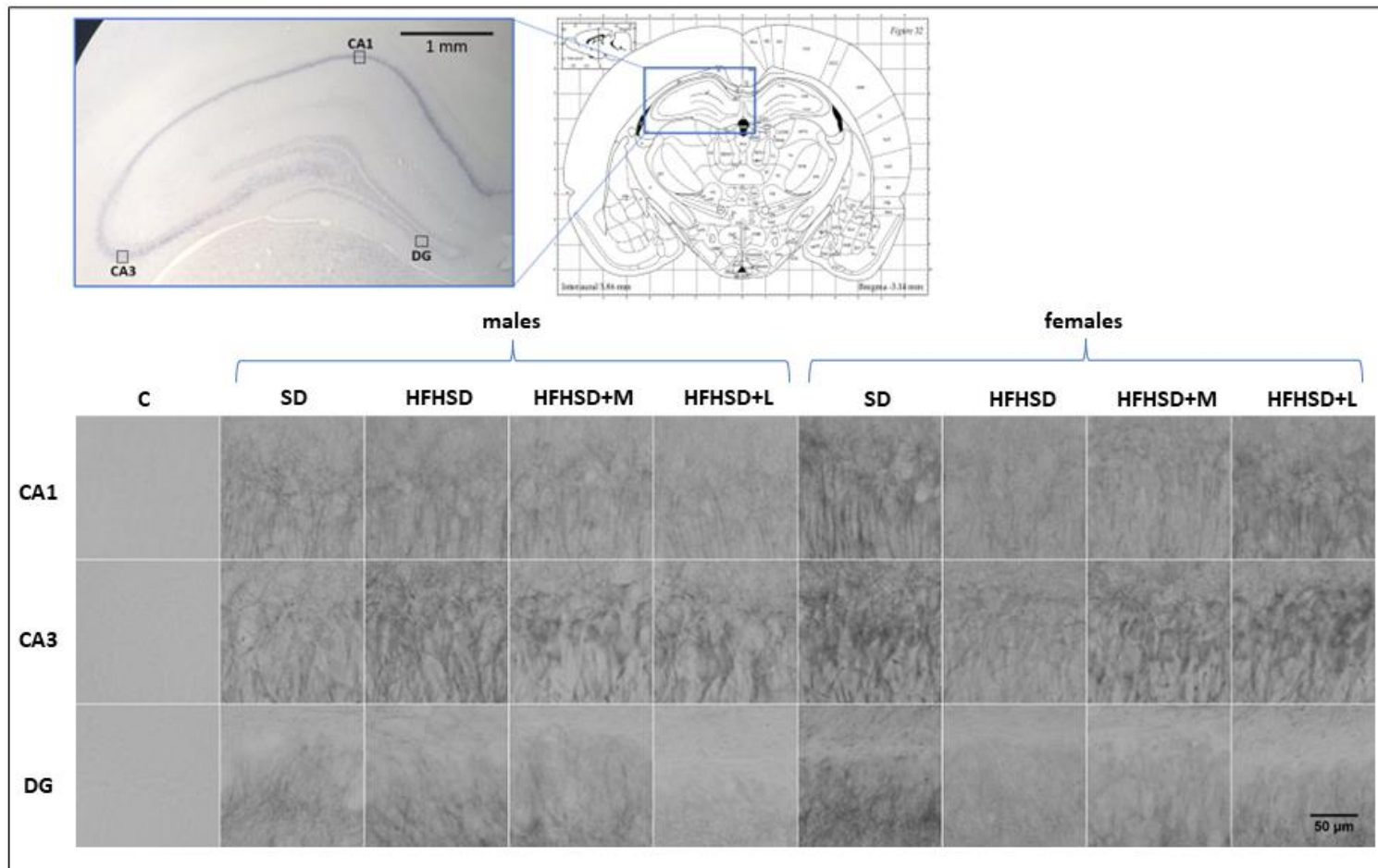
Figure 5.8. Expression of phosphorylated Tau protein in all animal group hippocampi, organized by region of interest, sex and group. C – negative control; CA1 – Cornu Ammonis region 1; CA3 – Cornu Ammonis region 3; DG – dentate gyrus; HFHSD – high-fat high-sugar diet; HFHSD+L – HFHSD treated with liraglutide; HFHSD+M – HFHSD treated with metformin; SD – standard diet.

Table 5.66. Integrated density values for the phosphorylated Tau protein in the dentate gyrus

Variable	IDV mean	Two-way ANOVA	
		F value (df)	*P*
Sex			
Male	4.26×10^7	3.009 (1, 112)	0.09
Female	3.96×10^7		
Group			
SD	5.64×10^7		
HFHSD	3.46×10^7	32.949 (3, 112)	**< 0.001**
HFHSD+M	4.05×10^7		
HFHSD+L	3.29×10^7		
Interaction	-	30.318 (3, 112)	**< 0.001**

df = degrees of freedom; HFHSD = high-fat high-sugar diet; HFHSD+L = high-fat high-sugar diet treated with liraglutide; HFHSD+M = high-fat high-sugar diet treated with metformin; IDV = integrated density value; SD = standard diet.

Table 5.67. Group-specific pairwise comparisons of integrated density values for the phosphorylated Tau protein in the dentate gyrus

Compared groups	IDV difference mean[*]	*P*[†]
SD vs HFHSD	2×10^7	**< 0.001**
SD vs HFHSD+M	1.6×10^7	**< 0.001**
SD vs HFHSD+L	2.39×10^7	**< 0.001**
HFHSD vs HFHSD+M	-3.99×10^6	0.33
HFHSD vs HFHSD+L	3.97×10^6	0.35
HFHSD+M vs HFHSD+L	7.96×10^6	**0.004**

HFHSD = high-fat high-sugar diet; HFHSD+L = high-fat high-sugar diet treated with liraglutide; HFHSD+M = high-fat high-sugar diet treated with metformin; IDV = integrated density value; SD = standard diet; *estimated marginal means; [†]Tukey's post hoc HSD.

Table 5.68. Relevant group-specific and sex-specific pairwise comparisons of integrated density values for the phosphorylated Tau protein in the dentate gyrus

Compared groups	IDV difference mean[*]	$P^{\dagger}$
M - SD vs M - HFHSD	1.12×10^7	**0.02**
M - SD vs F - SD	-2.37×10^6	> 0.9
M - HFHSD vs M - HFHSD+M	-4.79×10^6	0.81
M - HFHSD vs M - HFHSD+L	2.14×10^7	**< 0.001**
M - HFHSD vs F - HFHSD	1.87×10^7	**< 0.001**
M - HFHSD+M vs F - HFHSD+M	1.66×10^7	**< 0.001**
M - HFHSD+L vs F - HFHSD+L	-2.07×10^7	**< 0.001**
F - SD vs F - HFHSD	3.23×10^7	**< 0.001**
F - HFHSD vs F - HFHSD+M	-6.89×10^6	0.51
F - HFHSD vs F - HFHSD+L	-1.8×10^7	**< 0.001**

F = female; HFHSD = high-fat high-sugar diet; HFHSD+L = high-fat high-sugar diet treated with liraglutide; HFHSD+M = high-fat high-sugar diet treated with metformin; IDV = integrated density value; M = male; SD = standard diet; [*]estimated marginal means; [†]Tukey's post hoc HSD.

Table 5.69. Integrated density values for the phosphorylated Tau protein in the Cornu Ammonis 1 region

Variable	IDV mean	Two-way ANOVA	
		F value (df)	P
Sex			
Male	5.93×10^7	0.230 (1, 118)	0.63
Female	5.84×10^7		
Group			
SD	6.91×10^7		
HFHSD	6.04×10^7	17.318 (3, 118)	**< 0.001**
HFHSD+M	5.48×10^7		
HFHSD+L	5.1×10^7		
Interaction	-	30.021 (3, 118)	**< 0.001**

df = degrees of freedom; HFHSD = high-fat high-sugar diet; HFHSD+L = high-fat high-sugar diet treated with liraglutide; HFHSD+M = high-fat high-sugar diet treated with metformin; IDV = integrated density value; SD = standard diet.

Table 5.70. Group-specific pairwise comparisons of integrated density values for the phosphorylated Tau protein in the Cornu Ammonis 1 region

Compared groups	IDV difference mean*	$P^{\dagger}$
SD vs HFHSD	8.14×10^{6}	**0.01**
SD vs HFHSD+M	1.32×10^{7}	**< 0.001**
SD vs HFHSD+L	1.69×10^{7}	**< 0.001**
HFHSD vs HFHSD+M	5.05×10^{6}	0.18
HFHSD vs HFHSD+L	8.75×10^{6}	**0.002**
HFHSD+M vs HFHSD+L	3.7×10^{6}	0.46

HFHSD = high-fat high-sugar diet; HFHSD+L = high-fat high-sugar diet treated with liraglutide; HFHSD+M = high-fat high-sugar diet treated with metformin; IDV = integrated density value; SD = standard diet; *estimated marginal means; †Tukey's post hoc HSD.

Table 5.71. Relevant group-specific and sex-specific pairwise comparisons of integrated density values for the phosphorylated Tau protein in the Cornu Ammonis 1 region

Compared groups	IDV difference mean*	$P^{\dagger}$
M - SD vs M - HFHSD	-2.21×10^{6}	> 0.9
M - SD vs F - SD	-6.85×10^{6}	0.68
M - HFHSD vs M - HFHSD+M	3.7×10^{6}	> 0.9
M - HFHSD vs M - HFHSD+L	2.83×10^{7}	**< 0.001**
M - HFHSD vs F - HFHSD	1.49×10^{7}	**0.001**
M - HFHSD+M vs F - HFHSD+M	1.83×10^{7}	**< 0.001**
M - HFHSD+L vs F - HFHSD+L	-2.29×10^{7}	**< 0.001**
F - SD vs F - HFHSD	1.95×10^{7}	**< 0.001**
F - HFHSD vs F - HFHSD+M	7.36×10^{6}	0.46
F - HFHSD vs F - HFHSD+L	-9.46×10^{6}	0.1

F = female; HFHSD = high-fat high-sugar diet; HFHSD+L = high-fat high-sugar diet treated with liraglutide; HFHSD+M = high-fat high-sugar diet treated with metformin; IDV = integrated density value; M = male; SD = standard diet; *estimated marginal means; †Tukey's post hoc HSD.

Table 5.72. Integrated density values for the phosphorylated Tau protein in the Cornu Ammonis 3 region

Variable	IDV mean	Two-way ANOVA	
		F value (df)	*P*
Sex			
Male	6.17×10^7	2.242 (1, 123)	0.14
Female	6.47×10^7		
Group			
SD	7.58×10^7		
HFHSD	6.11×10^7	17.045 (3, 123)	**< 0.001**
HFHSD+M	6.03×10^7		
HFHSD+L	5.56×10^7		
Interaction	-	24.083 (3, 123)	**< 0.001**

df = degrees of freedom; HFHSD = high-fat high-sugar diet; HFHSD+L = high-fat high-sugar diet treated with liraglutide; HFHSD+M = high-fat high-sugar diet treated with metformin; IDV = integrated density value; SD = standard diet.

Table 5.73. Group-specific pairwise comparisons of integrated density values for the phosphorylated Tau protein in the Cornu Ammonis 3 region

Compared groups	IDV difference mean[*]	*P*[†]
SD vs HFHSD	1.47×10^7	**< 0.001**
SD vs HFHSD+M	1.54×10^7	**< 0.001**
SD vs HFHSD+L	2.01×10^7	**< 0.001**
HFHSD vs HFHSD+M	7.39×10^5	0.8
HFHSD vs HFHSD+L	5.46×10^6	0.05
HFHSD+M vs HFHSD+L	4.73×10^6	0.09

HFHSD = high-fat high-sugar diet; HFHSD+L = high-fat high-sugar diet treated with liraglutide; HFHSD+M = high-fat high-sugar diet treated with metformin; IDV = integrated density value; SD = standard diet; *estimated marginal means; †Tukey's post hoc HSD.

Table 5.74. Relevant group-specific and sex-specific pairwise comparisons of integrated density values for the phosphorylated Tau protein in the Cornu Ammonis 3 region

Compared groups	IDV difference mean[*]	P[†]
M - SD vs M - HFHSD	-4.24×10^6	> 0.9
M - SD vs F - SD	-1.92×10^7	**< 0.001**
M - HFHSD vs M - HFHSD+M	5.46×10^6	0.88
M - HFHSD vs M - HFHSD+L	2.52×10^7	**< 0.001**
M - HFHSD vs F - HFHSD	1.86×10^7	**< 0.001**
M - HFHSD+M vs F - HFHSD+M	9.18×10^6	0.3
M - HFHSD+L vs F - HFHSD+L	-2.08×10^7	**< 0.001**
F - SD vs F - HFHSD	3.36×10^7	**< 0.001**
F - HFHSD vs F - HFHSD+M	-3.98×10^6	> 0.9
F - HFHSD vs F - HFHSD+L	-1.43×10^7	**0.011**

F = female; HFHSD = high-fat high-sugar diet; HFHSD+L = high-fat high-sugar diet treated with liraglutide; HFHSD+M = high-fat high-sugar diet treated with metformin; IDV = integrated density value; M = male; SD = standard diet; *estimated marginal means; †Tukey's post hoc HSD.

5.3. MALDI-TOF mass spectrometric analysis

The MALDI-TOF mass spectrometric analysis identified significant ($P < 0.05$) changes in signals between compared animal groups for 53 unique compounds. 26 of these compounds were lipids, with an additional ten compounds directly related to the ethiopathogenesis of the researched topic (five carbohydrates and five vitamins and cofactors). The remaining identified compounds were amino acids and purine and pyrimidine metabolites.

In terms of the sex-specific distribution of these compounds, there was a 64.15% overlap in identified compounds (34 of 53). There were seven compounds uniquely identified in male rats and 12 compounds uniquely identified in female rats, for a total of 41 compounds identified in male rats and 46 compounds identified in female rats.

All the identified compounds were grouped based on their structure:

- Lipids
    - Fatty acids
    - Steroids
    - Sphingolipids and glycerophospholipids
- Vitamins and cofactors
- Carbohydrates
- Other compounds
    - Purines and pyrimidines
    - Amino acids
    - Miscellaneous compounds

Several compounds identified by the MALDI-TOF spectrometric analysis (not included in the final count of 54 compounds) were excluded from the final results and analysis since the only statistically significant differences were found between the SD group and groups treated with either metformin or liraglutide. This difference was deemed irrelevant to the aims of the research, since it did not reveal changes to the lipidome following a HFHSD, nor did it reveal significant changes following pharmacotherapy in comparison with the HFHSD group.

The tables are separated by sex and include only compounds with significantly altered signal changes and show t values between groups of most significant to the research – SD vs HFHSD to confirm changes following the HFHSD diet and HFHSD vs HFHSD-M and HFHSD-L to show effects of metformin and liraglutide treatment. The t values are a direct

reflection of changes of the spectrometric signal and have both positive and negative values, based on whether or not a certain animal group showed a significant increase (positive value) or decrease (negative value) in signal of a compound when compared to another group. Since not all identified compounds showed significant signal changes between all three of the observed comparisons, those spaces were left blank. The tables include the compounds' KEGG identification numbers as well as all of their used names, full and abbreviated.

Using the KEGG database, the spectrometric analysis also produced a list of all the significantly altered metabolic pathways based on the identified compounds.

5.3.1. Identified compounds

A total of 16 unique fatty acid metabolites were identified. Five of these were unique to female rats, while one was unique to male rats. Coenzyme A (CoA) was added to this table, even though it is featured in the tables showing identified vitamins and cofactors (Table 5.81, Table 5.82), due to its relevance and role in multiple metabolic pathways regarding lipid metabolism.

A majority of the identified compounds were significantly altered after a HFHSD. Male rats showed a better response to liraglutide treatment, while female rats showed a better response to metformin treatment. Identified lipids included polyunsaturated fatty acids (PUFA), fatty acyl-CoAs, and FFAs. Every identified compound in male rats showed a significantly increased signal between the SD and HFHSD groups, while most, but not all identified compounds in female rats had the same alteration.

Two compounds identified in male rats and three compounds identified in female rats reacted with multiple adducts.

Table 5.75. Identified compounds related to fatty acid biosynthesis and metabolism showing statistically significant differences in signal following MALDI-TOF spectrometry between male rat groups ($P < 0.05$)

Identifier				t score		
KEGG ID	**m/z ratio**	**Adducts**	**Compound**	**SD vs HFHSD**	**HFHSD vs HFHSD-M**	**HFHSD vs HFHSD-L**
C01571	231,2	HAc-H	Decanoic acid; Decanoate; Decylic acid; n-Capric acid	*NI*	-3.36	*NI*
C01530	283,3	M-H	Octadecanoic acid; Stearate; Stearic acid	5.25	*NI*	-4.64
C16525	291,3	M+H-H2O	Icosadienoic acid; Eicosadienoic acid; 11,14-Icosadienoic acid; (11Z,14Z)-Icosa-11,14-dienoic acid; 11,14-Eicosadienoic acid; (11Z,14Z)-Eicosa-11,14-dienoic acid	17.49	*NI*	*NI*
C16526	291,3	M-H2O-H	Icosenoic acid; Eicosenoic acid; 11-Icosenoic acid; 11-Eicosenoic acid; (11Z)-Icosenoic acid; (11Z)-Eicosenoic acid; (Z)-Icosa-11-enoic acid	14.43	*NI*	5.04
C16526	293,3	M+H-H2O	Icosenoic acid; Eicosenoic acid; 11-Icosenoic acid; 11-Eicosenoic acid; (11Z)-Icosenoic acid; (11Z)-Eicosenoic acid; (Z)-Icosa-11-enoic acid	8.97	*NI*	*NI*
C16526	309,3	M-H	Icosenoic acid; Eicosenoic acid; 11-Icosenoic acid; 11-Eicosenoic acid; (11Z)-Icosenoic acid; (11Z)-Eicosenoic acid; (Z)-Icosa-11-enoic acid	5.13	*NI*	3.76

KEGG = Kyoto Encyclopaedia of Genes and Genomes; HFHSD = high-fat high-sugar diet; HFHSD+L = high-fat high-sugar diet treated with liraglutide; HFHSD+M = high-fat high-sugar diet treated with metformin; MALDI-TOF = matrix-assisted laser desorption/ionization time-of-flight; m/z = mass to charge; NI = not identified; SD = standard diet.

Table 5.75. (continued) Identified compounds related to fatty acid biosynthesis and metabolism showing statistically significant differences in signal following MALDI-TOF spectrometry between male rat groups ($P < 0.05$)

Identifier				t score		
KEGG ID	m/z ratio	Adducts	Compound	SD vs HFHSD	HFHSD vs HFHSD-M	HFHSD vs HFHSD-L
C08281	323,3	M+H-H2O	Docosanoic acid; Docosanoate; Behenic acid	18.42	*NI*	*NI*
C16527	331,3	M-H	Adrenic acid; 7,10,13,16-Docosatetraenoic acid; (7Z,10Z,13Z,16Z)-Docosa-7,10,13,16-tetraenoic acid; 7Z,10Z,13Z,16Z-Docosatetraenoic acid	5.72	*NI*	-5.93
C16533	335,3	M-H	(13Z,16Z)-Docosadienoic acid; (13Z,16Z)-Docosa-13,16-dienoic acid; 13Z,16Z-Docosadienoic acid	*NI*	21.45	20.1
C16533	337,3	M+H	(13Z,16Z)-Docosadienoic acid; (13Z,16Z)-Docosa-13,16-dienoic acid; 13Z,16Z-Docosadienoic acid	2.83	*NI*	*NI*
C02990	438,3	M+K	L-Palmitoylcarnitine	6.46	*NI*	-3.06
C00010	750,1	M+H-H2O	CoA; Coenzyme A; CoA-SH	2.27	*NI*	-3.12
C05269	878,2	M-H	3-Oxohexanoyl-CoA; 3-Ketohexanoyl-CoA	10.44	*NI*	-3.66
C05267	888,2	M-H2O-H	3-Oxooctanoyl-CoA	6.89	*NI*	*NI*
C14794	307,2	M-H2O-H	2,3-Dinor-8-iso prostaglandin F2α; 2,3-Dinor-8-iso PGF2α	8.43	-2.49	-5.94

KEGG = Kyoto Encyclopaedia of Genes and Genomes; HFHSD = high-fat high-sugar diet; HFHSD+L = high-fat high-sugar diet treated with liraglutide; HFHSD+M = high-fat high-sugar diet treated with metformin; MALDI-TOF = matrix-assisted laser desorption/ionization time-of-flight; m/z = mass to charge; NI = not identified; SD = standard diet.

Table 5.76. Identified compounds related to fatty acid biosynthesis and metabolism showing statistically significant differences in signal following MALDI-TOF spectrometry between female rat groups ($P < 0.05$)

KEGG ID	m/z ratio	Adducts	Compound	SD vs HFHSD	HFHSD vs HFHSD-M	HFHSD vs HFHSD-L
			Identifier		**t score**	
C01530	283,3	M-H	Octadecanoic acid; Stearate; Stearic acid	-5.41	*NI*	-3.81
C16525	289,3	M-H2O-H	Icosadienoic acid; Eicosadienoic acid; 11,14-Icosadienoic acid; (11Z,14Z)-Icosa-11,14-dienoic acid; 11,14-Eicosadienoic acid; (11Z,14Z)-Eicosa-11,14-dienoic acid	27.41	5.62	*NI*
C16526	291,3	M-H2O-H	Icosenoic acid; Eicosenoic acid; 11-Icosenoic acid; 11-Eicosenoic acid; (11Z)-Icosenoic acid; (11Z)-Eicosenoic acid; (Z)-Icosa-11-enoic acid	12.69	-7.32	-8.36
C16526	293,3	M+H-H2O	Icosenoic acid; Eicosenoic acid; 11-Icosenoic acid; 11-Eicosenoic acid; (11Z)-Icosenoic acid; (11Z)-Eicosenoic acid; (Z)-Icosa-11-enoic acid	*NI*	-3.35	*NI*
C08281	323,3	M+H-H2O	Docosanoic acid; Docosanoate; Behenic acid	4.52	-3.46	*NI*
C16527	331,3	M-H	Adrenic acid; 7,10,13,16-Docosatetraenoic acid; (7Z,10Z,13Z,16Z)-Docosa-7,10,13,16-tetraenoic acid; 7Z,10Z,13Z,16Z-Docosatetraenoic acid	*NI*	-29.64	*NI*

KEGG = Kyoto Encyclopaedia of Genes and Genomes; HFHSD = high-fat high-sugar diet; HFHSD+L = high-fat high-sugar diet treated with liraglutide; HFHSD+M = high-fat high-sugar diet treated with metformin; MALDI-TOF = matrix-assisted laser desorption/ionization time-of-flight m/z = mass to charge; NI = not identified; SD = standard diet.

Table 5.76. (continued) Identified compounds related to fatty acid biosynthesis and metabolism showing statistically significant differences in signal following MALDI-TOF spectrometry between female rat groups ($P < 0.05$)

Identifier				t score		
KEGG ID	**m/z ratio**	**Adducts**	**Compound**	**SD vs HFHSD**	**HFHSD vs HFHSD-M**	**HFHSD vs HFHSD-L**
C16533	335,3	M-H	(13Z,16Z)-Docosadienoic acid; (13Z,16Z)-Docosa-13,16-dienoic acid; 13Z,16Z-Docosadienoic acid	9.74	-8.22	-7.2
C16533	337,3	M+H	(13Z,16Z)-Docosadienoic acid; (13Z,16Z)-Docosa-13,16-dienoic acid; 13Z,16Z-Docosadienoic acid	*NI*	-3.62	*NI*
C02990	438,3	M+K	L-Palmitoylcarnitine	-5.38	*NI*	*NI*
C00010	750,1	M+H-H2O	CoA; Coenzyme A; CoA-SH	-4.35	*NI*	*NI*
C05269	878,2	M-H	3-Oxohexanoyl-CoA; 3-Ketohexanoyl-CoA	-22.3	*NI*	*NI*
C05267	888,2	M-H2O-H	3-Oxooctanoyl-CoA	-7.8	-3.69	-3.05
C05267	906,2	M-H	3-Oxooctanoyl-CoA	26.65	*NI*	*NI*
C05270	888,2	M+Na	Hexanoyl-CoA	*NI*	-2.69	*NI*
C05276	909,2	M+NH4	trans-Oct-2-enoyl-CoA; (2E)-Octenoyl-CoA	2.72	-3.13	*NI*
C05266	910,2	M+H	(S)-3-Hydroxyoctanoyl-CoA; (S)-3-Hydroxycapryloyl-CoA; (S)-Hydroxyoctanoyl-CoA	3.31	-3.08	*NI*
C01944	916,2	M+Na	Octanoyl-CoA	4.48	-3.65	*NI*
C02232	948,1	M+K	3-Oxoadipyl-CoA; beta-Ketoadipyl-CoA	*NI*	-2.69	*NI*
C14794	307,2	M-H2O-H	2,3-Dinor-8-iso prostaglandin F2α; 2,3-Dinor-8-iso PGF2α	-6.12	*NI*	-4.32

KEGG = Kyoto Encyclopaedia of Genes and Genomes; HFHSD = high-fat high-sugar diet; HFHSD+L = high-fat high-sugar diet treated with liraglutide; HFHSD+M = high-fat high-sugar diet treated with metformin; MALDI-TOF = matrix-assisted laser desorption/ionization time-of-flight; m/z = mass to charge; NI = not identified; SD = standard diet.

A total of five sphingolipid and glycerophospholipid metabolites were identified with significant changes in signal. One compound was unique to male rats [cytidine diphosphate (CDP)-ethanolamine]. CDP-ethanolamine was also the only compound not to show a significant change in signal between the SD and HFHSD groups. While Table 5.79 and Table 5.80 show certain gaps in the SD vs HFHSD group column for other compounds, these are all compounds with reactions with multiple adducts, with at least one showing a significant change in signal between these two groups. Groups treated with metformin or liraglutide showed significant differences in signal compared to the HFHSD group, with male rats responding better to liraglutide treatment and female rats responding better to metformin treatment.

A total of five compounds with significant changes in signal were identified that are related to steroid hormone biosynthesis and metabolism. These metabolites were more affected in male rats, as two identified compounds were unique to them (androstenedione and pregnenolone sulfate). Pharmacotherapy showed certain significant changes in signal, with liraglutide showing no effect in female rats. Estrone glucuronide reacted with multiple adducts in female rats.

Table 5.77. Identified compounds related to sphingolipid and glycerophospholipid biosynthesis and metabolism showing statistically significant differences in signal following MALDI-TOF spectrometry between male rat groups ($P < 0.05$)

Identifier				t score		
KEGG ID	**m/z ratio**	**Adducts**	**Compound**	**SD vs HFHSD**	**HFHSD vs HFHSD-M**	**HFHSD vs HFHSD-L**
C00836	282,3	M-H2O-H	Sphinganine; Dihydrosphingosine; 2-Amino-1,3-dihydroxyoctadecane	4.36	*NI*	*NI*
C01120	404,3	M+Na	Sphinganine 1-phosphate; Dihydrosphingosine 1-phosphate	*NI*	2.91	3.65
C01120	420,2	M+K	Sphinganine 1-phosphate; Dihydrosphingosine 1-phosphate	4.45	*NI*	*NI*
C00570	445,1	M-H	CDP-ethanolamine; Cytidine diphosphate ethanolamine	*NI*	*NI*	7.72
C20518	755,6	M+Na	2,3-Bis-(O-phytanyl)-sn-glycerol 1-phosphate	4.27	*NI*	-3.89
C20466	804,6	M+H	2,3-Bis-O-(geranylgeranyl)-sn-glycero-1-phospho-L-serine	6.42	*NI*	-4.22
C20466	821,6	M+NH4	2,3-Bis-O-(geranylgeranyl)-sn-glycero-1-phospho-L-serine	*NI*	7.04	*NI*
C20466	862,6	HAc-H	2,3-Bis-O-(geranylgeranyl)-sn-glycero-1-phospho-L-serine	7.51	*NI*	*NI*

KEGG = Kyoto Encyclopaedia of Genes and Genomes; HFHSD = high-fat high-sugar diet; HFHSD+L = high-fat high-sugar diet treated with liraglutide; HFHSD+M = high-fat high-sugar diet treated with metformin; MALDI-TOF = matrix-assisted laser desorption/ionization time-of-flight; m/z = mass to charge; NI = not identified; SD = standard diet.

Table 5.78. Identified compounds related to sphingolipid and glycerophospholipid biosynthesis and metabolism showing statistically significant differences in signal following MALDI-TOF spectrometry between female rat groups ($P < 0.05$)

Identifier				t score		
KEGG ID	**m/z ratio**	**Adducts**	**Compound**	**SD vs HFHSD**	**HFHSD vs HFHSD-M**	**HFHSD vs HFHSD-L**
C00836	282,3	M-H2O-H	Sphinganine; Dihydrosphingosine; 2-Amino-1,3-dihydroxyoctadecane	-5.87	*NI*	-3.39
C00836	336,3	M+Cl	Sphinganine; Dihydrosphingosine; 2-Amino-1,3-dihydroxyoctadecane	11.6	-9.37	-8.37
C01120	404,3	M+Na	Sphinganine 1-phosphate; Dihydrosphingosine 1-phosphate	5.24	-4.04	*NI*
C20518	755,6	M+Na	2,3-Bis-(O-phytanyl)-sn-glycerol 1-phosphate	-3.63	*NI*	*NI*
C20466	804,6	M+H	2,3-Bis-O-(geranylgeranyl)-sn-glycero-1-phospho-L-serine	-2.8	-2.76	*NI*
C20466	821,6	M+NH4	2,3-Bis-O-(geranylgeranyl)-sn-glycero-1-phospho-L-serine	-3.91	*NI*	*NI*

KEGG = Kyoto Encyclopaedia of Genes and Genomes; HFHSD = high-fat high-sugar diet; HFHSD+L = high-fat high-sugar diet treated with liraglutide; HFHSD+M = high-fat high-sugar diet treated with metformin; MALDI-TOF = matrix-assisted laser desorption/ionization time-of-flight; m/z = mass to charge; NI = not identified; SD = standard diet.

Table 5.79. Identified compounds related to steroid hormone biosynthesis and metabolism showing statistically significant differences in signal following MALDI-TOF spectrometry between male rat groups ($P < 0.05$)

Identifier				t score		
KEGG ID	m/z ratio	Adducts	Compound	SD vs HFHSD	HFHSD vs HFHSD-M	HFHSD vs HFHSD-L
C00280	321,2	M+Cl	Androstenedione; Androst-4-ene-3,17-dione; 4-Androstene-3,17-dione	-9.1	-5.05	-2.46
C18044	419,2	M+Na	3beta-Hydroxypregn-5-en-20-one sulfate; Pregnenolone sulfate	4.44	*NI*	*NI*
C08358	439,1	HAc-H	2-Methoxyestrone 3-sulfate	6.48	-3.24	*NI*
C11133	469,2	M+Na	Estrone glucuronide; Estrone 3-glucuronide; Estrone beta-D-glucuronide	13.93	*NI*	*NI*
C18043	505,3	M+K	Cholesterol sulfate; Cholest-5-en-3beta-ol sulfate	4.5	*NI*	-4.59

KEGG = Kyoto Encyclopaedia of Genes and Genomes; HFHSD = high-fat high-sugar diet; HFHSD+L = high-fat high-sugar diet treated with liraglutide; HFHSD+M = high-fat high-sugar diet treated with metformin; MALDI-TOF = matrix-assisted laser desorption/ionization time-of-flight; m/z = mass to charge; NI = not identified; SD = standard diet.

Table 5.80. Identified compounds related to steroid hormone biosynthesis and metabolism showing statistically significant differences in signal following MALDI-TOF spectrometry between female rat groups ($P < 0.05$)

Identifier				t score		
KEGG ID	m/z ratio	Adducts	Compound	SD vs HFHSD	HFHSD vs HFHSD-M	HFHSD vs HFHSD-L
C08358	439,1	HAc-H	2-Methoxyestrone 3-sulfate	-3.2	*NI*	*NI*
C11133	464,2	M+NH4	Estrone glucuronide; Estrone 3-glucuronide; Estrone beta-D-glucuronide	4.54	-3.69	*NI*
C11133	469,2	M+Na	Estrone glucuronide; Estrone 3-glucuronide; Estrone beta-D-glucuronide	*NI*	-2.82	*NI*
C18043	505,3	M+K	Cholesterol sulfate; Cholest-5-en-3beta-ol sulfate	-5.49	*NI*	*NI*

KEGG = Kyoto Encyclopaedia of Genes and Genomes; HFHSD = high-fat high-sugar diet; HFHSD+L = high-fat high-sugar diet treated with liraglutide; HFHSD+M = high-fat high-sugar diet treated with metformin; MALDI-TOF = matrix-assisted laser desorption/ionization time-of-flight; m/z = mass to charge; NI = not identified; SD = standard diet.

In the group of vitamins and cofactors, a total of five compounds were identified showing significant changes in signal between observed groups. Three of these were unique to both sexes, with each sex having one unique compound – reduced nicotinamide adenine dinucleotide (NADH) in male rats and thiamine diphosphate in female rats. Significant changes in signal in all three observed comparisons were present, with female rats showing a predominant response to metformin treatment.

In the relevant observed comparisons, a total of five carbohydrates were identified. Two of them were unique to female rats - GDP-mannose and stachyose. There were significant changes in signal following both metformin and liraglutide treatment in male rats, while female rats responded better to metformin treatment.

Table 5.81. Identified vitamins and cofactors showing statistically significant differences in signal following MALDI-TOF spectrometry between male rat groups ($P < 0.05$)

Identifier				t score		
KEGG ID	m/z ratio	Adducts	Compound	SD vs HFHSD	HFHSD vs HFHSD-M	HFHSD vs HFHSD-L
C00101	444,2	M-H	Tetrahydrofolate; 5,6,7,8-Tetrahydrofolate; Tetrahydrofolic acid; THF; (6S)-Tetrahydrofolate; (6S)-Tetrahydrofolic acid; (6S)-THFA	*NI*	*NI*	6.02
C00061	455,1	M-H	FMN; Riboflavin-5-phosphate; Flavin mononucleotide	4.86	-2.53	*NI*
C00061	479,1	M+Na	FMN; Riboflavin-5-phosphate; Flavin mononucleotide	5.32	*NI*	*NI*
C00004	704,1	M+K	NADH; DPNH; Reduced nicotinamide adenine dinucleotide	-2.74	*NI*	*NI*
C00010	750,1	M+H-H2O	CoA; Coenzyme A; CoA-SH	2.27	*NI*	-3.12

KEGG = Kyoto Encyclopaedia of Genes and Genomes; HFHSD = high-fat high-sugar diet; HFHSD+L = high-fat high-sugar diet treated with liraglutide; HFHSD+M = high-fat high-sugar diet treated with metformin; MALDI-TOF = matrix-assisted laser desorption/ionization time-of-flight; m/z = mass to charge; NI = not identified; SD = standard diet.

Table 5.82. Identified vitamins and cofactors showing statistically significant differences in signal following MALDI-TOF spectrometry between female rat groups (*P* < 0.05)

Identifier				t score		
KEGG ID	**m/z ratio**	**Adducts**	**Compound**	**SD vs HFHSD**	**HFHSD vs HFHSD-M**	**HFHSD vs HFHSD-L**
C00101	444,2	M-H	Tetrahydrofolate; 5,6,7,8-Tetrahydrofolate; Tetrahydrofolic acid; THF; (6S)-Tetrahydrofolate; (6S)-Tetrahydrofolic acid; (6S)-THFA	33.8	-18.32	-18.63
C00061	455,1	M-H	FMN; Riboflavin-5-phosphate; Flavin mononucleotide	3.37	-5.35	-4.43
C05125	487,1	M+NH4	2-(α-Hydroxyethyl)thiamine diphosphate; 2-Hydroxyethyl-ThPP	*NI*	-2.74	*NI*
C05125	492,1	M+Na	2-(α-Hydroxyethyl)thiamine diphosphate; 2-Hydroxyethyl-ThPP	*NI*	-3.16	*NI*
C00010	750,1	M+H-H2O	CoA; Coenzyme A; CoA-SH	-4.35	*NI*	*NI*

KEGG = Kyoto Encyclopaedia of Genes and Genomes; HFHSD = high-fat high-sugar diet; HFHSD+L = high-fat high-sugar diet treated with liraglutide; HFHSD+M = high-fat high-sugar diet treated with metformin; MALDI-TOF = matrix-assisted laser desorption/ionization time-of-flight; m/z = mass to charge; NI = not identified; SD = standard diet.

Table 5.83. Identified compounds related to carbohydrate biosynthesis and metabolism showing statistically significant differences in signal following MALDI-TOF spectrometry between male rat groups ($P < 0.05$)

Identifier				t score		
KEGG ID	**m/z ratio**	**Adducts**	**Compound**	**SD vs HFHSD**	**HFHSD vs HFHSD-M**	**HFHSD vs HFHSD-L**
C02262	238,1	HAc-H	D-Galactosamine; D-Chondrosamine; 2-Amino-2-deoxy-D-galactose	8.04	-7.69	*NI*
C06188	347,1	M-H2O-H	Salicin 6-phosphate; Salicin-6P	10.65	*NI*	4.11
C01222	605,1	M+NH4	GDP-4-dehydro-6-deoxy-D-mannose; GDP-4-dehydro-6-deoxy-D-talose; GDP-4-oxo-6-deoxy-D-mannose; GDP-4-dehydro-D-rhamnose; GDP-4-keto-6-deoxy-D-mannose; GDP-4-dehydro-α-D-rhamnose; GDP-4-dehydro-6-deoxy-α-D-mannose	3.41	*NI*	*NI*

KEGG = Kyoto Enclopaedia of Genes and Genomes; HFHSD = high-fat high-sugar diet; HFHSD+L = high-fat high-sugar diet treated with liraglutide; HFHSD+M = high-fat high-sugar diet treated with metformin; MALDI-TOF = matrix-assisted laser desorption/ionization time-of-flight; m/z = mass to charge; NI = not identified; SD = standard diet.

Table 5.84. Identified compounds related to carbohydrate biosynthesis and metabolism showing statistically significant differences in signal following MALDI-TOF spectrometry between female rat groups ($P < 0.05$)

Identifier				t score		
KEGG ID	**m/z ratio**	**Adducts**	**Compound**	**SD vs HFHSD**	**HFHSD vs HFHSD-M**	**HFHSD vs HFHSD-L**
C02262	238,1	HAc-H	D-Galactosamine; D-Chondrosamine; 2-Amino-2-deoxy-D-galactose	10.95	-8.91	-7.49
C06188	347,1	M-H2O-H	Salicin 6-phosphate; Salicin-6P	5.23	-5.35	-5.04
C01222	605,1	M+NH4	GDP-4-dehydro-6-deoxy-D-mannose; GDP-4-dehydro-6-deoxy-D-talose; GDP-4-oxo-6-deoxy-D-mannose; GDP-4-dehydro-D-rhamnose; GDP-4-keto-6-deoxy-D-mannose; GDP-4-dehydro-α-D-rhamnose; GDP-4-dehydro-6-deoxy-α-D-mannose	*NI*	-2.25	*NI*
C00096	606,1	M+H	GDP-mannose; GDP-D-mannose; GDP-α-D-mannose	-2.26	*NI*	*NI*
C01613	705,2	M+K	Stachyose	*NI*	4.01	*NI*

KEGG = Kyoto Encyclopaedia of Genes and Genomes; HFHSD = high-fat high-sugar diet; HFHSD+L = high-fat high-sugar diet treated with liraglutide; HFHSD+M = high-fat high-sugar diet treated with metformin; MALDI-TOF = matrix-assisted laser desorption/ionization time-of-flight; m/z = mass to charge; NI = not identified; SD = standard diet.

The remaining identified compounds were grouped as either purine and pyrimidine metabolites, amino acid metabolites or miscellaneous compounds. There is a degree of overlap, where certain compounds could have been added to both the purine and pyrimidine group and the amino acid group, but they are included only in a single group where they have a predominant role. CoA is the only exception to this, as it was added to the fatty acid group to highlight its changes in signal in comparison with fatty acid metabolites as that directly pertains to a key aim of the research.

There was a total of six compounds identified relating to purine and pyrimidine metabolism. Five of them were seen in both sexes, with one unique compound identified in female rats (adenosine 5'-triphosphate 5'-adenosine). All the purine and pyrimidine metabolites showed significant changes in signal between the SD and HFHSD group in male rats, while only two metabolites in the comparison of those female groups did not. Male rats showed little response to either pharmacotherapeutic agent when compared to the HFHSD group, while female rats showed a predominant response to metformin treatment. Two compounds in male rats reacted with multiple adducts.

In the group of amino acid metabolites, there was a total of eight identified compounds, five of which were seen in both sexes. One compound was unique to male rats [S-(hercyn-2-yl)-L-cysteine S-oxide] and two were unique to female rats (phenylglyoxylyl-CoA and 3-oxo-5,6-didehydrosuberoyl-CoA). Only two metabolites in female rats did not show significant changes between the SD and HFHSD groups. When comparing the HFHSD group with both the HFHSD-M and HFHSD-L groups, male rats responded to both metformin and liraglutide treatment, while female rats predominantly responded to metformin treatment.

Three miscellaneous compounds were identified, one seen in both sexes and one unique to each sex, both showing significant changes in signal between their respective SD and HFHSD group.

Table 5.85. Identified compounds related to purine and pyrimidine biosynthesis and metabolism showing statistically significant differences in signal following MALDI-TOF spectrometry between male rat groups ($P < 0.05$)

Identifier				t score		
KEGG ID	**m/z ratio**	**Adducts**	**Compound**	**SD vs HFHSD**	**HFHSD vs HFHSD-M**	**HFHSD vs HFHSD-L**
C00360	330,1	M-H	dAMP; 2'-Deoxyadenosine 5'-phosphate; 2'-Deoxyadenosine 5'-monophosphate; Deoxyadenylic acid; Deoxyadenosine monophosphate	5.65	-4.83	*NI*
C03997	355,1	M+NH4	5-Hydroxymethyldeoxycytidylate; 5-Hydroxymethyldeoxycytidylic acid; 2'-Deoxy-5-hydroxymethylcytidine 5'-phosphate	8.48	*NI*	*NI*
C02354	364,1	HAc-H	2',3'-Cyclic CMP	-3.09	*NI*	8.36
C22395	463,1	M+H	N6-Succino-2-amino-2'-deoxyadenylate; dSMP; 2-Amino-2'-deoxy-N6-[(2S)-succino]adenylate	4.45	*NI*	*NI*
C22395	485,1	M+Na	N6-Succino-2-amino-2'-deoxyadenylate; dSMP; 2-Amino-2'-deoxy-N6-[(2S)-succino]adenylate	4.21	*NI*	*NI*
C03794	486,1	M+Na	N6-(1,2-Dicarboxyethyl)-AMP; N6-(1,2-Dicarboxyethyl)AMP; Adenylosuccinate; Adenylosuccinic acid	4.16	*NI*	*NI*
C03794	444,1	M-H2O-H	N6-(1,2-Dicarboxyethyl)-AMP; N6-(1,2-Dicarboxyethyl)AMP; Adenylosuccinate; Adenylosuccinic acid	4.58	*NI*	20.8

KEGG = Kyoto Encyclopaedia of Genes and Genomes; HFHSD = high-fat high-sugar diet; HFHSD+L = high-fat high-sugar diet treated with liraglutide; HFHSD+M = high-fat high-sugar diet treated with metformin; MALDI-TOF = matrix-assisted laser desorption/ionization time-of-flight; m/z = mass to charge; NI = not identified; SD = standard diet.

Table 5.86. Identified compounds related to purine and pyrimidine biosynthesis and metabolism showing statistically significant differences in signal following MALDI-TOF spectrometry between female rat groups ($P < 0.05$)

Identifier				t score		
KEGG ID	**m/z ratio**	**Adducts**	**Compound**	**SD vs HFHSD**	**HFHSD vs HFHSD-M**	**HFHSD vs HFHSD-L**
C00360	330,1	M-H	dAMP; 2'-Deoxyadenosine 5'-phosphate; 2'-Deoxyadenosine 5'-monophosphate; Deoxyadenylic acid; Deoxyadenosine monophosphate	2.62	-2.57	*NI*
C03997	355,1	M+NH4	5-Hydroxymethyldeoxycytidylate; 5-Hydroxymethyldeoxycytidylic acid; 2'-Deoxy-5-hydroxymethylcytidine 5'-phosphate	5.76	-4.43	*NI*
C02354	364,1	HAc-H	2',3'-Cyclic CMP	9.36	-5.83	-5.85
C22395	485,1	M+Na	N6-Succino-2-amino-2'-deoxyadenylate; dSMP; 2-Amino-2'-deoxy-N6-[(2S)-succino]adenylate	*NI*	-2.77	*NI*
C03794	486,1	M+Na	N6-(1,2-Dicarboxyethyl)-AMP; N6-(1,2-Dicarboxyethyl)AMP; Adenylosuccinate; Adenylosuccinic acid	*NI*	-2.82	*NI*
C06197	779,1	M+Na	P1,P3-Bis(5'-adenosyl) triphosphate; ApppA; Adenosine 5'-triphosphate 5'-adenosine	-3.9	NI	*NI*

KEGG = Kyoto Encyclopaedia of Genes and Genomes; HFHSD = high-fat high-sugar diet; HFHSD+L = high-fat high-sugar diet treated with liraglutide; HFHSD+M = high-fat high-sugar diet treated with metformin; MALDI-TOF = matrix-assisted laser desorption/ionization time-of-flight; m/z = mass to charge; NI = not identified; SD = standard diet.

Table 5.87. Identified compounds related to amino acid biosynthesis and metabolism showing statistically significant differences in signal following MALDI-TOF spectrometry between male rat groups ($P < 0.05$)

Identifier				t score		
KEGG ID	**m/z ratio**	**Adducts**	**Compound**	**SD vs HFHSD**	**HFHSD vs HFHSD-M**	**HFHSD vs HFHSD-L**
C00135	214,1	HAc-H	L-Histidine; (S)-alpha-Amino-1H-imidazole-4-propionic acid	6.97	-4.22	*NI*
C04479	273,1	HAc-H	2-Hydroxy-6-oxonona-2,4-diene-1,9-dioate; (2Z,4E)-2-Hydroxy-6-oxonona-2,4-diene-1,9-dioate	21.94	-6.78	-2.64
C17935	315,1	M-H	Cysteinyldopa; 5-S-Cysteinyl-DOPA	7.98	*NI*	-2.9
C00021	383,1	M-H	S-Adenosyl-L-homocysteine; S-Adenosylhomocysteine	4.23	-5.56	*NI*
C20994	392,1	HAc-H	S-(Hercyn-2-yl)-L-cysteine S-oxide	20.01	*NI*	-13
C16517	427,1	HAc-H	Indolylmethyl-desulfoglucosinolate; Desulfoglucobrassicin	2.97	-4.58	*NI*

KEGG = Kyoto Encyclopaedia of Genes and Genomes; HFHSD = high-fat high-sugar diet; HFHSD+L = high-fat high-sugar diet treated with liraglutide; HFHSD+M = high-fat high-sugar diet treated with metformin; MALDI-TOF = matrix-assisted laser desorption/ionization time-of-flight; m/z = mass to charge; NI = not identified; SD = standard diet.

Table 5.88. Identified compounds related to amino acid biosynthesis and metabolism showing statistically significant differences in signal following MALDI-TOF spectrometry between female rat groups ($P < 0.05$)

Identifier				t score		
KEGG ID	m/z ratio	Adducts	Compound	SD vs HFHSD	HFHSD vs HFHSD-M	HFHSD vs HFHSD-L
C00135	214,1	HAc-H	L-Histidine; (S)-alpha-Amino-1H-imidazole-4-propionic acid	3.44	-2.46	*NI*
C04479	273,1	HAc-H	2-Hydroxy-6-oxonona-2,4-diene-1,9-dioate; (2Z,4E)-2-Hydroxy-6-oxonona-2,4-diene-1,9-dioate	3.05	-10.75	-7.41
C17935	315,1	M-H	Cysteinyldopa; 5-S-Cysteinyl-DOPA	*NI*	-2.64	-3.54
C00021	383,1	M-H	S-Adenosyl-L-homocysteine; S-Adenosylhomocysteine	11.03	*NI*	-4.07
C16517	427,1	HAc-H	Indolylmethyl-desulfoglucosinolate; Desulfoglucobrassicin	26.37	-7.14	*NI*
C15524	938,1	M+K	Phenylglyoxylyl-CoA	4.21	-3.63	*NI*
C19945	953,2	M+NH4	3-Oxo-5,6-dehydrosuberyl-CoA; 3-Oxo-5,6-didehydrosuberoyl-CoA	*NI*	-4.44	*NI*

KEGG = Kyoto Encyclopaedia of Genes and Genomes; HFHSD = high-fat high-sugar diet; HFHSD+L = high-fat high-sugar diet treated with liraglutide; HFHSD+M = high-fat high-sugar diet treated with metformin; MALDI-TOF = matrix-assisted laser desorption/ionization time-of-flight; m/z = mass to charge; NI = not identified; SD = standard diet.

Table 5.89. Unspecified miscellaneous compounds showing statistically significant differences in signal following MALDI-TOF spectrometry between male rat groups ($P < 0.05$)

Identifier				t score		
KEGG ID	m/z ratio	Adducts	Compound	SD vs HFHSD	HFHSD vs HFHSD-M	HFHSD vs HFHSD-L
C04722	485,3	M+Cl	3α,7α,12α-Trihydroxy-5β-cholestanoate; 3α,7α,12α-Trihydroxy-5β-cholestan-26-oate; 3α,7α,12α-Trihydroxy-5 β-cholestanate	-4.77	*NI*	*NI*
C22116	509,3	M+K	3β-Hydroxy-4β,14α-dimethyl-9β,19-cyclo-5α-ergost-24(24(1))-en-4α-carboxylate	4.1	*NI*	-4.33

KEGG = Kyoto Encyclopaedia of Genes and Genomes; HFHSD = high-fat high-sugar diet; HFHSD+L = high-fat high-sugar diet treated with liraglutide; HFHSD+M = high-fat high-sugar diet treated with metformin; MALDI-TOF = matrix-assisted laser desorption/ionization time-of-flight; m/z = mass to charge; NI = not identified; SD = standard diet.

Table 5.90. Unspecified miscellaneous compounds showing statistically significant differences in signal following MALDI-TOF spectrometry between female rat groups ($P < 0.05$)

Identifier				t score		
KEGG ID	m/z ratio	Adducts	Compound	SD vs HFHSD	HFHSD vs HFHSD-M	HFHSD vs HFHSD-L
C17651	483,3	HAc-H	α-Phocaecholic acid; 3α,7α,12α,23R-Tetrahydroxycholanic acid	4.92	-4.89	-3.93
C22116	509,3	M+K	3β-Hydroxy-4β,14α-dimethyl-9β,19-cyclo-5α-ergost-24(24(1))-en-4α-carboxylate	-5.42	*NI*	*NI*

KEGG = Kyoto Encyclopaedia of Genes and Genomes; HFHSD = high-fat high-sugar diet; HFHSD+L = high-fat high-sugar diet treated with liraglutide; HFHSD+M = high-fat high-sugar diet treated with metformin; MALDI-TOF = matrix-assisted laser desorption/ionization time-of-flight; m/z = mass to charge; NI = not identified; SD = standard diet.

5.3.2. Identified metabolic pathways

The online KEGG database was used to identify metabolic pathways affected by the HFHSD as well as metformin and liraglutide treatment. The identified pathways are a direct reflection of identified compounds using MALDI-TOF mass spectrometry. Similarly to the analysis of identified compounds and final result selection, the initial list of identified metabolic pathways had included certain significant pairwise differences that were not deemed as relevant to the research (SD vs HFHSD-M and HFHSD-L), due to the fact that no direct effects by HFHSD or metformin and liraglutide treatment could be interpreted from those results. If significant differences for a specific metabolic pathway were found only between the aforementioned group pairs, the pathway was excluded from the final list. Therefore, only three relevant, sex-specific pairwise comparisons were included – SD vs HFHSD, HFHSD vs HFHSD-M and HFHSD vs HFHSD-L. Since not all the identified metabolic pathways showed significant changes between all three of the observed comparisons, those spaces were left blank.

Once the initial results were filtered, sex-specific significant differences between animal groups were identified for a total of 43 pathways. These pathways are listed in Tables 5.89 to 5.92, with pathways specifically affected by InR-related metabolic and lipidomic changes shown in Table 5.91 and Table 5.93.

Each sex had a total of 34 identified pathways with significant differences. Nine pathways were unique to each sex, which translates to a 25 pathways showing significant differences in both sexes for an overlap of 58.14%. This is illustrated in Figure 5.9.

Table 5.91. Identified metabolic pathways affected by insulin resistance-related metabolic and lipidomic changes in hippocampal tissue showing statistical significance (*P* < 0.05) between analyzed groups of male Sprague Dawley rats

KEGG ID	Pathway	*P*		
		SD vs HFHSD	HFHSD vs HFHSD-M	HFHSD vs HFHSD-L
rno00010	Glycolysis/Gluconeogenesis	0.026		0.0193
rno00052	Galactose metabolism		0.0159	
rno00062	Fatty acid elongation	0.0092		0.0172
rno00071	Fatty acid degradation			0.0497
rno00140	Steroid hormone biosynthesis	0.0134	0.0105	
rno00532	GAG biosynthesis - chondroitin sulfate/dermatan sulfate	0.0208	0.0135	
rno00534	GAG biosynthesis - heparan sulfate/heparin	0.0056	0.0128	
rno00563	Glycosylphosphatidylinositol (GPI)-anchor biosynthesis		0.0317	0.0232
rno00564	Glycerophospholipid metabolism	0.0206	0.0197	0.0016
rno00600	Sphingolipid metabolism			0.0419
rno01040	Biosynthesis of unsaturated fatty acids	< 0.0001	0.0234	0.0001
rno01212	Fatty acid metabolism	0.0113	0.0474	0.0367
rno03320	PPAR signaling pathway	0.047792		0.0482
rno04020	Calcium signaling pathway		0.0405	
rno04071	Sphingolipid signaling pathway	0.0045	0.0263	0.0299
rno04072	Phospholipase D signaling pathway	0.0186	0.0110	0.0122
rno04080	Neuroactive ligand-receptor interaction		0.0228	
rno04150	mTOR signaling pathway		0.0426	
rno04151	PI3K-Akt signaling pathway			0.0436
rno04152	AMPK signaling pathway	0.0265		0.0145
rno04216	Ferroptosis	0.0066		0.0022
rno04725	Cholinergic synapse			0.0329
rno04920	Adipocytokine signaling pathway	0.011		0.0052
rno04922	Glucagon signaling pathway	0.0371		0.0289
rno04931	Insulin resistance	0.028		0.0179

AMPK = AMP-activated protein kinase; GAG = glycosaminoglycan; HFHSD = high-fat high-sugar diet; HFHSD-L = high-fat high-sugar diet treated with liraglutide; HFHSD-M = high-fat high-sugar diet treated with metformin; KEGG = Kyoto Encyclopedia of Genes and Genomes; mTOR = mechanistic target of rapamycin; PI3K-Akt = phosphoinositide 3-kinase-protein kinase B; PPAR = peroxisome-proliferator-activated receptor; SD = standard diet

Table 5.92. Remaining identified metabolic pathways in hippocampal tissue showing statistical significance ($P < 0.05$) between analyzed groups of male Sprague Dawley rats

KEGG ID	Pathway	P		
		SD vs HFHSD	HFHSD vs HFHSD-M	HFHSD vs HFHSD-L
rno00240	Pyrimidine metabolism	0.0063		0.0320
rno00350	Tyrosine metabolism	0.0298		0.0132
rno01522	Endocrine resistance	0.0426	0.0133	0.0248
rno03008	Ribosome biogenesis in eukaryotes	0.0065	0.0083	
rno04370	VEGF signaling pathway		0.0241	0.0395
rno04371	Apelin signaling pathway	0.0382	0.0213	0.0378
rno04666	Fc gamma R-mediated phagocytosis	0.0066	0.0087	0.0089
rno04936	Alcoholic liver disease	0.008		0.0025
rno05231	Choline metabolism in cancer			0.0343

Fc = crystallizable fragment; HFHSD = high-fat high-sugar diet; HFHSD-L = high-fat high-sugar diet treated with liraglutide; HFHSD-M = high-fat high-sugar diet treated with metformin; KEGG = Kyoto Encyclopedia of Genes and Genomes; SD = standard diet; VEGF = vascular endothelial growth factor

Table 5.93. Identified metabolic pathways affected by insulin resistance-related metabolic and lipidomic changes in hippocampal tissue showing statistical significance ($P < 0.05$) between analyzed groups of female Sprague Dawley rats

KEGG ID	Pathway	P		
		SD vs HFHSD	HFHSD vs HFHSD-M	HFHSD vs HFHSD-L
rno00010	Glycolysis / Gluconeogenesis	0.0167	0.0043	0.0099
rno00052	Galactose metabolism	0.0471		
rno00061	Fatty acid biosynthesis	0.0446		
rno00062	Fatty acid elongation	0.0018	0.0064	0.0222
rno00071	Fatty acid degradation	0.0418		
rno00190	Oxidative phosphorylation	0.0484		
rno00513	Various types of N-glycan biosynthesis	0.0413		
rno00532	GAG biosynthesis - chondroitin sulfate/dermatan sulfate		0.0398	
rno00534	GAG biosynthesis - heparan sulfate/heparin		0.0389	
rno00564	Glycerophospholipid metabolism	0.0121		
rno01040	Biosynthesis of unsaturated fatty acids	< 0.0001	< 0.0001	0.0001
rno01212	Fatty acid metabolism	0.0137	0.0139	0.0304
rno03320	PPAR signaling pathway	0.0216	0.0434	
rno04071	Sphingolipid signaling pathway	0.003	0.0046	0.0191
rno04072	Phospholipase D signaling pathway	0.0115	0.0192	
rno04146	Peroxisome	< 0.0001		
rno04151	PI3K-Akt signaling pathway	0.0294		0.0384
rno04152	AMPK signaling pathway	0.0189		
rno04216	Ferroptosis		0.0067	
rno04920	Adipocytokine signaling pathway	0.0084		
rno04922	Glucagon signaling pathway	0.0332	0.0260	
rno04931	Insulin resistance	< 0.0001		

AMPK = AMP-activated protein kinase; Fc = crystallizable fragment; GAG = glycosaminoglycan; HFHSD = high-fat high-sugar diet; HFHSD-L = high-fat high-sugar diet treated with liraglutide; HFHSD-M = high-fat high-sugar diet treated with metformin; KEGG = Kyoto Encyclopedia of Genes and Genomes; PI3K-Akt = phosphoinositide 3-kinase-protein kinase B; PPAR = peroxisome-proliferator-activated receptor; SD = standard diet

Table 5.94. Remaining identified metabolic pathways in hippocampal tissue showing statistical significance ($P < 0.05$) between analyzed groups of female Sprague Dawley rats

KEGG ID	Pathway	P		
		SD vs HFHSD	HFHSD vs HFHSD-M	HFHSD vs HFHSD-L
rno00240	Pyrimidine metabolism	0.0043	0.0036	0.0124
rno00250	Alanine, aspartate and glutamate metabolism		0.0457	
rno00350	Tyrosine metabolism		0.0261	0.0072
rno00360	Phenylalanine metabolism	0.0356	0.0043	0.0465
rno00670	One carbon pool by folate	0.0478	0.0331	
rno03008	Ribosome biogenesis in eukaryotes	0.0156	0.0021	
rno04066	HIF-1 signaling pathway		0.0379	
rno04370	VEGF signaling pathway	0.0327		
rno04371	Apelin signaling pathway	0.0191	0.0408	
rno04666	Fc gamma R-mediated phagocytosis	0.0028	0.0065	
rno04742	Taste transduction	< 0.0001	0.0391	0.0147
rno04936	Alcoholic liver disease	0.0002	0.0133	

Fc = crystallizable fragment; HFHSD = high-fat high-sugar diet; HFHSD-L = high-fat high-sugar diet treated with liraglutide; HFHSD-M = high-fat high-sugar diet treated with metformin; HIF = hypoxia-inducible factor-1; KEGG = Kyoto Encyclopedia of Genes and Genomes; SD = standard diet; VEGF = vascular endothelial growth factor
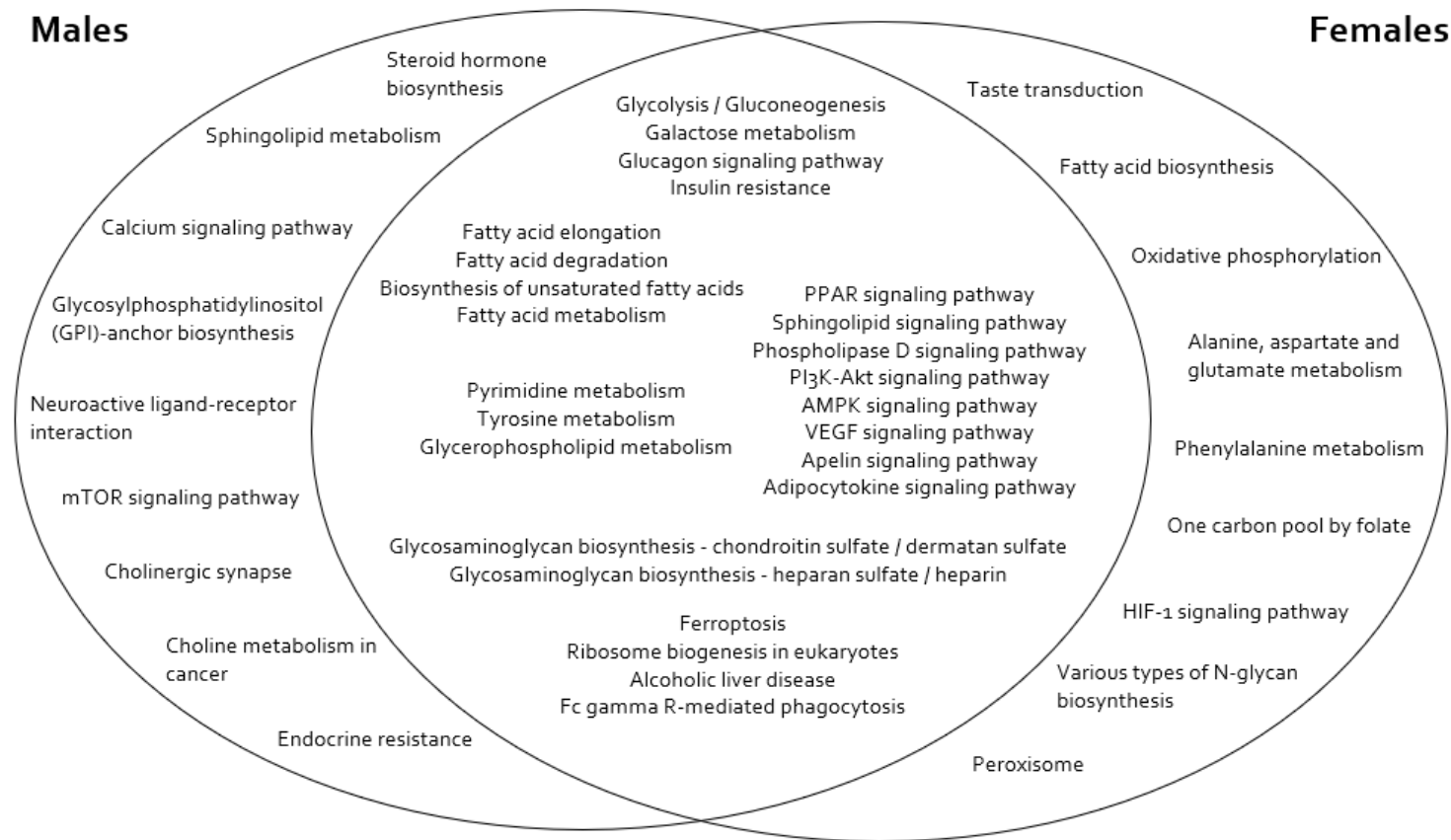
Figure 5.9. Overlapping and uniquely identified altered metabolic pathways in rat hippocampi between sexes.

6. DISCUSSION

This study aimed at investigating and identifying sex-specific differences in hippocampal tissue composition in a rat model of InR, as well as changes following treatment with metformin or liraglutide, two commonly used pharmacotherapeutic agents in the treatment of T2DM. Immunohistochemical analysis was used to identify differences in the expression of relevant membrane proteins and myelin gangliosides, while MALDI-TOF mass spectrometric analysis was used to identify significant alterations in the hippocampal lipidome and in other relevant groups of compounds between observed groups.

6.1. Immunohistochemical analysis

A free-floating immunohistochemical analysis was performed to determine the expression changes in eight epitopes – four gangliosides and four proteins, all relevant to the topic of InR and neurodegeneration. The importance of gangliosides in the context of these topics lies in their abundance in the CNS – the brain is the most ganglioside-rich organ. The four investigated gangliosides (GM1, GD1a, GD1b and GT1b) are the most common gangliosides found in the brain, specifically in the neuronal membrane and myelin sheath (195). The highest levels of gangliosides in the neuronal membrane can be found in lipid rafts, specialized microdomains that consist of certain membrane proteins and have a specific composition of lipids. They carry out an entire spectrum of functions in the CNS, including signal transduction, maintenance of synapse and dendritic spine integrity, etc. (196) Out of the four mentioned gangliosides, GM1 is the most common one seen in lipid rafts (197). Over the past couple of decades, several research studies have been conducted that identify lipid rafts as ground zero of amyloidogenesis. Zampagni et al. (198) demonstrated that amyloid-related oxidative stress in neurons is enhanced and mediated by lipid rafts in human cell cultures. Rushworth JV and Hooper NM published a review paper on this topic in 2011 (199), showing overwhelming evidence that all key events regarding amyloidogenesis and neuronal dysfunction happen within lipid rafts – from Aβ peptide formation to oligomerization to their interference with neuronal homeostasis. The term oligomerization, specifically, should be noted because, contrary to long-lasting popular belief, amyloid plaques/fibrils are not the main culprits in AD pathogenesis – be it extracellular or intracellular, but rather Aβ oligomers (200). Although there is a certain variety in their fine shape and structure, the oligomers

generally have been linked to neuronal pathologies reflective of AD – LTP and LTD impairment, changes in dendritic spine density, and other (201), all leading to memory loss and cognitive disorders (202). These toxic and deleterious Aβ molecules have a strong affinity for sialic acid, which is part of certain gangliosides, including GM1.

The connection between InR and AD must start by defining what comes first – Aβ and pTau accumulation or dysfunctional neurons resistant to insulin? The answer might be both. The overall, general conclusion from all research papers investigating this area is that Aβ itself can render neuronal cells insensitive to insulin. Studies have described Aβ reducing phosphorylation of the IR (115), binding to it (203) as well as initiating neuroinflammatory processes (204). With both IR and IGF-1R expression increased following metformin and liraglutide treatment in male rats, it might represent a way of counteracting the Aβ actions by increasing the number of available receptors and, subsequently, increasing insulin sensitivity. One region that, for unknown reasons, saw a completely opposite effect, was the CA1 region. When flipping the initial pathologic trigger to T2DM and InR, it is easily understandable that increased resistance of neuronal tissue to insulin action would further impair many processes and the overall metabolic scheme. Still, it must be pointed out that Aβ and pTau themselves could inflict InR-inducing damage.

When observing the results of the immunohistochemical analysis, there is a clear pattern and dynamic of changes in male rats – the expression of GM1 is not changed significantly in any of the ROIs in HFHSD rats, while the most striking change happens in rats treated with liraglutide, where there is a drastically higher expression of this ganglioside. Female rats across the board had much weaker IDVs and the observed changes did not yield any significance to conclude whether or not metformin or liraglutide had an effect on GM1 expression. In the comparison of GM1 expression changes with those of APP in male rats, the key observation is that APP expression changes drastically not with liraglutide, but with metformin treatment. As APP is an integral part of neuronal membranes with a plethora of functions itself, its presence and its across-group dynamic changes alone should not be confused or equated with the presence of pathological Aβ accumulation. Interestingly, metformin treatment had the same effect on both sexes – increasing the APP expression above levels seen in the SD or HFHSD group, while liraglutide treatment had a stronger impact on male rats. Since no significant similarities were found between GM1 and APP expression levels, the protein of interest that was next in line to potentially elucidate the neuronal dynamics in this animal model was pTau. While no uniformly significant changes were observed between the male SD and HFHSD groups, liraglutide treatment drastically

decreased the expression of pTau in all three ROIs to levels well below any other group. Therefore, these results suggest that already observed positive neuroprotective properties of liraglutide (185, 205) are reflected in an increase of GM1 (possibly to restructure and strengthen lipid raft domains), with the decrease in pTau levels serving as secondary confirmation because of its known status as an AD biomarker (99). The importance of GM1 has been already noted in research studies demonstrating its neuroprotective properties (206) but it is also relevant to note that CA1 and CA3 regions of the hippocampus in both sexes showed very little to almost no immunoreactivity whatsoever, which coincides precisely with a study by Vajn et al. (207) that provided detailed mapping and localization of all the significant gangliosides within CNS structures in adult mice. The effects of liraglutide treatment did, however, extend to those regions in both sexes, which was an interesting finding.

GD1a is another ganglioside that has been associated with neuroprotection – one study identified this in a model of Parkinson's disease and Huntington's disease (208). While there were not many significant alterations in the three analyzed ROIs, the overall dynamic of changes observed for this ganglioside also shows a larger influence of liraglutide on its expression, both in male and female rats. The increase in expression following liraglutide treatment further backs the aforementioned theory that neuroprotective effects of this agent are carried out through gangliosidic restructuring within the membrane and/or myelin sheath. GD1b, on the other hand, was almost uniformly significantly altered, including differences between the SD and HFHSD groups of both sexes. The important difference here, however, is that female rats on a HFHSD experienced much lower expression of GD1b compared to their respective SD group, while the opposite was seen in male rats. Significant decreases were seen in groups receiving treatment of both sexes for almost every ROI (except for metformin treatment in female rats in the DG), a completely reversed situation compared to the expression of GM1 and GD1a, at least when it comes to liraglutide treatment. The biggest difference in expression, while also not showing many notable, significant changes, was observed for GT1b. This is the only trisialoganglioside in the investigated group and there were almost no significant changes following pharmacotherapy, save for an increase in the CA1 region in female rats treated with liraglutide.

The expression levels of IR and IGF-1R in the SD and HFHSD groups reflect the neuronal sensitivity to insulin. The IDV values in male rats showed much more extensive changes. A curious finding in this analysis was a remarkably high IDV value of IR in the CA1 region following a HFHSD. Following metformin and liraglutide treatment, its expression

dropped to very low levels, while a large increase in expression was observed in the DG and the CA3 region. The CA1 region was also the "odd man out" among all ROIs in IGF-1R expression, but not in the HFHSD group, but rather in the liraglutide-treated group, where liraglutide failed to increase its expression.

Overall, more effects were observed in male rats and they were more responsive to liraglutide treatment than metformin. As a GLP-1 analogue, it makes sense that liraglutide would help change the expression of certain gangliosides and especially membrane proteins since the GLP-1 receptors share a certain overlap in function with IR and IGF-1R (209) and therefore it might be beneficial to neurons by promoting a positive autoregulatory loop to increase its sensitivity to insulin and to restructure the membrane to strengthen the cell itself following the nosogenic effects of a HFHSD.

6.2. Mass spectrometric analysis

The MALDI-TOF spectrometric analysis revealed numerous differences in the observed lipidomes, including group-specific and sex-specific changes. Compounds involved in lipid metabolism included PUFAs and their metabolites, saturated fatty acids, acyl-CoAs, phospholipids (glycerophospholipids and sphingolipids) and lipids involved in steroid hormone metabolism and biosynthesis. There were also observable changes in several carbohydrates, compounds involved in amino acid and purine and pyrimidine metabolism, as well as vitamins and cofactors.

6.2.1. Lipidomic changes are a reflection of lipid peroxidation and mitochondrial dysfunction

When taking compounds relating to sphingolipid, glycerophospholipid and steroid biosynthesis and metabolism out of the picture, several lipid compounds were identified – they were PUFAs, saturated fatty acids such as stearic acid and multiple fatty acyl-CoAs that were much more extensively represented in female rats. When observing these results generally, there were two striking findings. The first was significant increases in most of the identified compounds in both sexes on a HFHSD compared with their respective SD group, which was an expected finding that is in line with a rat model of obesity and InR. The second was a sex-specific response to pharmacotherapeutics – the majority of identified compounds saw significant decreases when compared with the HFHSD, but these decreases were,

generally speaking, observed in the female rats treated with metformin and in male rats treated with liraglutide. Not only are these observations in line with immunohistochemical findings, but they are also in line with identified compounds related to phospholipid and steroid biosynthesis and metabolism as well. The observation that only three of ten compounds identified in male rats and none of the sixteen compounds in female rats (excluding CoA which is included in Table 5.75 and 5.76, but is technically not a lipid) showed no changes following pharmacotherapy indicates that metformin and liraglutide indeed alter the hippocampal lipidomic profile following a HFHSD. There were several metabolic pathways identified as significantly altered relating to lipid metabolism, directly or indirectly, in both sexes, such as biosynthesis of unsaturated fatty acids, fatty acid elongation and degradation etc. In fact, biosynthesis of unsaturated fatty acids was the most prominently affected metabolic pathway in female rats, with P values well under 0.0001 in all three comparisons. Insulin signaling pathways were affected as well – the significant changes in the metabolic pathway "insulin resistance" between the SD and HFHSD group in both sexes were yet another confirmation that this animal model was successful in inducing InR and all the metabolic and pathologic changes that follow it. The PI3K/PKB and AMPK signaling pathways were also among identified metabolic pathways and it was liraglutide treatment in both sexes that showed significant changes compared to the HFHSD group. The key takeaway point from these general observations is an overwhelming indication that the lipidomic profile of observed rat groups is indeed altered following a HFHSD that successfully induced InR, with observable changes following treatment with both metformin and liraglutide, to a larger or lesser extent based on sex.

Several of the identified lipid compounds were PUFAs. As these are essential fatty acids, i.e. they cannot be synthesized endogenously in mammals, their levels are a reflection of dietary intake. Therefore, expectedly, levels of eicosadienoic acid, icosenoic (gondoic) acid and docosanoic (behenic) acid were significantly elevated in both sexes on a HFHSD. It was in female rats only that significant decreases were observed for all of these compounds following pharmacotherapy, specifically and predominantly metformin treatment. PUFAs are a major component of the neuronal lipid profile, especially the neuronal membrane, with large roles in neuroinflammation and neurotransmission, to name just a couple (210). Being such an important presence in the CNS, PUFAs have also been linked to numerous pathologies affecting the CNS, including neurodegenerative entities (211). Three major PUFAs found in the CNS – eicosapentaenoic acid, docosapentaenoic acid and docosahaexaenoic acid, all synthesized from linoleic acid, an ω-3 PUFA, did not show up in the spectrometric analysis.

Results from a recently published study by Xu J et al. (212) demonstrated that treatment with docosahaexaenoic acid actually improves cognitive function in Sprague Dawley rats on a high-fat diet.

The effects of PUFAs on hippocampal structural and functional integrity, nonetheless, are reflected in the findings, specifically in terms of lipid peroxidation and ferroptosis. The two compounds with significant changes between compared groups relating to the mentioned metabolic pathways were adrenic (docosatetraenoic) acid and 2,3-dinor-8-iso prostaglandin F2α (2,3-dinor-8-iso PGF2α). These two compounds are directly related to the metabolism of arachidonic acid, an ω-6 PUFA with four double bonds that is a precursor to several groups of eicosanoids that are major regulators of neuroinflammatory and neuroimmune response (prostaglandins, prostacyclins, tromboxanes, leukotrienes, etc.) (213). Male rats on a HFHSD saw an increase in adrenic acid levels compared to the SD group, while there were no significant changes between the two groups in female rats. As previously mentioned, male rats responded to liraglutide treatment, seeing a decrease in adrenic acid levels compared to the HFHSD group, while female rats responded to metformin treatment, also with a decrease in adrenic acid levels that was much more substantial than the male liraglutide response (t = -29.63733 and t = -5.9261952, respectively). Adrenic acid is an arachidonic acid metabolite that is synthesized by elongating its hydrocarbon chain. Reactive oxygen species, generated mostly by mitochondria, induce lipid peroxidation specifically affecting PUFAs. Once overwhelmed with reactive oxygen species, i.e. free radicals, neurons might initiate cell survival or cell death.

Another process that has been closely followed and investigated in recent years is ferroptosis. Despite the fact that exact molecular mechanisms that trigger ferroptosis still remain unknown, it has garnered attention in the field of neuroscience as well since it occurs in many pathological states affecting the CNS, including T2DM changes. It is a regulated cell death that is mostly mediated by iron-dependent lipid peroxides and it is often accompanied by mitochondrial dysfunction (214). Recently published studies highlight ferroptosis as a potential therapeutic target in treating InR-related cognitive dysfunction since ferroptosis has been proven to occur in hippocampal neurons (215). Meanwhile, 2,3-dinor-8-iso PGF2α has already been proven to be a reliable marker of lipid peroxidation and oxidative stress (216). Laight DW et al. (217) specifically demonstrated an increase 2,3-dinor-8-iso PGF2α levels in obese Zucker rats. The spectrometric analysis for this compound once again showed sex-specific differences – male rats on a HFHSD had increased levels compared to the SD group, while both metformin and liraglutide treatment decreased them (more effectively liraglutide),

while female rats on a HFHSD showed decreased levels in the HFHSD group, with an additional decrease in those treated with liraglutide. This was also one of the few instances where liraglutide showed a significant effect on female rats. This finding suggests that both pharmacotherapeutics might help reduce oxidative stress in the hippocampal neurons.

The processes of lipid peroxidation and ferroptosis are intertwined with additional complex processes that affect neurons negatively, leading to InR-induced neurodegeneration, such as mitochondrial dysfunction and metabolic changes due to InR. Additionally, it should be noted that alterations in the hippocampal lipidomic profiles are a reflection of both systemic and local InR-related changes in the CNS. Since InR was induced systemically in this experiment, a delineation between findings that are a direct reflection of CNS dysfunction and those that mirror pathologic changes that occurred elsewhere, in other metabolically active tissue (liver, adipose tissue, etc.) was not possible. Even though glucose is the primary source of fuel for the CNS, fatty acid mobilization and utilization for ATP production is also seen in neuronal tissue. It has been estimated that fatty acid oxidation accounts for approximately 20% of the total energy production in the CNS and that this metabolic pathway occurs mainly in astrocytes (218). Results of the mass spectrometry showed changes in levels of L-palmitoylcarnitine. In male rats, there was an increase in L-palmitoylcarnitine levels following HFHSD and a decrease following liraglutide treatment. In female rats, however, there was a decrease in L-palmitoylcarnitine levels following HFHSD and no significant changes following either metformin or liraglutide treatment. L-palmitoylcarnitine is an intermediate metabolite in the process of palmitic acid β-oxidation that is created by carnitine O-palmitoyltransferase in order for it to cross the inner mitochondrial membrane which eventually leads to its β-oxidation (219). The observed changes in the L-palmitoylcarnitine levels suggest that InR affects fatty acid β-oxidation in the hippocampus and that increased levels of the compound might be a consequence of either oversaturation of the carnitine O-palmitoyltransferases or their dysfunction. These changes are presented in Tables 5.75. and 5.76., but they also include CoA changes, which follow the same pattern as L-palmitoylcarnitine. While CoA is an omnipresent compound in a multitude of metabolic pathways, its pattern follows the changes seen in most compounds related to fatty acid β-oxidation. To further elaborate on the theory of altered fatty acid metabolism, i.e. β-oxidation, there are certain indices of mitochondrial dysfunction. In addition to the aforementioned L-palmitoylcarnitine, the spectrometric analysis yielded alterations for several fatty acyl-CoAs affected by the HFHSD and pharmacotherapeutic intervention, as was reflected in the identified metabolic pathways pertaining to them (fatty acid elongation, fatty acid

metabolism) – 3-oxohexanoyl-CoA and 3-oxooctanoyl-CoA in both sexes, hexanoyl-CoA, octanoyl-CoA, (2E)-Octenoyl-CoA, (S)-3-hydroxyoctanoyl-CoA and 3-oxoadipyl-CoA in female rats specifically. Interestingly, pharmacological agents decreased levels of these compounds compared to the HFHSD group – liraglutide in male rats, metformin in female rats. This finding could be an indirect indicator of mitochondrial function recovery or simply that these compounds were used up for energy production, which is in line with findings from a 1997 research study by Lenhard JM et al. (220) where metformin was found to increase mitochondrial and peroxisomal fatty acid β-oxidation. The HFHSD groups, however, did not follow a uniform trajectory – the two compounds identified in male rats were increased, while there was an uneven split between increases and decreases among the several compounds identified in female rats, compared to their respective SD group, with more compounds showing increases. These findings could be a consequence of an increased intracellular lipid burden due to InR, but are also highly suggestive of mitochondrial dysfunction leading to fatty acyl-CoA accumulation, as was seen in most compounds identified in the HFHSD groups. Yao J et al. (221) even showed that compromised function of mitochondria is present in female mice prior to AD degeneration, suggesting that not only do InR-related metabolic changes affect mitochondrial homeostasis, but that they also foretell neurodegeneration. That finding is in line with female rats from this study, as it was only in female rats that a significant change in oxidative phosphorylation was found between the SD and HFHSD groups. Pharmacotherapy, however, did not result in any additional significant changes. Physiological mitochondrial function is closely related to insulin and IGF-1 action since it heavily relies on their signaling cascades to correctly alter metabolism based on neuronal needs. It was previously mentioned that immunohistochemical analysis revealed that changes to both IR and IGF-1R expression were very lopsided in favor of male rats, where both metformin and liraglutide increased the expression of both receptors, especially in the DG and CA3 region.

The discussed lipidomic changes that were potentially affected by lipid peroxidation/ferroptosis, mitochondrial dysfunction and subsequent changes in fatty acid β-oxidation have already been linked to neurodegenerative diseases such as AD. One example is the aforementioned Yao J et al. study, but there have also been clinical studies elucidating this matter. In a study carried out by Casadesus G et al. in 2007 (222), increased levels of 15-Keto-13,14-dihydroprostaglandin E2 and the already discussed 2,3-dinor-8-iso PGF2α were revealed in pyramidal neurons of hippocampi of AD subjects, implying the effects of free radical damage in the pathogenesis of AD. Thomas MH et al. (223) wrote a review paper

highlighting the numerous effects of arachidonic acid and its metabolites in the development and progression of AD, through synaptic dysregulation and LTP changes, creating a proinflammatory environment mediated by its metabolites and even an indirect contribution to tau protein phosphorylation. The immunohistochemical analysis, however, did not provide significant and clear changes in pTau protein expression in HFHSD groups to come to a specific conclusion for both sexes. Still, there were significant decreases following liraglutide treatment, as was already discussed.

6.2.2. Sphingolipid and glycerophospholipid alterations affect insulin signaling, membrane and myelin structure

Shining light on another aspect of the complex pathophysiological cellular changes in an insulin-resistant hippocampal neuron is the change in sphinganine levels. This, in addition to fatty acids, PUFAs and fatty acyl-CoAs, brings sphingolipid metabolism into the discussion. Also called dihydrosphingosine, this compound is created from serine and palmitoyl-CoA and it is an intermediate metabolite in the biosynthesis of ceramide. Ceramide has been identified as one of the key culprits in insulin signaling disruption through the inhibition of PKC (34). When compared to their respective SD group, both male and female rats on a HFHSD showed an increase in sphinganine levels. Female rats showed a decrease in sphinganine levels following both metformin and liraglutide treatment, while only liraglutide decreased its levels in male rats. When discussing the effects of InR in the CNS, ceramide levels are of special interest because it is part of the molecular structure of gangliosides, compounds that are some of the most abundant and most important components of the membrane and myelin sheath. Ceramide itself was not identified in the mass spectrometric analysis, but the presence of its precursor compounds suggests that the HFHSD did indeed cause intraneuronal lipid accumulation that would impair insulin signaling effects, causing extensive metabolic changes that are closely associated with numerous other nosogenic factors that were already highlighted (lipid peroxidation, mitochondrial dysfunction). When these findings are observed as one collective piece of information, it is apparent that HFHSD caused expected disruptions in the hippocampal lipidome that reflect a collection of points of dysfunction that together close a vicious cycle that is difficult, near impossible to break – even with the treatment options that were introduced to the animals in this experiment.

On the other hand, sphinganine-1-phosphate, also known as dihydrosphingosine-1-phosphate, is a sphingolipid that has not been extensively researched and its properties and function in the body, especially in the CNS, are yet to be elucidated. Both male and female rats saw an increase in sphinganine-1-phosphate following a HFHSD. Following both metformin and liraglutide treatment, its levels were even greater in male rats, while female rats experienced a decrease following metformin treatment compared to those without any treatment. It is clear that sphinganine-1-phosphate is not a mere analog of sphingosine-1-phosphate and that it has its own unique function (224). In a study carried out by Bu S et al. (225) that observed human dermal fibroblast cultures, sphinganine-1-phosphate was shown to have an opposite effect on transforming growth factor-β regulation and an important connection to phosphatase and tensin homolog (PTEN) signaling. In the CNS, this signaling pathway has been known to have an antagonistic effect on the PI3K/PKB pathway (226), which indirectly places sphinganine-1-phosphate in the role of a possible insulin signaling disruptor.

Due to the homogenization of hippocampal tissue samples and the inability to pinpoint the precise anatomical location of a detected altered compound within the sample, it is impossible to state whether or not these findings are a consequence of membrane and myelin sheath changes, intraneuronal ceramide accumulation or a combination of both. The immunohistochemical analysis, however, as a useful complementary tool, was used to steer the interpretation in the right direction. Since the immunohistochemical results regarding the ganglioside composition differences did not show a clear sex-specific predominance, it is then possible that the observed changes in sphinganine levels are a reflection of intraneuronal ceramide accumulation and changes in metabolism. Therefore, both metformin and liraglutide might potentially have positive effects on intracellular lipid accumulation by decreasing levels of sphinganine and sphinganine-1-phosphate (metformin only), i.e. on reestablishing normal function of intracellular signaling pathways in female rats.

Despite the observations regarding sphinganine and sphinganine-1-phosphate, neuronal membranes and myelin sheaths might still have been affected in the hippocampi. Male rats showed a sevenfold increase in CDP-ethanolamine levels when on a liraglutide treatment. This compound is an important intermediate metabolite in the synthesis of ethanolamine plasmalogens in the ER. Plasmalogens are a group of membrane glycerophospholipids that are found not only in brain tissue (including myelin sheaths) but elsewhere in the body as well (bone, lens, heart, etc.) Ethanolamine plasmalogens are more prevalent in neuronal tissue compared to the other type, choline plasmalogens (227). These

compounds also show specific changes in concentration throughout the developmental stages of the CNS as well as a decline with age (228). It is therefore unusual to observe an increase in CDP-ethanolamine in rats that were at 65 weeks of age when they were terminated for the purposes of the experiment, which suggests that liraglutide treatment played a role in this increase. The value and importance of ethanolamine plasmalogens lie in their antioxidative properties and their role in stabilizing neuronal membranes and maintaining synaptic homeostasis (229, 230). They have also been identified in synaptic vesicles (231). The potential of ethanolamine plasmalogens as an AD biomarker was discussed in a review paper by Su XQ et al. (232) where it was summarized that different mechanisms (most of which were already discussed in this chapter), such as lipid peroxidation, neuroinflammation, lipid metabolism and structural changes in the membrane all contribute to decreased levels of ethanolamine plasmalogens, ultimately leading to synaptic dysfunction, increased neuroinflammatory processes, membrane and myelin restructuring as well as Aβ fiber deposition. These plasmalogens themselves were not identified in the mass spectrometric analysis, but the presence of significant changes following liraglutide treatment in an important precursor suggests a possible therapeutic target.

The story of CDP-ethanolamine does not end with plasmalogens. This compound represents one of two ways to synthesize one of the most abundant phospholipids found intracellularly (233) – phosphatidylethanolamine. An important piece to this puzzle lies in the identified metabolic pathways in the mass spectrometric analysis. There was a significant change observed in the glycosylphosphatidylinositol (GPI)-anchor biosynthesis pathway in male rats treated with liraglutide, as well as metformin – CDP-ethanolamine plays an important part in their synthesis. They are complex glycolipids that are normally found in lipid rafts, specific microdomains of the cell membrane (already discusses in 6.1). Their roles have been extensively researched, including the hippocampus specifically, where they have been found to influence synaptic plasticity, promote neurogenesis (234) and regulate myelination (235). Puzzo D et al., for example, identified contactin-1 as a significant GPI anchor in hippocampal neurons that improves synaptic plasticity and memory in elderly mice, while also regulating APP processing and Aβ levels (236).

6.2.3. Relevance of the changes in steroid hormone biosynthesis and metabolism

The notion that steroid hormones are not only synthesized in the CNS but also have several CNS-specific functions, has been heavily investigated since the turn of the century when the term "neurosteroids" was coined to differentiate between hormones synthesized in gonadal and adrenal glands from those synthesized in the central and peripheral nervous system (237). The hippocampus was found to be one of the key regions in the brain affected by locally synthesized and circulating steroid hormone modulation, as both androgen receptors and estrogen receptors are found in cell membranes, nuclei and even synaptic vesicles of hippocampal neurons (238, 239). Furthermore, sex-specific differences in androgen hormone expression, levels and function have also been noted, specifically concerning sex hormones (240).

The mass spectrometric analysis identified five compounds involved in biosynthesis and metabolism of steroid hormones with observable differences between male and female rats. More changes following the HFHSD regimen were noted in male rats. It is also worth noting that steroid biosynthesis, as a metabolic pathway, was identified as significantly altered in male rats only (as seen in Table 5.91). While androstenedione was not identified as a compound showing significant changes in expression between female groups, it showed significant changes between several male groups. In this pathway, androstenedione is a precursor molecule synthesized from either dehydroepiandrosterone or 17α-hydroxyprogesterone. It can then be converted to either testosterone, which can then be converted to its more potent metabolite, 5α-dihydrotestosterone, or it can be used in the estrogen pathway for synthesis of one of the estrogen hormones, including the most potent one, estradiol-17β. There was a significant, ninefold decrease in androstenedione levels in the HFHSD group compared to the SD group. Both metformin and liraglutide-treated male groups showed additional significant decreases in androstenedione levels when compared to the HFHSD group, but less extensive ones (fivefold and twofold, respectively). Although studies have been published suggesting a testosterone-mediated impairment of LTP (241), the majority of both clinical and animal studies point in the direction of neuroprotective properties of testosterone and androgens in general (242, 243). Estrogenic hippocampal modulation has been well documented and observed. Estrogen receptors are present in the synapses for modulation of LTD and spinogenesis (244), while estrogenic effects in pyramidal cells in terms of dendritic spine density have also been described (245).

There have been interesting findings concerning the effects of androgens on hippocampal neurons in studies investigating androgen antagonists. MacLusky NJ et al. (246) studied the effects of androgens and flutamide, a nonsteroidal antiandrogen, on the density of dendritic spine synapses in the CA1 hippocampal regions and found that both DHEA and flutamide, the antagonist itself, had positive effects on the CA1 region in both sexes. These findings were backed by Nguyen TV et al. (247) in a study using hippocampal cultures. They showed neuroprotective effects of both flutamide and cyproterone acetate, a synthetic antiandrogen and progesterone derivative, respectively, in the sense that both failed to inhibit dihydrotestosterone and its neuroprotective properties. This specificity of neuronal tissue with regards to androgen response compared to other tissues is currently thought to be linked to a larger role of transmembrane androgen and estrogen receptors, rather than cytoplasmic/nuclear ones (239, 248). Gatson JW et al. (249) demonstrated a difference in androgen function by using a BSA-conjugated androgen (dihydrotestosterone) that cannot cross the cell membrane – these androgens, when bound to cell-surface androgen receptors, exerted opposite effects that were not affected by flutamide, as was demonstrated in previously mentioned studies. A 2004 study carried out by Tabori NE et al. (239) that focused specifically on hippocampal neurons showed prominent immunoreactivity of androgen receptors in the nuclei of CA1 pyramidal cells, but also diffuse androgen receptor immunoreactivity within the stratum lucidum of CA3 axons. The immunohistochemical analysis showed significant changes in the expression of both the IR and IGF-1R when comparing the HFHSD group with both metformin and liraglutide-treated groups. These findings were exclusive to male rats and were found specifically in the CA3 region, as was previously discussed in 6.1. Both IR and IGF-1R had a significant reduction in expression, whereas treatment with both metformin and liraglutide significantly increased their expression. The initial drop in expression following the HFHSD could be a consequence of receptor resistance and subsequent ligand hyperexpression. Two pieces of the puzzle connect immunohistochemical findings with mass spectrometric findings. The first one is the fact that cytoplasmic, inactive androgen receptors can be activated by the growth factor protein family, including IGF-1, in states with low levels of androgens, i.e. dihydrotestosterone (250). The second one is cross-linking and reciprocity of both androgen and estrogen receptors and IGF-1R, specifically in the context of downstream signaling cascades and nuclear transcription activation (especially through the RAS/MAPK pathway which was found to be involved in synaptic plasticity). This connection was heavily discussed in a paper by Huffman J et al. (251) where the highlight was mainly on estrogens, simply due to the fact that most research

into sex hormone effects on hippocampal function and morphology has been focused on them. This does not, however, negate the findings that the most significant differences in the mass spectrometric analysis were found in male rat groups since both testosterone and estrogens have a strong presence and function in both sexes.

The finding that estrone glucoronide and 2-methoxyestrone-3-sulfate had significant differences between the SD group and the HFHSD group in both male and female groups is suggestive of a probability that the effects of a HFHSD altered estrogen, rather than (or in addition to) testosterone synthesis. The findings could also be a reflection of a systemic change in circulating estrogen levels, which have already been extensively researched and proven (252, 253). Androstenedione levels might have been reduced, i.e. depleted in male rats in order to synthesize an increased amount of estrogens. This scenario implicates not only the previously discussed intracellular signaling and its effects, but also introduces the topic of neuroinflammation. The overlapping consequences of MetS in terms of effects of InR and a chronic, systemic proinflammatory state that extends to the CNS make it difficult to differentiate and delineate between the two when investigating changes in tissue morphology and metabolomics. Studies have shown that ovariectomised mice demonstrate an exaggeration of acute inflammatory mediators and changes in microglia and astroglia (254). To expand on this, we must also take animal age into account as an important factor when attempting to elucidate these findings. A paper by Villa A et al. (255) discusses the diminishing function of estrogen receptors with aging, leading to elevated levels of circulating estrogens, which may, in part, explain the findings due to the fact that rats were terminated at 65 weeks of age. While these papers primarily refer to female animals, it is to be expected and assumed that an age-dependent decrease in functionality of steroid hormone receptors affects males as well. An opposing finding that further complicates matters lies in the relationship between androstenedione and estrogens in the male sex. A study carried out by Hojo et al. (240) revealed a weak conversion of androstenedione to estrogens, indicating that hippocampal estrogens in males are synthesized primarily through testosterone.

When analyzing and interpreting the effects of pharmacological agents, it was interesting to find that specific, not extensive, but nonetheless significant decreases in estrogen metabolites were found in both sexes only when treated with metformin. The liraglutide-treated group, on the other hand, besides the aforementioned change in androstenedione, showed a significant decrease in cholesterol sulfate when compared with the HFHSD group in males. While cholesterol sulfate was found to be not only a precursor in steroid biosynthesis, but also a relevant neuroprotective agent that alters astrocyte metabolism

and protects neurons from oxidative stress (256), this finding could be reflective of liraglutide-mediated changes in circulating and membrane lipid levels.

6.2.4. Changes in other metabolites

Besides lipidomic changes, the mass spectrometric analysis provided insight into multiple other compounds from other molecular groups. In the group of carbohydrates, only a few compounds were identified (three in male rats, five in female rats), which was, to a certain degree, expected, since direct effects of InR in neuronal (hippocampal) tissue regarding carbohydrate metabolism are not main concerns and crucial components, simply due to the fact that CNS does not rely on insulin for glucose uptake and utilization. The crucial aspects of metabolic changes in hippocampal neurons are related to ceramide, FFA and complex lipid synthesis, degradation and circulation. The most prominent changes, carbohydrate-wise, in both sexes were observed in D-galactosamine levels. HFHSD groups of both sexes saw large increases compared to their respective SD groups, with female rats seeing decreases when treated with metformin and liraglutide and male rats after metformin treatment. This aminosugar represents one of the many building blocks of gangliosides, which is why its presence in the mass spectrometric analysis stands out as a relevant finding. Its eightfold and tenfold increase in male and female rats, respectively, in the HFHSD group demonstrates a neuronal accumulation that could be a reflection of structural changes to the membrane and myelin sheath, including ganglioside composition, spread and overall share in membrane lipids. One ganglioside that is of specific interest in this context is GM1. It contains, among other components, two galactose residues and an N-acetylgalactosamine group (257). The aforementioned effects of a HFHSD and metformin and liraglutide treatment on GM1 expression (Chapter 6.1.) can be linked to galactosamine levels, even though a response to liraglutide treatment was not observed in male rats, as was seen for GM1. Furthermore, there were extensive changes between female groups in galactosamine levels, while GM1 expression levels did not significantly change following pharmacotherapy. The findings regarding these two compounds, while not fully comprehendible and complimentary, are important to point out due to the fact that GM1 is the most abundant ganglioside in lipid rafts (197). Lipid rafts are also rich in GPI-anchors that play a significant role in myelin stability (235). This brings CDP-ethanolamine back into the discussion, since a sevenfold increase was observed in liraglutide-treated male rats compared to those on a

HFHSD without intervention, which correlates well with the GM1 immunohistochemical findings, where IDV values in liraglutide-treated male rats were significantly higher than even the control group. Once again, with both galactosamine and CDP-ethanolamine, only intermediate compounds in certain metabolic pathways related to the pathology of interest were identified, but the combined results of the immunohistochemical and mass spectrometric analysis are solid enough to support the initial hypothesis of changes in the hippocampal lipidome following a HFHSD and pharmacotherapy.

Small, but still significant changes in unspecific compounds were found related to mannose metabolism – GDP-4-dehydro-6-deoxy-D-mannose in both sexes and GDP-mannose in female rats. Salicin-6-phosphate showed an increase in HFHSD groups of both sexes compared to the SD group, with opposite effects observed following pharmacotherapy. Female rats also showed an increase in stachyose levels following treatment with metformin.

There were significant differences in levels of several vitamins and cofactors. In line with previously observed compounds, female rats predominantly responded to metformin treatment, while treatment-related changes in male rats were less prominent, but they responded to both metformin and liraglutide. The most striking sex-specific difference was observed for tetrahydrofolate, which showed an extremely large increase in the HFHSD group compared to the SD group (t = 33.80319), while male rats did not show any significant changes between those two groups. Interestingly, both metformin and liraglutide treatment somewhat decreased its levels in female rats, while liraglutide treatment in male rats increased it. The role of folate compounds in the CNS has been known since the 1980s (258) and, more recently, its positive effects on oxidative stress inhibition have been described (259). A similar pattern of changes between sexes was observed for the coenzyme flavin mononucleotide, which showed increases following a HFHSD and decreases following pharmacotherapy (metformin in male rats, both metformin and liraglutide in female rats). A small, but significant decrease following metformin treatment in 2-hydroxyethyl-thiamine diphosphate levels was observed in female rats, which is a finding that should not be ignored because this compound is closely related to several key metabolic pathways, including the citrate cycle and glucose and pyruvate metabolism. Minor alterations were observed for NADH and the previously discussed CoA.

When it comes to compounds related to purine and pyrimidine metabolism, it is evident that metformin treatment had a significant effect on female rats in terms of decreasing the levels of identified compounds. In male rats, on the other hand, there were fewer treatment-mediated changes. Two compounds that had drastically increased in male rats

treated with liraglutide compared to the HFHSD group were 2',3'-cyclic CMP and adenylosuccinate. Their place in the metabolic puzzle lies in the biosynthesis and degradation of nucleotides. Several other intermediate metabolites of this group were identified, with no clear and distinctive relation to lipidomic changes.

One compound that has recently garnered attention in the context of brain atrophy and neurodegeneration, including AD, is homocysteine. In a 2021 meta-analysis, Wang Q et al. (260) concluded that increased levels of homocysteine increase the risk of AD. Our analysis identified S-adenosylhomocysteine, which is an intermediate compound in the synthesis of homocysteine. HFHSD groups of both sexes showed increases in S-adenosylhomocysteine levels compared to their respective SD groups. This was one of the rare instances where an atypical response to pharmacotherapy was observed – metformin decreased its levels in male rats, while liraglutide decreased them in female rats. Nonetheless, the mere existence of this compound in the analysis points to another potential, not yet fully elucidated, aspect of InR and neurodegeneration. Several other compounds related to different amino acid metabolism (tyrosine, tryptophan, histidine) were identified, with female rats once again showing better response to metformin therapy, while male rats similarly responded to both metformin and liraglutide.

6.2.5. A sex-specific response to pharmacotherapeutic agents

An overwhelming number of identified compounds in the mass spectrometric analysis showed changes following metformin or liraglutide treatment. While there is a certain share of compounds that were affected by both pharmacotherapeutic agents, most compounds that showed changes following treatment with only a single agent show a very clear sex-specific delineation: male rats responded better to liraglutide, while female rats responded better to metformin. Tables 5.75 and 5.76 best illustrate this observation – such a distinctly different effect of treatment on a compound group is seen among identified fatty acids. This has been a common thread throughout the discussion of changes, not just in that particular compound group, but in every one of them and the additional factor that supports this finding is the immunohistochemical analysis. While not as clear-cut as the mass spectrometric findings, immunohistochemical stains did reveal that liraglutide treatment changed the expression of certain gangliosides in several ROIs in male rats, while protein expression was more affected in female rats treated with metformin. Many aspects of neuronal metabolism and structural

integrity disruption at play in the context of InR in the brain were uncovered through the spectrometric analysis – lipid peroxidation, ferroptosis, mitochondrial dysfunction, signaling disruption, as well as membrane and myelin integrity and composition. Treatment with neither metformin nor liraglutide showed clear unidirectional changes compared to a non-treated HFHSD to be able to come to a conclusion of undisputable certainty that they positively or negatively impact any of the InR- and neurodegeneration-related cellular dysfunction in the hippocampus.

6.3. Prospects of the study

T2DM and MetS are extensively researched topics with both animal and clinical studies being published on a daily basis. This research specifically has a large translational potential regarding modifications of T2DM treatment, especially in the context of neurodegeneration. Metformin and liraglutide are commonly used antidiabetics in daily practice. The gravity of the deleterious effects T2DM has on the CNS, however, is still not fully embedded in the minds of all primary care physicians and clinicians. With the rise of modern and sophisticated methodologies used to analyse the entire composition of certain tissues, coupled with the rise of modern *in vivo* imaging techniques in a clinical setting that are in the domain of radiology (e.g. magnetic resonance spectrometry), a field of medicine currently seeing extensive progress in imaging techniques thanks to artificial intelligence and biomarker identification, there is large potential to shift these types of studies from animal models to a clinical setting where patients who are struggling with the nosogenic effects of T2DM on the CNS and hippocampus, specifically, can be observed (261, 262). An important step towards achieving this would be identifying potential biomarkers of treatment response to certain pharmacotherapeutic agents in an animal model hippocampus and then applying and translating that knowledge into a clinical setting.

6.4. Limitations of the study

The MALDI-TOF spectrometric analysis was carried out on samples of tissue homogenate, which did not allow for a spatial correlation of changes in the lipidome with the immunohistochemical results. A repeat of the experiment using a method that would provide this information, e.g. imaging mass spectrometry, could be performed for more specific

information. Immunohistochemical analysis was performed by observing the expression of four neuronal gangliosides and four neuronal proteins. Expanding the number of epitopes, or perhaps using different methodology could provide additional and more specific changes in hippocampal neurons to build on the findings of this study. InR in this study was induced on a systemic level through a HFHSD – CNS-specific changes and those that are a reflection of circulating metabolites from distal tissues (liver, adipose tissue, muscle tissue, etc.) have been blended. A locally induced InR (e.g. via a lentiviral vector expressing an IR antisense sequence) has already been used to observe changes in Sprague Dawley rats (Grillo, Reagan), so this methodology could provide more specific answers to InR-mediated changes in the hippocampal lipidome.

7. CONCLUSIONS

Based on the research results, the following conclusions can be made:

- A HFHSD, as well as metformin and liraglutide treatment, caused significant changes in the expression of common neuronal gangliosides and proteins that serve as biomarkers for AD;

- The expression of ganglioside GM1 following liraglutide treatment was significantly increased in all hippocampal ROIs in male rats, even in regions where it is not normally found, while expression of ganglioside GT1b was significantly decreased in both sexes following metformin and liraglutide treatment;

- Liraglutide treatment significantly decreased pTau expression in the DG, CA1 and CA3 regions of male rats;

- Metformin and liraglutide treatment caused sex-specific changes in the hippocampal lipidome;

- Effects of liraglutide treatment were more prominent in male rats, while effects of metformin treatment were more prominent in female rats;

- Lipidomic analysis revealed that altered compounds included PUFAs, FFAs, fatty acyl-CoAs, sphingolipids, glycerophospholipids and steroid hormones;

- The alterations of the HFHSD group hippocampal lipidome were suggestive of changes due to mitochondrial dysfunction, lipid peroxidation, intracellular signaling disruption and an InR-related shift in metabolism;

- Sphinganine and CDP-ethanolamine changes were a reflection of membrane and myelin sheath disruption following a HFHSD;

- Lipidomic analysis revealed HFHSD-related changes in steroid hormone metabolism that were more prominent in male rats;

- Lipidomic analysis revealed HFHSD-related changes to carbohydrate, amino acid and purine and pyrimidine metabolism, with unspecific changes observed following treatment with metformin and liraglutide;

- Based on the overall spectrometric and immunohistochemical analysis, treatment with neither metformin nor liraglutide exhibited uniform alterations of the lipidome to suggest a reversal of HFHSD-related changes of undisputable certainty.

8. SUMMARY

Objectives. To determine sex-specific changes in the hippocampal lipidome in a HFHSD rat model following treatment with metformin and liraglutide and to determine expression levels of relevant neuronal gangliosides and proteins.

Study Design. Paired research.

Materials and Methods. The study included 64 Sprague Dawley rats divided by sex into four groups based on diet and treatment with either metformin or liraglutide, including a control group on a standard diet. After a 20-week regimen of a HFHSD and pharmacotherapy, rat brains were isolated and halved. Once hippocampal tissue was isolated, one half was used for immunohistochemical analysis of common neuronal gangliosides and proteins relevant to InR, while the other half was used for MALDI-TOF spectrometric analysis to identify alterations in the hippocampal lipidome.

Results. Immunohistochemical analysis showed changes in the expression of all gangliosides, with the most notable changes seen in GM1 in male rats, where liraglutide increased its expression, even in regions where it is not usually expressed. Liraglutide significantly decreased pTau levels throughout the hippocampus in male rats. Non-specific changes were observed in IR and IGF-1R expression predominantly in male rats. The lipidomic analysis revealed changes following a HFHSD, as well as metformin and liraglutide treatment. Changes following liraglutide treatment were more prevalent in male rats, while metformin changes were more prevalent in female rats. Multiple groups of lipids were affected, suggestive of changes due to mitochondrial dysfunction, lipid peroxidation, intracellular signaling disruption and membrane and myelin sheath composition changes. Neither metformin nor liraglutide exhibited uniformly specific changes to suggest a reversal of HFHSD-induced changes.

Conclusion. A HFHSD changed the hippocampal lipidome in both sexes. There were notable alterations following pharmacotherapy, with certain differences observed between sexes.

Keywords. Diabetes mellitus; hippocampus; insulin resistance; lipidome; MALDI-TOF.

9. SAŽETAK

Cilj istraživanja. Ispitati spolno specifične razlike lipidoma hipokampusa u modelu štakora na dijeti obogaćenoj mastima i ugljikohidratima, kao i nakon primjene metformina i liraglutida te utvrditi ekspresiju značajnih gangliozida i bjelančevina.

Ustroj istraživanja. Istraživanje parova.

Materijali i metode. 64 Sprague Dawley štakora odvojeno je po spolu i podijeljeno u četiri skupine na temelju prehrane i primjene metformina ili liraglutida, uključujući kontrolnu skupinu na standardnoj dijeti. Nakon 20 tjedana dijete obogaćene mastima i ugljikohidratima i farmakoterapije, mozgovi štakora su izolirani i podijeljeni u sagitalnoj ravnini. Jedna je polovica korištena za hipokampalnu imunohistokemijsku analizu čestih neuronalnih gangliozida i značajnih bjelančevina u etiopatogenezi inzulinske rezistencije, dok je druga polovica nakon izolacije hipokampusa korištena za MALDI-TOF spektrometrijsku analizu lipidoma.

Rezultati. Imunohistokemijska analiza pokazala je promjene u ekspresiji svih gangliozida, s najvećim promjenama u ekspresiji GM1 kod mužjaka, kod kojih je liraglutid značajno povećao njegovu ekspresiju, čak i u regijama gdje uobičajeno nije prisutan. Liraglutid je značajno smanjio razinu pTau u svim analiziranim regijama u mužjaka. Nespecifične promjene zabilježene su u ekspresiji IR i IGF-1R, dominantno kod mužjaka. Analizom lipidoma zabilježene su promjene nakon dijete obogaćene mastima i ugljikohidratima, kao i nakon primjene metformina i liraglutida. Mužjaci su pokazali bolji odgovor na terapiju liraglutidom, dok su ženke pokazale bolji odgovor na terapiju metforminom. Promijenjeno je više skupina lipida, što je ukazalo na promjene uslijed disfunkcije mitohondrija, lipidne peroksidacije, poremećaja unutarstanične signalizacije te promjene u strukturi membrane i mijelina. Liječenje metforminom i liraglutidom nije dovelo do jedinstvene i jasne promjene lipidomske strukture hipokampusa koja bi ukazivala na eliminaciju promjena induciranih dijetom.

Zaključak. Dijeta obogaćena mastima i ugljikohidratima promijenila je lipidom hipokampusa u oba spola. Značajne promjene zabilježene su nakon farmakoterapije s vidljivim razlikama i između spolova.

Ključne riječi: hipokampus; inzulinska rezistencija; lipidom, MALDI-TOF, šećerna bolest tipa 2.

10. REFERENCES

1. World Health Organization. Noncommunicable diseases. Available at: https://www.who.int/news-room/fact-sheets/detail/noncommunicable-diseases. Date of access: October 12th, 2021.

2. The Global Economic Burden of Non-communicable Diseases - A report by the World Economic Forum and the Harvard School of Public Health. Available at: http://www3.weforum.org/docs/WEF_Harvard_HE_GlobalEconomicBurdenNonCommu nicableDiseases_2011.pdf. Date of access: October 12th, 2021.

3. Haller H, Hanefeld M. Synoptische Betrachtung metabolischer Risikofaktoren. Haller H, Hanefeld M, Jaross W eds. Lipidstoffwechselstörungen. 1975; 254-264: Gustav Fischer Verlag Jena.

4. Grundy SM. Overnutrition, ectopic lipid and the metabolic syndrome. J Investig Med. 2016;64(6):1082-6.

5. Saklayen MG. The Global Epidemic of the Metabolic Syndrome. Curr Hypertens Rep. 2018;20(2):12.

6. Alwan A, King H, editors. Department of Noncommunicable Disease Surveillance. Geneva: World Health Organization; 1999. World Health Organization: Definition, Diagnosis, and Classification of Diabetes Mellitus and its Complications. Part 1: Diagnosis and Classification of Diabetes Mellitus: Report of a WHO consultation; pp. 1– 59.

7. The IDF consensus worldwide definition of the metabolic syndrome. International Diabetes Federation, 2006. Available at: https://www.idf.org/component/attachments/attachments.html?id=705&task=download. Date of access: November 3rd, 2021.

8. National Cholesterol Education Program Expert Panel on Detection E, Treatment of High Blood Cholesterol in A. Third Report of the National Cholesterol Education Program (NCEP) Expert Panel on Detection, Evaluation, and Treatment of High Blood Cholesterol in Adults (Adult Treatment Panel III) final report. Circulation. 2002;106(25):3143-421.

9. Bluher M. Metabolically Healthy Obesity. Endocr Rev. 2020;41(3).

10. Osadnik K, Osadnik T, Lonnie M, Lejawa M, Regula R, Fronczek M, et al. Metabolically healthy obese and metabolic syndrome of the lean: the importance of diet quality. Analysis of MAGNETIC cohort. Nutr J. 2020;19(1):19.

11. Nielsen J. Systems Biology of Metabolism: A Driver for Developing Personalized and Precision Medicine. Cell Metab. 2017;25(3):572-9.

12. Marchiani S, Tamburrino L, McPherson N, Baldi E. Editorial: The Role of Obesity and Metabolic Syndrome in Couple Infertility. Front Endocrinol (Lausanne). 2021;12:784716.

13. Esposito K, Chiodini P, Colao A, Lenzi A, Giugliano D. Metabolic syndrome and risk of cancer: a systematic review and meta-analysis. Diabetes Care. 2012;35(11):2402-11.

14. Lee MK, Han K, Kim MK, Koh ES, Kim ES, Nam GE, et al. Changes in metabolic syndrome and its components and the risk of type 2 diabetes: a nationwide cohort study. Sci Rep. 2020;10(1):2313.

15. Petersen MC, Shulman GI. Mechanisms of Insulin Action and Insulin Resistance. Physiol Rev. 2018;98(4):2133-223.

16. Belfiore A, Malaguarnera R, Vella V, Lawrence MC, Sciacca L, Frasca F, et al. Insulin Receptor Isoforms in Physiology and Disease: An Updated View. Endocr Rev. 2017;38(5):379-431.

17. De Meyts P. The insulin receptor: a prototype for dimeric, allosteric membrane receptors? Trends Biochem Sci. 2008;33(8):376-84.

18. Kido Y, Burks DJ, Withers D, Bruning JC, Kahn CR, White MF, et al. Tissue-specific insulin resistance in mice with mutations in the insulin receptor, IRS-1, and IRS-2. J Clin Invest. 2000;105(2):199-205.

19. Withers DJ, Gutierrez JS, Towery H, Burks DJ, Ren JM, Previs S, et al. Disruption of IRS-2 causes type 2 diabetes in mice. Nature. 1998;391(6670):900-4.

20. Huang X, Liu G, Guo J, Su Z. The PI3K/AKT pathway in obesity and type 2 diabetes. Int J Biol Sci. 2018;14(11):1483-96.

21. Geraldes P, King GL. Activation of protein kinase C isoforms and its impact on diabetic complications. Circ Res. 2010;106(8):1319-31.

22. Saltiel AR, Kahn CR. Insulin signalling and the regulation of glucose and lipid metabolism. Nature. 2001;414(6865):799-806.

23. Copps KD, White MF. Regulation of insulin sensitivity by serine/threonine phosphorylation of insulin receptor substrate proteins IRS1 and IRS2. Diabetologia. 2012;55(10):2565-82.

24. Liu GY, Sabatini DM. mTOR at the nexus of nutrition, growth, ageing and disease. Nat Rev Mol Cell Biol. 2020;21(4):183-203.

25. Barthel A, Schmoll D, Unterman TG. FoxO proteins in insulin action and metabolism. Trends Endocrinol Metab. 2005;16(4):183-9.

26. Luo Z, Fujio Y, Kureishi Y, Rudic RD, Daumerie G, Fulton D, et al. Acute modulation of endothelial Akt/PKB activity alters nitric oxide-dependent vasomotor activity in vivo. J Clin Invest. 2000;106(4):493-9.

27. Boucher J, Kleinridders A, Kahn CR. Insulin receptor signaling in normal and insulin-resistant states. Cold Spring Harb Perspect Biol. 2014;6(1).

28. Terrell EM, Morrison DK. Ras-Mediated Activation of the Raf Family Kinases. Cold Spring Harb Perspect Med. 2019;9(1).

29. DeFronzo RA, Ferrannini E, Groop L, Henry RR, Herman WH, Holst JJ, et al. Type 2 diabetes mellitus. Nat Rev Dis Primers. 2015;1:15019.

30. Lebovitz HE. Insulin resistance: definition and consequences. Exp Clin Endocrinol Diabetes. 2001;109 Suppl 2:S135-48.

31. Matthews DR, Hosker JP, Rudenski AS, Naylor BA, Treacher DF, Turner RC. Homeostasis model assessment: insulin resistance and beta-cell function from fasting plasma glucose and insulin concentrations in man. Diabetologia. 1985;28(7):412-9.

32. Gayoso-Diz P, Otero-Gonzalez A, Rodriguez-Alvarez MX, Gude F, Garcia F, De Francisco A, et al. Insulin resistance (HOMA-IR) cut-off values and the metabolic syndrome in a general adult population: effect of gender and age: EPIRCE cross-sectional study. BMC Endocr Disord. 2013;13:47.

33. Hanley AJ, Williams K, Stern MP, et al. Homeostasis model assessment of insulin resistance in relation to the incidence of cardiovascular disease: the San Antonio Heart Study. Diabetes Care. 2002;25:1177–1184.

34. Sokolowska E, Blachnio-Zabielska A. The Role of Ceramides in Insulin Resistance. Front Endocrinol (Lausanne). 2019;10:577.

35. Erion DM, Shulman GI. Diacylglycerol-mediated insulin resistance. Nat Med. 2010;16(4):400-2.

36. Zhang D, Liu ZX, Choi CS, Tian L, Kibbey R, Dong J, et al. Mitochondrial dysfunction due to long-chain Acyl-CoA dehydrogenase deficiency causes hepatic steatosis and hepatic insulin resistance. Proc Natl Acad Sci U S A. 2007;104(43):17075-80.

37. Ellis BA, Poynten A, Lowy AJ, Furler SM, Chisholm DJ, Kraegen EW, et al. Long-chain acyl-CoA esters as indicators of lipid metabolism and insulin sensitivity in rat and human muscle. Am J Physiol Endocrinol Metab. 2000;279(3):E554-60.

38. Gregor MF, Hotamisligil GS. Inflammatory mechanisms in obesity. Annu Rev Immunol. 2011;29:415-45.

39. Perseghin G, Scifo P, De Cobelli F, Pagliato E, Battezzati A, Arcelloni C, et al. Intramyocellular triglyceride content is a determinant of in vivo insulin resistance in humans: a 1H-13C nuclear magnetic resonance spectroscopy assessment in offspring of type 2 diabetic parents. Diabetes. 1999;48(8):1600-6.

40. Allen JA, Halverson-Tamboli RA, Rasenick MM. Lipid raft microdomains and neurotransmitter signalling. Nat Rev Neurosci. 2007;8(2):128-40.

41. Glatz JFC, Luiken J. Dynamic role of the transmembrane glycoprotein CD36 (SR-B2) in cellular fatty acid uptake and utilization. J Lipid Res. 2018;59(7):1084-93.

42. Ehehalt R, Sparla R, Kulaksiz H, Herrmann T, Fullekrug J, Stremmel W. Uptake of long chain fatty acids is regulated by dynamic interaction of FAT/CD36 with cholesterol/sphingolipid enriched microdomains (lipid rafts). BMC Cell Biol. 2008;9:45.

43. Frühbeck G, Lopez M, Dieguez C. Role of caveolins in body weight and insulin resistance regulation. Trends Endocrinol Metab. 2007;18(5):177-82.

44. Yu C, Chen Y, Cline GW, et al.. Mechanism by which fatty acids inhibit insulin activation of insulin receptor substrate-1 (IRS-1)-associated phosphatidylinositol 3-kinase activity in muscle. J Biol Chem. 2002;277(52):50230–50236.

45. Summers SA, Garza LA, Zhou H, Birnbaum MJ. Regulation of insulin-stimulated glucose transporter GLUT4 translocation and Akt kinase activity by ceramide. Mol Cell Biol. 1998;18(9):5457-64.

46. Hyde R, Hajduch E, Powell DJ, Taylor PM, Hundal HS. Ceramide down-regulates System A amino acid transport and protein synthesis in rat skeletal muscle cells. FASEB J. 2005;19(3):461-3.

47. Kashyap SR, Roman LJ, Lamont J, Masters BS, Bajaj M, Suraamornkul S, et al. Insulin resistance is associated with impaired nitric oxide synthase activity in skeletal muscle of type 2 diabetic subjects. J Clin Endocrinol Metab. 2005;90(2):1100-5.

48. Chennamsetty I, Coronado M, Contrepois K, Keller MP, Carcamo-Orive I, Sandin J, et al. Nat1 Deficiency Is Associated with Mitochondrial Dysfunction and Exercise Intolerance in Mice. Cell Rep. 2016;17(2):527-40.

49. Knowles JW, Xie W, Zhang Z, Chennamsetty I, Assimes TL, Paananen J, et al. Identification and validation of N-acetyltransferase 2 as an insulin sensitivity gene. J Clin Invest. 2015;125(4):1739-51.

50. Ritov VB, Menshikova EV, He J, Ferrell RE, Goodpaster BH, Kelley DE. Deficiency of subsarcolemmal mitochondria in obesity and type 2 diabetes. Diabetes. 2005;54(1):8-14.

51. Stump CS, Short KR, Bigelow ML, Schimke JM, Nair KS. Effect of insulin on human skeletal muscle mitochondrial ATP production, protein synthesis, and mRNA transcripts. Proc Natl Acad Sci U S A. 2003;100(13):7996-8001.

52. Newsom SA, Everett AC, Hinko A, Horowitz JF. A single session of low-intensity exercise is sufficient to enhance insulin sensitivity into the next day in obese adults. Diabetes Care. 2013;36(9):2516-22.

53. Menshikova EV, Ritov VB, Toledo FG, Ferrell RE, Goodpaster BH, Kelley DE. Effects of weight loss and physical activity on skeletal muscle mitochondrial function in obesity. Am J Physiol Endocrinol Metab. 2005;288(4):E818-25.

54. Tan J, Guo L. Swimming intervention alleviates insulin resistance and chronic inflammation in metabolic syndrome. Exp Ther Med. 2019;17(1):57-62.

55. Eizirik DL, Cardozo AK, Cnop M. The role for endoplasmic reticulum stress in diabetes mellitus. Endocr Rev. 2008;29(1):42-61.

56. Ozcan U, Cao Q, Yilmaz E, Lee AH, Iwakoshi NN, Ozdelen E, et al. Endoplasmic reticulum stress links obesity, insulin action, and type 2 diabetes. Science. 2004;306(5695):457-61.

57. Boden G, Duan X, Homko C, Molina EJ, Song W, Perez O, et al. Increase in endoplasmic reticulum stress-related proteins and genes in adipose tissue of obese, insulin-resistant individuals. Diabetes. 2008;57(9):2438-44.

58. Cho JH, Kim JW, Shin JA, Shin J, Yoon KH. beta-cell mass in people with type 2 diabetes. J Diabetes Investig. 2011;2(1):6-17.

59. Muoio DM, Newgard CB. Mechanisms of disease: Molecular and metabolic mechanisms of insulin resistance and beta-cell failure in type 2 diabetes. Nat Rev Mol Cell Biol. 2008;9(3):193-205.

60. Gupta D, Leahy JL. Islet amyloid and type 2 diabetes: overproduction or inadequate clearance and detoxification? J Clin Invest. 2014;124(8):3292-4.

61. Rahier J, Guiot Y, Goebbels RM, Sempoux C, Henquin JC. Pancreatic beta-cell mass in European subjects with type 2 diabetes. Diabetes Obes Metab. 2008;10 Suppl 4:32-42.

62. Dienel GA. Brain Glucose Metabolism: Integration of Energetics with Function. Physiol Rev. 2019 Jan 1;99(1):949-1045.

63. Harris JJ, Jolivet R, Attwell D. Synaptic energy use and supply. Neuron. 2012 Sep 6;75(5):762-77.

64. Attwell D, Laughlin SB. An energy budget for signaling in the grey matter of the brain. J Cereb Blood Flow Metab. 2001 Oct;21(10):1133-45.

65. Rangaraju V, Calloway N, Ryan TA. (2014). Activity-driven local ATP synthesis is required for synaptic function. Cell. 2014 Feb 13;156(4):825-35.

66. Pathak D, Shields LY, Mendelsohn BA, Haddad D, Lin W, Gerencser AA, et al. The role of mitochondrially derived ATP in synaptic vesicle recycling. J Biol Chem. 2015;290(37):22325-36.

67. Grillo CA, Piroli GG, Hendry RM, Reagan LP. Insulin-stimulated translocation of GLUT4 to the plasma membrane in rat hippocampus is PI3-kinase dependent. Brain Res. 2009;1296:35-45.

68. Vecchio I, Tornali C, Bragazzi NL, Martini M. The Discovery of Insulin: An Important Milestone in the History of Medicine. Front Endocrinol (Lausanne). 2018;9:613.

69. Havrankova J, Schmechel D, Roth J, Brownstein M. Identification of insulin in rat brain. Proc Natl Acad Sci U S A. 1978 Nov;75(11):5737-41.

70. Woods SC, Lotter EC, McKay LD, Porte D, Jr. Chronic intracerebroventricular infusion of insulin reduces food intake and body weight of baboons. Nature. 1979;282(5738):503-5.

71. Strubbe JH, Porte D Jr, Woods SC. Insulin responses and glucose levels in plasma and cerebrospinal fluid during fasting and refeeding in the rat. Physiol Behav. 1988;44:205–8.

72. Wallum BJ, Taborsky GJ Jr, Porte D Jr, Figlewicz DP, Jacobson L, et al. Cerebrospinal fluid insulin levels increase during intravenous insulin infusions in man. J Clin Endocrinol Metab. 1987 Jan;64(1):190–4.

73. Kern W, Benedict C, Schultes B, Plohr F, Moser A, Born J, et al. Low cerebrospinal fluid insulin levels in obese humans. Diabetologia. 2006;49(11):2790-2.

74. Schwartz MW, Sipols A, Kahn SE, Lattemann DF, Taborsky GJ, Jr., Bergman RN, et al. Kinetics and specificity of insulin uptake from plasma into cerebrospinal fluid. Am J Physiol. 1990;259(3 Pt 1):E378-83.

75. Gray SM, Aylor KW, Barrett EJ. Unravelling the regulation of insulin transport across the brain endothelial cell. Diabetologia. 2017;60(8):1512-21.

76. Wilhelm I, Nyul-Toth A, Suciu M, Hermenean A, Krizbai IA. Heterogeneity of the blood-brain barrier. Tissue Barriers. 2016;4(1):e1143544.

77. Csajbok EA, Tamas G. Cerebral cortex: a target and source of insulin? Diabetologia. 2016;59(8):1609-15.

78. Rhea EM, Rask-Madsen C, Banks WA. Insulin transport across the blood–brain barrier can occur independently of the insulin receptor. J Physiol. 2018 Oct;596(19):4753-4765.

79. Brown C, Pemberton S, Babin A, Abdulhameed N, Noonan C, Brown MB, et al. Insulin blood-brain barrier transport and interactions are greater following exercise in mice. J Appl Physiol (1985). 2022;132(3):824-34.

80. Hill JM, Lesniak MA, Pert CB, Roth J. Autoradiographic localization of insulin receptors in rat brain: prominence in olfactory and limbic areas. Neuroscience. 1986 Apr;17(4):1127-38.

81. Werther GA, Hogg A, Oldfield BJ, McKinley MJ, Figdor R, Mendelsohn FA. Localization and Characterization of Insulin-Like Growth Factor-I Receptors in Rat Brain and Pituitary Gland Using in vitro Autoradiography and Computerized Densitometry* A Distinct Distribution from Insulin Receptors. J Neuroendocrinol. 1989 Oct 1;1(5):369-77.

82. Timper K, Bruning JC. Hypothalamic circuits regulating appetite and energy homeostasis: pathways to obesity. Dis Model Mech. 2017;10(6):679-89.

83. Obici S, Zhang BB, Karkanias G, Rossetti L. Hypothalamic insulin signaling is required for inhibition of glucose production. Nat Med. 2002;8(12):1376-82.

84. Clarke DW, Boyd FT, Jr., Kappy MS, Raizada MK. Insulin stimulates macromolecular synthesis in cultured glial cells from rat brain. Am J Physiol. 1985;249(5 Pt 1):C484-9.

85. Mielke JG, Taghibiglou C, Wang YT. Endogenous insulin signaling protects cultured neurons from oxygen-glucose deprivation-induced cell death. Neuroscience. 2006;143(1):165-73.

86. Xu QG, Li XQ, Kotecha SA, Cheng C, Sun HS, Zochodne DW. Insulin as an in vivo growth factor. Exp Neurol. 2004;188(1):43-51.

87. Schubert M, Brazil DP, Burks DJ, Kushner JA, Ye J, Flint CL, et al. Insulin receptor substrate-2 deficiency impairs brain growth and promotes tau phosphorylation. J Neurosci. 2003;23(18):7084-92.

88. Heidenreich KA, Toledo SP. Insulin receptors mediate growth effects in cultured fetal neurons. II. Activation of a protein kinase that phosphorylates ribosomal protein S6. Endocrinology. 1989;125(3):1458-63.

89. Lee CC, Huang CC, Wu MY, Hsu KS. Insulin stimulates postsynaptic density-95 protein translation via the phosphoinositide 3-kinase-Akt-mammalian target of rapamycin signaling pathway. J Biol Chem. 2005;280(18):18543-50.

90. Duarte AI, Proenca T, Oliveira CR, Santos MS, Rego AC. Insulin restores metabolic function in cultured cortical neurons subjected to oxidative stress. Diabetes. 2006;55(10):2863-70.

91. Duarte AI, Santos MS, Seica R, de Oliveira CR. Insulin affects synaptosomal GABA and glutamate transport under oxidative stress conditions. Brain Res. 2003;977(1):23-30.

92. Boyd FT, Jr., Clarke DW, Muther TF, Raizada MK. Insulin receptors and insulin modulation of norepinephrine uptake in neuronal cultures from rat brain. J Biol Chem. 1985;260(29):15880-4.

93. Zhao F, Siu JJ, Huang W, Askwith C, Cao L. Insulin Modulates Excitatory Synaptic Transmission and Synaptic Plasticity in the Mouse Hippocampus. Neuroscience. 2019;411:237-54.

94. Wang Q, Liu L, Pei L, Ju W, Ahmadian G, Lu J, et al. Control of synaptic strength, a novel function of Akt. Neuron. 2003;38(6):915-28.

95. Sliwowska JH, Fergani C, Gawalek M, Skowronska B, Fichna P, Lehman MN. Insulin: its role in the central control of reproduction. Physiol Behav. 2014;133:197-206.

96. Arias P, Rodriguez M, Szwarcfarb B, Sinay IR, Moguilevsky JA. Effect of insulin on LHRH release by perifused hypothalamic fragments. Neuroendocrinology. 1992;56(3):415-8.

97. Steen E, Terry BM, Rivera EJ, Cannon JL, Neely TR, Tavares R, et al. Impaired insulin and insulin-like growth factor expression and signaling mechanisms in Alzheimer's disease--is this type 3 diabetes? J Alzheimers Dis. 2005;7(1):63-80.

98. McKhann GM, Knopman DS, Chertkow H, Hyman BT, Jack CR, Jr., Kawas CH, et al. The diagnosis of dementia due to Alzheimer's disease: recommendations from the National Institute on Aging-Alzheimer's Association workgroups on diagnostic guidelines for Alzheimer's disease. Alzheimers Dement. 2011;7(3):263-9.

99. Blennow K, Zetterberg H. Biomarkers for Alzheimer's disease: current status and prospects for the future. J Intern Med. 2018;284(6):643-63.

100. Stephan BC, Matthews FE, Ma B, Muniz G, Hunter S, Davis D, et al. Alzheimer and vascular neuropathological changes associated with different cognitive States in a non-demented sample. J Alzheimers Dis. 2012;29(2):309-18.

101. Nelson PT, Alafuzoff I, Bigio EH, Bouras C, Braak H, Cairns NJ, et al. Correlation of Alzheimer disease neuropathologic changes with cognitive status: a review of the literature. J Neuropathol Exp Neurol. 2012;71(5):362-81.

102. Bove J, Perier C. Neurotoxin-based models of Parkinson's disease. Neuroscience. 2012;211:51-76.

103. Karch CM, Goate AM. Alzheimer's disease risk genes and mechanisms of disease pathogenesis. Biol Psychiatry. 2015;77(1):43-51.

104. Priller C, Bauer T, Mitteregger G, Krebs B, Kretzschmar HA, Herms J. Synapse formation and function is modulated by the amyloid precursor protein. J Neurosci. 2006;26(27):7212-21.

105. Duce JA, Tsatsanis A, Cater MA, James SA, Robb E, Wikhe K, et al. Iron-export ferroxidase activity of beta-amyloid precursor protein is inhibited by zinc in Alzheimer's disease. Cell. 2010;142(6):857-67.

106. Turner PR, O'Connor K, Tate WP, Abraham WC. Roles of amyloid precursor protein and its fragments in regulating neural activity, plasticity and memory. Prog Neurobiol. 2003;70(1):1-32.

107. Chow VW, Mattson MP, Wong PC, Gleichmann M. An overview of APP processing enzymes and products. Neuromolecular Med. 2010;12(1):1-12.

108. Serpell LC. Alzheimer's amyloid fibrils: structure and assembly. Biochim Biophys Acta. 2000;1502(1):16-30.

109. Sengupta U, Nilson AN, Kayed R. The Role of Amyloid-beta Oligomers in Toxicity, Propagation, and Immunotherapy. EBioMedicine. 2016;6:42-9.

110. Villemagne VL, Rowe CC. Amyloid imaging. Int Psychogeriatr. 2011;23 Suppl 2:S41-9.

111. O'Nuallain B, Freir DB, Nicoll AJ, Risse E, Ferguson N, Herron CE, et al. Amyloid beta-protein dimers rapidly form stable synaptotoxic protofibrils. J Neurosci. 2010;30(43):14411-9.

112. Garzon-Rodriguez W, Vega A, Sepulveda-Becerra M, Milton S, Johnson DA, Yatsimirsky AK, et al. A conformation change in the carboxyl terminus of Alzheimer's Abeta (1-40) accompanies the transition from dimer to fibril as revealed by fluorescence quenching analysis. J Biol Chem. 2000;275(30):22645-9.

113. Forloni G, Artuso V, La Vitola P, Balducci C. Oligomeropathies and pathogenesis of Alzheimer and Parkinson's diseases. Mov Disord. 2016;31(6):771-81.

114. Mroczko B, Groblewska M, Litman-Zawadzka A, Kornhuber J, Lewczuk P. Cellular Receptors of Amyloid beta Oligomers (AbetaOs) in Alzheimer's Disease. Int J Mol Sci. 2018;19(7).

115. Xie L, Helmerhorst E, Taddei K, Plewright B, Van Bronswijk W, Martins R. Alzheimer's beta-amyloid peptides compete for insulin binding to the insulin receptor. J Neurosci. 2002;22(10):RC221.

116. Yasumoto T, Takamura Y, Tsuji M, Watanabe-Nakayama T, Imamura K, Inoue H, et al. High molecular weight amyloid beta1-42 oligomers induce neurotoxicity via plasma membrane damage. FASEB J. 2019;33(8):9220-34.

117. Kayed R, Lasagna-Reeves CA. Molecular mechanisms of amyloid oligomers toxicity. J Alzheimers Dis. 2013;33 Suppl 1:S67-78.

118. Hong S, Ostaszewski BL, Yang T, O'Malley TT, Jin M, Yanagisawa K, et al. Soluble Abeta oligomers are rapidly sequestered from brain ISF in vivo and bind GM1 ganglioside on cellular membranes. Neuron. 2014;82(2):308-19.

119. Swerdlow RH. Mitochondria and Mitochondrial Cascades in Alzheimer's Disease. J Alzheimers Dis. 2018;62(3):1403-16.

120. Andreadis A. Tau gene alternative splicing: expression patterns, regulation and modulation of function in normal brain and neurodegenerative diseases. Biochim Biophys Acta. 2005;1739(2-3):91-103.

121. Metaxas A, Kempf SJ. Neurofibrillary tangles in Alzheimer's disease: elucidation of the molecular mechanism by immunohistochemistry and tau protein phospho-proteomics. Neural Regen Res. 2016;11(10):1579-81.

122. Holmes BB, Diamond MI. Prion-like properties of Tau protein: the importance of extracellular Tau as a therapeutic target. J Biol Chem. 2014;289(29):19855-61.

123. Pereira JB, Ossenkoppele R, Palmqvist S, Strandberg TO, Smith R, Westman E, et al. Amyloid and tau accumulate across distinct spatial networks and are differentially associated with brain connectivity. Elife. 2019;8.

124. Bloom GS. Amyloid-beta and tau: the trigger and bullet in Alzheimer disease pathogenesis. JAMA Neurol. 2014;71(4):505-8.

125. Hardy JA, Higgins GA. Alzheimer's disease: the amyloid cascade hypothesis. Science. 1992;256(5054):184-5.

126. Ricciarelli R, Fedele E. The Amyloid Cascade Hypothesis in Alzheimer's Disease: It's Time to Change Our Mind. Curr Neuropharmacol. 2017;15(6):926-35.

127. Giap BT, Jong CN, Ricker JH, Cullen NK, Zafonte RD. The hippocampus: anatomy, pathophysiology, and regenerative capacity. J Head Trauma Rehabil. 2000;15(3):875-94.

128. Zemla R, Basu J. Hippocampal function in rodents. Curr Opin Neurobiol. 2017;43:187-97.

129. Kjonigsen LJ, Lillehaug S, Bjaalie JG, Witter MP, Leergaard TB. Waxholm Space atlas of the rat brain hippocampal region: three-dimensional delineations based on magnetic resonance and diffusion tensor imaging. Neuroimage. 2015;108:441-9.

130. Braak H, Braak E, Yilmazer D, Bohl J. Functional anatomy of human hippocampal formation and related structures. J Child Neurol. 1996;11(4):265-75.

131. Agster KL, Burwell RD. Hippocampal and subicular efferents and afferents of the perirhinal, postrhinal, and entorhinal cortices of the rat. Behav Brain Res. 2013;254:50-64.

132. Miranda AM, Bravo FV, Chan RB, Sousa N, Di Paolo G, Oliveira TG. Differential lipid composition and regulation along the hippocampal longitudinal axis. Transl Psychiatry. 2019;9(1):144.

133. Bear MF. A synaptic basis for memory storage in the cerebral cortex. Proc Natl Acad Sci U S A. 1996;93(24):13453-9.

134. Ming GL, Song H. Adult neurogenesis in the mammalian brain: significant answers and significant questions. Neuron. 2011;70(4):687-702.

135. de Flores R, La Joie R, Chetelat G. Structural imaging of hippocampal subfields in healthy aging and Alzheimer's disease. Neuroscience. 2015;309:29-50.

136. Mufson EJ, Mahady L, Waters D, Counts SE, Perez SE, DeKosky ST, et al. Hippocampal plasticity during the progression of Alzheimer's disease. Neuroscience. 2015;309:51-67.

137. Goedert M, Spillantini MG. A century of Alzheimer's disease. Science. 2006;314(5800):777-81.

138. Cope EC, LaMarca EA, Monari PK, Olson LB, Martinez S, Zych AD, et al. Microglia Play an Active Role in Obesity-Associated Cognitive Decline. J Neurosci. 2018;38(41):8889-904.

139. Gerges NZ, Aleisa AM, Alkadhi KA. Impaired long-term potentiation in obese zucker rats: possible involvement of presynaptic mechanism. Neuroscience. 2003;120(2):535-9.

140. Alzoubi KH, Aleisa AM, Alkadhi KA. Impairment of long-term potentiation in the CA1, but not dentate gyrus, of the hippocampus in Obese Zucker rats: role of calcineurin and phosphorylated CaMKII. J Mol Neurosci. 2005;27(3):337-46.

141. Wu A, Ying Z, Gomez-Pinilla F. The interplay between oxidative stress and brain-derived neurotrophic factor modulates the outcome of a saturated fat diet on synaptic plasticity and cognition. Eur J Neurosci. 2004;19(7):1699-707.

142. Stranahan AM, Norman ED, Lee K, Cutler RG, Telljohann RS, Egan JM, et al. Diet-induced insulin resistance impairs hippocampal synaptic plasticity and cognition in middle-aged rats. Hippocampus. 2008;18(11):1085-8.

143. Kanoski SE, Zhang Y, Zheng W, Davidson TL. The effects of a high-energy diet on hippocampal function and blood-brain barrier integrity in the rat. J Alzheimers Dis. 2010;21(1):207-19.

144. Freeman LR, Granholm AC. Vascular changes in rat hippocampus following a high saturated fat and cholesterol diet. J Cereb Blood Flow Metab. 2012;32(4):643-53.

145. Lindqvist A, Mohapel P, Bouter B, Frielingsdorf H, Pizzo D, Brundin P, et al. High-fat diet impairs hippocampal neurogenesis in male rats. Eur J Neurol. 2006;13(12):1385-8.

146. Park HR, Park M, Choi J, Park KY, Chung HY, Lee J. A high-fat diet impairs neurogenesis: involvement of lipid peroxidation and brain-derived neurotrophic factor. Neurosci Lett. 2010;482(3):235-9.

147. Boitard C, Etchamendy N, Sauvant J, Aubert A, Tronel S, Marighetto A, et al. Juvenile, but not adult exposure to high-fat diet impairs relational memory and hippocampal neurogenesis in mice. Hippocampus. 2012;22(11):2095-100.

148. Park HS, Cho HS, Kim TW. Physical exercise promotes memory capability by enhancing hippocampal mitochondrial functions and inhibiting apoptosis in obesity-induced insulin resistance by high fat diet. Metab Brain Dis. 2018;33(1):283-92.

149. Duffy CM, Hofmeister JJ, Nixon JP, Butterick TA. High fat diet increases cognitive decline and neuroinflammation in a model of orexin loss. Neurobiol Learn Mem. 2019;157:41-7.

150. Reagan LP, Cowan HB, Woodruff JL, Piroli GG, Erichsen JM, Evans AN, et al. Hippocampal-specific insulin resistance elicits behavioral despair and hippocampal dendritic atrophy. Neurobiol Stress. 2021;15:100354.

151. Grillo CA, Piroli GG, Lawrence RC, Wrighten SA, Green AJ, Wilson SP, et al. Hippocampal Insulin Resistance Impairs Spatial Learning and Synaptic Plasticity. Diabetes. 2015;64(11):3927-36.

152. Soto M, Cai W, Konishi M, Kahn CR. Insulin signaling in the hippocampus and amygdala regulates metabolism and neurobehavior. Proc Natl Acad Sci U S A. 2019;116(13):6379-84.

153. Costello DA, Claret M, Al-Qassab H, Plattner F, Irvine EE, Choudhury AI, et al. Brain deletion of insulin receptor substrate 2 disrupts hippocampal synaptic plasticity and metaplasticity. PLoS One. 2012;7(2):e31124.

154. Chell JM, Brand AH. Nutrition-responsive glia control exit of neural stem cells from quiescence. Cell. 2010;143(7):1161-73.

155. Aberg MA, Aberg ND, Palmer TD, Alborn AM, Carlsson-Skwirut C, Bang P, et al. IGF-I has a direct proliferative effect in adult hippocampal progenitor cells. Mol Cell Neurosci. 2003;24(1):23-40.

156. Diem P. [The Discovery of Insulin]. Ther Umsch. 2020;77(7):289-96.

157. Williams DM, Jones H, Stephens JW. Personalized Type 2 Diabetes Management: An Update on Recent Advances and Recommendations. Diabetes Metab Syndr Obes. 2022;15:281-95.

158. Swinnen SG, Hoekstra JB, DeVries JH. Insulin therapy for type 2 diabetes. Diabetes Care. 2009;32 Suppl 2:S253-9.

159. Zaccardi F, Khunti K, Marx N, Davies MJ. First-line treatment for type 2 diabetes: is it too early to abandon metformin? Lancet. 2020;396(10264):1705-7.

160. Rena G, Hardie DG, Pearson ER. The mechanisms of action of metformin. Diabetologia. 2017;60(9):1577-85.

161. Raptis SA, Dimitriadis GD. Oral hypoglycemic agents: insulin secretagogues, alpha-glucosidase inhibitors and insulin sensitizers. Exp Clin Endocrinol Diabetes. 2001;109 Suppl 2:S265-87.

162. Hauner H. The mode of action of thiazolidinediones. Diabetes Metab Res Rev. 2002;18 Suppl 2:S10-5.

163. Kim W, Egan JM. The role of incretins in glucose homeostasis and diabetes treatment. Pharmacol Rev. 2008;60(4):470-512.

164. Rosenwasser RF, Sultan S, Sutton D, Choksi R, Epstein BJ. SGLT-2 inhibitors and their potential in the treatment of diabetes. Diabetes Metab Syndr Obes. 2013;6:453-67.

165. Pernicova I, Korbonits M. Metformin--mode of action and clinical implications for diabetes and cancer. Nat Rev Endocrinol. 2014;10(3):143-56.

166. DeFronzo R, Fleming GA, Chen K, Bicsak TA. Metformin-associated lactic acidosis: Current perspectives on causes and risk. Metabolism. 2016;65(2):20-9.

167. He L, Sabet A, Djedjos S, Miller R, Sun X, Hussain MA, et al. Metformin and insulin suppress hepatic gluconeogenesis through phosphorylation of CREB binding protein. Cell. 2009;137(4):635-46.

168.	Hawley SA, Ross FA, Chevtzoff C, Green KA, Evans A, Fogarty S, et al. Use of cells expressing gamma subunit variants to identify diverse mechanisms of AMPK activation. Cell Metab. 2010;11(6):554-65.

169.	Wang J, Gallagher D, DeVito LM, Cancino GI, Tsui D, He L, et al. Metformin activates an atypical PKC-CBP pathway to promote neurogenesis and enhance spatial memory formation. Cell Stem Cell. 2012;11(1):23-35.

170.	Correia S, Carvalho C, Santos MS, Proenca T, Nunes E, Duarte AI, et al. Metformin protects the brain against the oxidative imbalance promoted by type 2 diabetes. Med Chem. 2008;4(4):358-64.

171.	Hwang IK, Kim IY, Joo EJ, Shin JH, Choi JW, Won MH, et al. Metformin normalizes type 2 diabetes-induced decrease in cell proliferation and neuroblast differentiation in the rat dentate gyrus. Neurochem Res. 2010;35(4):645-50.

172.	Chen Y, Zhao S, Fan Z, Li Z, Zhu Y, Shen T, et al. Metformin attenuates plaque-associated tau pathology and reduces amyloid-beta burden in APP/PS1 mice. Alzheimers Res Ther. 2021;13(1):40.

173.	Farr SA, Roesler E, Niehoff ML, Roby DA, McKee A, Morley JE. Metformin Improves Learning and Memory in the SAMP8 Mouse Model of Alzheimer's Disease. J Alzheimers Dis. 2019;68(4):1699-710.

174.	Hsu CC, Wahlqvist ML, Lee MS, Tsai HN. Incidence of dementia is increased in type 2 diabetes and reduced by the use of sulfonylureas and metformin. J Alzheimers Dis. 2011;24(3):485-93.

175.	Koenig AM, Mechanic-Hamilton D, Xie SX, Combs MF, Cappola AR, Xie L, et al. Effects of the Insulin Sensitizer Metformin in Alzheimer Disease: Pilot Data From a Randomized Placebo-controlled Crossover Study. Alzheimer Dis Assoc Disord. 2017;31(2):107-13.

176.	Wu CY, Ouk M, Wong YY, Anita NZ, Edwards JD, Yang P, et al. Relationships between memory decline and the use of metformin or DPP4 inhibitors in people with type 2 diabetes with normal cognition or Alzheimer's disease, and the role APOE carrier status. Alzheimers Dement. 2020;16(12):1663-73.

177.	Imfeld P, Bodmer M, Jick SS, Meier CR. Metformin, other antidiabetic drugs, and risk of Alzheimer's disease: a population-based case-control study. J Am Geriatr Soc. 2012;60(5):916-21.

178. Kuan YC, Huang KW, Lin CL, Hu CJ, Kao CH. Effects of metformin exposure on neurodegenerative diseases in elderly patients with type 2 diabetes mellitus. Prog Neuropsychopharmacol Biol Psychiatry. 2017;79(Pt B):77-83.

179. Bassil F, Fernagut PO, Bezard E, Meissner WG. Insulin, IGF-1 and GLP-1 signaling in neurodegenerative disorders: targets for disease modification? Prog Neurobiol. 2014;118:1-18.

180. Horowitz M, Flint A, Jones KL, Hindsberger C, Rasmussen MF, Kapitza C, et al. Effect of the once-daily human GLP-1 analogue liraglutide on appetite, energy intake, energy expenditure and gastric emptying in type 2 diabetes. Diabetes Res Clin Pract. 2012;97(2):258-66.

181. Mehta A, Marso SP, Neeland IJ. Liraglutide for weight management: a critical review of the evidence. Obes Sci Pract. 2017;3(1):3-14.

182. Watson E, Jonker DM, Jacobsen LV, Ingwersen SH. Population pharmacokinetics of liraglutide, a once-daily human glucagon-like peptide-1 analog, in healthy volunteers and subjects with type 2 diabetes, and comparison to twice-daily exenatide. J Clin Pharmacol. 2010;50(8):886-94.

183. Cork SC, Richards JE, Holt MK, Gribble FM, Reimann F, Trapp S. Distribution and characterisation of Glucagon-like peptide-1 receptor expressing cells in the mouse brain. Mol Metab. 2015;4(10):718-31.

184. Carranza-Naval MJ, Del Marco A, Hierro-Bujalance C, Alves-Martinez P, Infante-Garcia C, Vargas-Soria M, et al. Liraglutide Reduces Vascular Damage, Neuronal Loss, and Cognitive Impairment in a Mixed Murine Model of Alzheimer's Disease and Type 2 Diabetes. Front Aging Neurosci. 2021;13:741923.

185. McClean PL, Parthsarathy V, Faivre E, Holscher C. The diabetes drug liraglutide prevents degenerative processes in a mouse model of Alzheimer's disease. J Neurosci. 2011;31(17):6587-94.

186. Edison P, Femminella GD, Ritchie CW, Holmes C, Walker Z, Ridha BH, Raza S et al. Evaluation of liraglutide in the treatment of Alzheimer's disease. Alzheimer's Dement.2021;17(Suppl.9):e057848.

187. Kwitek AE. Rat Models of Metabolic Syndrome. Methods Mol Biol. 2019;2018:269-85.

188. Schindelin J, Arganda-Carreras I, Frise E, Kaynig V, Longair M, Pietzsch T, et al. Fiji: an open-source platform for biological-image analysis. Nat Methods. 2012 Jul;9(7):676–82.

189. Paxinos G, Watson C. The rat brain in stereotaxic coordinates. San Diego: Acad. Press; 2004.

190. Bligh EG, Dyer WJ. A rapid method of total lipid extraction and purification. Can J Biochem Physiol. 1959 Aug;37(8):911–7.

191. R Core Team R: A language and environment for statistical computing. R Foundation for Statistical Computing, Vienna, Austria; 2018. Available at: https://www.R-project.org/. Date of access: September 1st 2020.

192. Picart-Armada S, Fernández-Albert F, Vinaixa M, Yanes O, Perera-Lluna A. FELLA: an R package to enrich metabolomics data. BMC Bioinformatics. 2018;19(1):538.

193. Wishart DS, Feunang YD, Marcu A, Guo AC, Liang K, Vázquez-Fresno R, et al. HMDB 4.0: the human metabolome database for 2018. Nucleic acids res. 2018;46(D1):D608-D17.

194. Kanehisa M, Goto S. KEGG: kyoto encyclopedia of genes and genomes. Nucleic acids res. 2000;28(1):27-30.

195. Tettamanti G, Bonali F, Marchesini S, Zambotti V. A new procedure for the extraction, purification and fractionation of brain gangliosides. Biochim Biophys Acta. 1973;296(1):160-70.

196. Korade Z, Kenworthy AK. Lipid rafts, cholesterol, and the brain. Neuropharmacology. 2008;55(8):1265-73.

197. Yuan C, Furlong J, Burgos P, Johnston LJ. The size of lipid rafts: an atomic force microscopy study of ganglioside GM1 domains in sphingomyelin/DOPC/cholesterol membranes. Biophys J. 2002;82(5):2526-35.

198. Rushworth JV, Hooper NM. Lipid Rafts: Linking Alzheimer's Amyloid-beta Production, Aggregation, and Toxicity at Neuronal Membranes. Int J Alzheimers Dis. 2010;2011:603052.

199. Zampagni M, Evangelisti E, Cascella R, Liguri G, Becatti M, Pensalfini A, et al. Lipid rafts are primary mediators of amyloid oxidative attack on plasma membrane. J Mol Med (Berl). 2010;88(6):597-608.

200. Walsh DM, Selkoe DJ. A beta oligomers - a decade of discovery. J Neurochem. 2007;101(5):1172-84.

201. Shankar GM, Li S, Mehta TH, Garcia-Munoz A, Shepardson NE, Smith I, et al. Amyloid-beta protein dimers isolated directly from Alzheimer's brains impair synaptic plasticity and memory. Nat Med. 2008;14(8):837-42.

202. Lesne S, Koh MT, Kotilinek L, Kayed R, Glabe CG, Yang A, et al. A specific amyloid-beta protein assembly in the brain impairs memory. Nature. 2006;440(7082):352-7.

203. Lee HK, Kumar P, Fu Q, Rosen KM, Querfurth HW. The insulin/Akt signaling pathway is targeted by intracellular beta-amyloid. Mol Biol Cell. 2009;20(5):1533-44.

204. Lourenco MV, Clarke JR, Frozza RL, Bomfim TR, Forny-Germano L, Batista AF, et al. TNF-alpha mediates PKR-dependent memory impairment and brain IRS-1 inhibition induced by Alzheimer's beta-amyloid oligomers in mice and monkeys. Cell Metab. 2013;18(6):831-43.

205. Wicinski M, Socha M, Malinowski B, Wodkiewicz E, Walczak M, Gorski K, et al. Liraglutide and its Neuroprotective Properties-Focus on Possible Biochemical Mechanisms in Alzheimer's Disease and Cerebral Ischemic Events. Int J Mol Sci. 2019;20(5).

206. Finsterwald C, Dias S, Magistretti PJ, Lengacher S. Ganglioside GM1 Targets Astrocytes to Stimulate Cerebral Energy Metabolism. Front Pharmacol. 2021;12:653842.

207. Vajn K, Viljetic B, Degmecic IV, Schnaar RL, Heffer M. Differential distribution of major brain gangliosides in the adult mouse central nervous system. PLoS One. 2013;8(9):e75720.

208. Galleguillos D, Wang Q, Steinberg N, Zaidi A, Shrivastava G, Dhami K, et al. Anti-inflammatory role of GM1 and other gangliosides on microglia. J Neuroinflammation. 2022;19(1):9.

209. Candeias EM, Sebastiao IC, Cardoso SM, Correia SC, Carvalho CI, Placido AI, et al. Gut-brain connection: The neuroprotective effects of the anti-diabetic drug liraglutide. World J Diabetes. 2015;6(6):807-27.

210. Tracey TJ, Steyn FJ, Wolvetang EJ, Ngo ST. Neuronal Lipid Metabolism: Multiple Pathways Driving Functional Outcomes in Health and Disease. Front Mol Neurosci. 2018;11:10.

211. Bazinet RP, Laye S. Polyunsaturated fatty acids and their metabolites in brain function and disease. Nat Rev Neurosci. 2014;15(12):771-85.

212. Xu J, Ni B, Ma C, Rong S, Gao H, Zhang L, et al. Docosahexaenoic acid enhances hippocampal insulin sensitivity to promote cognitive function of aged rats on a high-fat diet. J Adv Res. 2022 Apr 30:S2090-1232(22)00111-4.

213. Rapoport SI. Arachidonic acid and the brain. J Nutr. 2008;138(12):2515-20.

214. Duan JY, Lin X, Xu F, Shan SK, Guo B, Li FX, et al. Ferroptosis and Its Potential Role in Metabolic Diseases: A Curse or Revitalization? Front Cell Dev Biol. 2021 Jul 9;9:701788.

215. Yang XD, Yang YY. Ferroptosis as a Novel Therapeutic Target for Diabetes and Its Complications. Front Endocrinol (Lausanne). 2022;13:853822.

216. Liang Y, Wei P, Duke RW, Reaven PD, Harman SM, Cutler RG, et al. Quantification of 8-iso-prostaglandin-F(2alpha) and 2,3-dinor-8-iso-prostaglandin-F(2alpha) in human urine using liquid chromatography-tandem mass spectrometry. Free Radic Biol Med. 2003;34(4):409-18.

217. Laight DW, Desai KM, Gopaul NK, Anggard EE, Carrier MJ. F2-isoprostane evidence of oxidant stress in the insulin resistant, obese Zucker rat: effects of vitamin E. Eur J Pharmacol. 1999;377(1):89-92.

218. Ebert D, Haller RG, Walton ME. Energy contribution of octanoate to intact rat brain metabolism measured by 13C nuclear magnetic resonance spectroscopy. J Neurosci. 2003;23(13):5928-35.

219. Wolfgang MJ, Cha SH, Millington DS, Cline G, Shulman GI, Suwa A, et al. Brain-specific carnitine palmitoyl-transferase-1c: role in CNS fatty acid metabolism, food intake, and body weight. J Neurochem. 2008;105(4):1550-9.

220. Lenhard JM, Kliewer SA, Paulik MA, Plunket KD, Lehmann JM, Weiel JE. Effects of troglitazone and metformin on glucose and lipid metabolism: alterations of two distinct molecular pathways. Biochem Pharmacol. 1997;54(7):801-8.

221. Yao J, Irwin RW, Zhao L, Nilsen J, Hamilton RT, Brinton RD. Mitochondrial bioenergetic deficit precedes Alzheimer's pathology in female mouse model of Alzheimer's disease. Proc Natl Acad Sci U S A. 2009;106(34):14670-5.

222. Casadesus G, Smith MA, Basu S, Hua J, Capobianco DE, Siedlak SL, et al. Increased isoprostane and prostaglandin are prominent in neurons in Alzheimer disease. Mol Neurodegener. 2007;2:2.

223. Thomas MH, Pelleieux S, Vitale N, Olivier JL. Arachidonic acid in Alzheimer's disease. J Neurol Neuromedicine. 2016;1(9):1-6.

224. Mishima Y, Kurano M, Kobayashi T, Nishikawa M, Ohkawa R, Tozuka M, et al. Dihydro-sphingosine 1-phosphate interacts with carrier proteins in a manner distinct from that of sphingosine 1-phosphate. Biosci Rep. 2018;38(5).

225. Bu S, Kapanadze B, Hsu T, Trojanowska M. Opposite effects of dihydrosphingosine 1-phosphate and sphingosine 1-phosphate on transforming growth factor-beta/Smad

signaling are mediated through the PTEN/PPM1A-dependent pathway. J Biol Chem. 2008;283(28):19593-602.

226.   Endersby R, Baker SJ. PTEN signaling in brain: neuropathology and tumorigenesis. Oncogene. 2008;27(41):5416-30.

227.   Macala LJ, Yu RK, Ando S. Analysis of brain lipids by high performance thin-layer chromatography and densitometry. J Lipid Res. 1983;24(9):1243-50.

228.   Pradas I, Jove M, Huynh K, Puig J, Ingles M, Borras C, et al. Exceptional human longevity is associated with a specific plasma phenotype of ether lipids. Redox Biol. 2019;21:101127.

229.   Braverman NE, Moser AB. Functions of plasmalogen lipids in health and disease. Biochim Biophys Acta. 2012;1822(9):1442-52.

230.   Farooqui AA, Horrocks LA. Plasmalogens: workhorse lipids of membranes in normal and injured neurons and glia. Neuroscientist. 2001;7(3):232-45.

231.   Takamori S, Holt M, Stenius K, Lemke EA, Gronborg M, Riedel D, et al. Molecular anatomy of a trafficking organelle. Cell. 2006;127(4):831-46.

232.   Su XQ, Wang J, Sinclair AJ. Plasmalogens and Alzheimer's disease: a review. Lipids Health Dis. 2019;18(1):100.

233.   Bleijerveld OB, Brouwers J, Vaandrager AB, Helms JB, Houweling M. The CDP-ethanolamine pathway and phosphatidylserine decarboxylation generate different phosphatidylethanolamine molecular species. J Biol Chem. 2007;282(39):28362-72.

234.   Tan RPA, Leshchyns'ka I, Sytnyk V. Glycosylphosphatidylinositol-Anchored Immunoglobulin Superfamily Cell Adhesion Molecules and Their Role in Neuronal Development and Synapse Regulation. Front Mol Neurosci. 2017;10:378.

235.   Çolakoğlu G, Bergstrom-Tyrberg U, Berglund EO, Ranscht B. Contactin-1 regulates myelination and nodal/paranodal domain organization in the central nervous system. Proc Natl Acad Sci U S A. 2014;111(3):E394-403.

236.   Puzzo D, Bizzoca A, Loreto C, Guida CA, Gulisano W, Frasca G, et al. Role of F3/contactin expression profile in synaptic plasticity and memory in aged mice. Neurobiol Aging. 2015;36(4):1702-15.

237.   EE Baulieu. Neurosteroids: of the nervous system, by the nervous system, for the nervous system. Recent Prog Horm Res. 1997;52:1-32.

238.   Prange-Kiel J, Wehrenberg U, Jarry H, Rune GM. Para/autocrine regulation of estrogen receptors in hippocampal neurons. Hippocampus. 2003;13(2):226-34.

239.   Tabori NE, Stewart LS, Znamensky V, Romeo RD, Alves SE, McEwen BS, et al. Ultrastructural evidence that androgen receptors are located at extranuclear sites in the rat hippocampal formation. Neuroscience. 2005;130(1):151-63.

240.   Hojo Y, Higo S, Ishii H, Ooishi Y, Mukai H, Murakami G, et al. Comparison between hippocampus-synthesized and circulation-derived sex steroids in the hippocampus. Endocrinology. 2009;150(11):5106-12.

241.   Harley CW, Malsbury CW, Squires A, Brown RA. Testosterone decreases CA1 plasticity in vivo in gonadectomized male rats. Hippocampus. 2000;10(6):693-7.

242.   Smith MD, Jones LS, Wilson MA. Sex differences in hippocampal slice excitability: role of testosterone. Neuroscience. 2002;109(3):517-30.

243.   Driscoll I, Resnick SM. Testosterone and cognition in normal aging and Alzheimer's disease: an update. Curr Alzheimer Res. 2007;4(1):33-45.

244.   Mukai H, Tsurugizawa T, Murakami G, Kominami S, Ishii H, Ogiue-Ikeda M, et al. Rapid modulation of long-term depression and spinogenesis via synaptic estrogen receptors in hippocampal principal neurons. J Neurochem. 2007;100(4):950-67.

245.   Pozzo-Miller LD, Inoue T, Murphy DD. Estradiol increases spine density and NMDA-dependent Ca2+ transients in spines of CA1 pyramidal neurons from hippocampal slices. J Neurophysiol. 1999;81(3):1404-11.

246.   MacLusky NJ, Hajszan T, Leranth C. Effects of dehydroepiandrosterone and flutamide on hippocampal CA1 spine synapse density in male and female rats: implications for the role of androgens in maintenance of hippocampal structure. Endocrinology. 2004;145(9):4154-61.

247.   Nguyen TV, Yao M, Pike CJ. Flutamide and cyproterone acetate exert agonist effects: induction of androgen receptor-dependent neuroprotection. Endocrinology. 2007;148(6):2936-43.

248.   Atwi S, McMahon D, Scharfman H, MacLusky NJ. Androgen Modulation of Hippocampal Structure and Function. Neuroscientist. 2016;22(1):46-60.

249.   Gatson JW, Kaur P, Singh M. Dihydrotestosterone differentially modulates the mitogen-activated protein kinase and the phosphoinositide 3-kinase/Akt pathways through the nuclear and novel membrane androgen receptor in C6 cells. Endocrinology. 2006;147(4):2028-34.

250.   Lonergan PE, Tindall DJ. Androgen receptor signaling in prostate cancer development and progression. J Carcinog. 2011;10:20.

251. Huffman J, Hoffmann C, Taylor GT. Integrating insulin-like growth factor 1 and sex hormones into neuroprotection: Implications for diabetes. World J Diabetes. 2017;8(2):45-55.

252. Riant E, Waget A, Cogo H, Arnal JF, Burcelin R, Gourdy P. Estrogens protect against high-fat diet-induced insulin resistance and glucose intolerance in mice. Endocrinology. 2009;150(5):2109-17.

253. De Paoli M, Zakharia A, Werstuck GH. The Role of Estrogen in Insulin Resistance: A Review of Clinical and Preclinical Data. Am J Pathol. 2021;191(9):1490-8.

254. Benedusi V, Meda C, Della Torre S, Monteleone G, Vegeto E, Maggi A. A lack of ovarian function increases neuroinflammation in aged mice. Endocrinology. 2012;153(6):2777-88.

255. Villa A, Vegeto E, Poletti A, Maggi A. Estrogens, Neuroinflammation, and Neurodegeneration. Endocr Rev. 2016;37(4):372-402.

256. Prah J, Winters A, Chaudhari K, Hersh J, Liu R, Yang SH. Cholesterol sulfate alters astrocyte metabolism and provides protection against oxidative stress. Brain Res. 2019;1723:146378.

257. Sipione S, Monyror J, Galleguillos D, Steinberg N, Kadam V. Gangliosides in the Brain: Physiology, Pathophysiology and Therapeutic Applications. Front Neurosci. 2020;14:572965.

258. Clifford DB, Ferrendelli JA. Neurophysiologic Effects of Folate Compounds in Hippocampus, in vitro. Brain Res. 1983;266:209-16.

259. Zhang X, Liu Z, Yang W, Zhao F, Zhang C, Feng H, et al. Tetrahydrofolate Alleviates the Inhibitory Effect of Oxidative Stress on Neural Stem Cell Proliferation through PTEN/Akt/mTOR Pathway. Oxid Med Cell Longev. 2022;2022:9021474.

260. Wang Q, Zhao J, Chang H, Liu X, Zhu R. Homocysteine and Folic Acid: Risk Factors for Alzheimer's Disease-An Updated Meta-Analysis. Front Aging Neurosci. 2021;13:665114.

261. Joe E, Medina LD, Ringman JM, O'Neill J. (1)H MRS spectroscopy in preclinical autosomal dominant Alzheimer disease. Brain Imaging Behav. 2019;13(4):925-32.

262. Maul S, Giegling I, Rujescu D. Proton Magnetic Resonance Spectroscopy in Common Dementias-Current Status and Perspectives. Front Psychiatry. 2020;11:769.

11. CURRICULUM VITAE

Name and surname: Marin Kuharić

Date and place of birth: August 7, 1992; Osijek, Croatia

Address: Ilica 253, 10000 Zagreb

Contact number: +385 91 199 2708

E-mail: mkuharic@fdmz.hr

Education:

2006 – 2010 – Jesuit Classical Secondary School Osijek

2010 – 2016 – Faculty of Medicine, J.J. Strossmayer University of Osijek

Work experience:

2016 – 2017 – medical internship, Sisters of Mercy Clinical Hospital Centre, Zagreb

2017 – 2018 – teaching and research assistant, Department for Pathophysiology, Faculty of Medicine, J.J. Strossmayer University of Osijek

2018 – today – teaching and research assistant, Department for Pathophysiology, Physiology and Immunology, Faculty of Dental Medicine and Health, J.J. Strossmayer University of Osijek

2018 – today – clinical radiology resident, Faculty of Dental Medicine and Health, J.J. Strossmayer University of Osijek and Clinical Hospital Holy Spirit, Zagreb

Published scientific papers:

1. Berlančić T, Kuharić M, Janković D, Milić J, Badak K. Croatian Translation and Linguistic Adaptation of the Short Assessment of Health Literacy for Spanish Adults (SAHLSA-50). Southeastern European Medical Journal. 2020; 4(2), 121-8.

2. Kuharić M, Zibar L. Screening for Carpal Tunnel Syndrome in Patients on Chronic Hemodialysis. Acta Med Acad. 2019; 48(2), 167-76.

3. Kuharić M, Janković D, Splavski B, Boop FA, Arnautović K. Hemangioblastomas of the posterior cranial fossa in adults: demographics, clinical, morphologic, pathologic, surgical features, and outcomes. A systematic review. World Neurosurg. 2018 Feb;110:e1049-e1062. doi: 10.1016/j.wneu.2017.11.173.

4. Zibar L, Ižaković I, Kuharić M. Ethics in Solid Organ Transplantation. [in Croatian.] Liječ Vjesn. 2018;140(5-6),0-0.

5. Kuharić M, Rozić D, Karner I. Thyroid Autoimmunity and Infertility. Southeastern European Medical Journal. 2018;1(2),1-10.